

# LINK ADAPTATION FOR ENERGY CONSTRAINED NETWORKS

by

ALI YILDIRIM ALEMDAR

A thesis submitted to the  
Department of Electrical and Computer Engineering  
in conformity with the requirements for  
the degree of Master of Science (Engineering)

Queen's University  
Kingston, Ontario, Canada

November 2008

Copyright © Ali Yıldırım Alemdar, 2008

# Abstract

Wireless sensor networks (WSNs) are a nascent technology that has recently garnered a significant amount of interest in academia and industry. Nodes in a sensor network often only have a finite amount of energy that can be used for sensing, signal processing, and communication. Understanding the trade off between battery life, signal processing and wireless communication is of paramount importance if we hope to maximize the operational lifetime of the network.

Relay terminals are often used in tandem in sensor networks to lessen nodal communication burden. In this light we investigate the problem of power allocation amongst nodes in a relay network in order to maximize the overall achievable rate using link adaptive transmission protocols. We focus on the physical layer characteristics and implementation issues of link adaptation in order to develop a bit-level simulator needed to accurately model the rate performance of such a system.

Optimal power allocation values, power adaptation policies, and switching levels for several link adaptive policies over a broad class of Rician fading channels are calculated. Furthermore, the maximum achievable rate for two and three link relay networks using our bit-level simulator and optimal power allocation values for collocated channel distributions is simulated. An overall achievable rate comparison between several link adaptive protocols is also investigated.

Finally, we show that discrete-rate continuous-power adaptation is a superior candidate

to other link adaptive protocols and that an appropriate design facilitates its incorporation as a communication protocol for energy constrained relay networks.

# Acknowledgments

I would like to express my sincere gratitude to my supervisor, Dr. Mohamed Ibnkahla, for his support, guidance, and encouragement. I would like to also thank the Ontario Centres of Excellence (OCE) and the Ontario Ministry of Natural Resources (OMNR) for their financial support.

To my parents and step-parents, Nedim Alemdar, Mojdeh Pourhamzeh, Nick Harris, and Sibel Sirakaya-Alemdar no words can express my gratitude. I would not be here if it was not for your hard work, sacrifice, and devotion. I love you with all of my heart.

I sincerely wish to thank Saeed Akhavan-Astaneh for his friendship, kindness, enthusiasm, and infinite patience. I will always cherish the memories that we have formed and rejoice in the prospect of continuing friendship.

I would also like to thank my colleagues, both past and present, in the Satellite and Mobile Communications Laboratory for their insight, friendship, and encouragement.

Finally, I would like to thank my friends. You have been an integral part of my life and I consider myself very lucky to have known you.

“A journey of a thousand miles begins with a single step.” -*Lao-tzu*

# Contents

<b>Abstract</b>	<b>ii</b>
<b>Acknowledgments</b>	<b>iv</b>
<b>Contents</b>	<b>v</b>
<b>List of Tables</b>	<b>viii</b>
<b>List of Figures</b>	<b>ix</b>
<b>List of Acronyms</b>	<b>xi</b>
<b>1 Introduction</b>	<b>1</b>
1.1 Background and Motivation . . . . .	2
1.1.1 The Role of Relay Nodes in Sensor Networks . . . . .	4
1.2 Thesis Contributions . . . . .	9
1.3 Thesis Overview . . . . .	9
<b>2 Analytical Framework</b>	<b>11</b>
2.1 Introduction . . . . .	11
2.2 System Architecture . . . . .	11
2.2.1 Information Source . . . . .	12
2.2.2 Transmitter . . . . .	12
2.2.3 Receiver . . . . .	13
2.2.4 Additive Noise Channels . . . . .	13
2.2.5 Wireless Fading Channel: Small Scale Fading . . . . .	13
2.2.6 Wireless Fading Channel: Large Scale Fading . . . . .	14
2.3 Clarke’s Rayleigh and Rician Fading Model . . . . .	15
2.3.1 Rayleigh Fading Channel Simulator . . . . .	15
2.3.2 Rician Fading Channel Simulator . . . . .	15
2.4 Probability Distributions for Rayleigh and Rician Fading Channels . . . . .	16
2.5 Capacity of Wireless Fading Channels . . . . .	17
2.6 Link Adaptation . . . . .	20

2.7	Energy Constrained Networks . . . . .	21
2.8	Conclusion . . . . .	23
<b>3</b>	<b>Adaptive Feedback Communication</b>	<b>24</b>
3.1	Introduction . . . . .	24
3.2	Adaptive Feedback Communication . . . . .	24
3.2.1	Single Hop Continuous Rate Continuous Power Adaptation . . . . .	25
3.2.2	Single Hop Fixed Rate Channel Inversion . . . . .	28
3.2.3	Single Hop Fixed Rate Truncated Channel Inversion . . . . .	29
3.2.4	Single Hop Discrete Rate Continuous Power Adaptation . . . . .	31
3.3	Conclusion . . . . .	35
<b>4</b>	<b>Link Adaptation for Energy Constrained Networks</b>	<b>38</b>
4.1	Introduction . . . . .	38
4.2	Multi-hop Discrete Rate Continuous Power Adaptation . . . . .	39
4.3	Multi-hop Fixed Rate Channel and Truncated Inversion . . . . .	40
4.4	Problem Formulation . . . . .	41
4.4.1	Problem Definition . . . . .	42
4.5	Conclusion . . . . .	43
<b>5</b>	<b>Simulation Results</b>	<b>44</b>
5.1	Introduction . . . . .	44
5.2	Simulation Objectives . . . . .	44
5.2.1	Simulation Parameters . . . . .	45
5.2.2	Simulation Assumptions . . . . .	45
5.3	Simulation Model, Methodology, and Metrics . . . . .	46
5.3.1	Methodology . . . . .	47
5.3.2	Effective Rate and Simulation Output . . . . .	52
5.4	Fixed Rate and Truncated Channel Inversion . . . . .	53
5.4.1	Received SNR and Switching Levels for Fixed Rate and Truncated Channel Inversion . . . . .	53
5.4.2	Power Adaptation Policies for Fixed Rate and Truncated Channel Inversion . . . . .	57
5.4.3	Effective Rate and Optimal Power Allocation for Fixed Rate and Truncated Channel Inversion over a Linear Relay Network . . . . .	57
5.4.4	Discussion: Results for Truncated and Channel Inversion Fixed Rate . . . . .	74
5.5	Discrete Rate Adaptation . . . . .	75
5.5.1	Switching Levels for Discrete Rate Adaptation . . . . .	75
5.5.2	Power Adaptation Policies for Adaptive Discrete Rate Transmission . . . . .	76
5.5.3	Effective Rate and Optimal Power Allocation for Adaptive Discrete Rate Transmission over a Linear Relay Network . . . . .	77
5.5.4	Discussion: Results for Adaptive Discrete Rate Transmission . . . . .	78
5.6	Achievable Rate Comparison between Link Adaptation Policies . . . . .	82

5.6.1	Discussion: Achievable Rate Comparison Between Adaptation Policies	86
5.7	Conclusion	87
<b>6</b>	<b>Conclusions and Future Work</b>	<b>88</b>
6.1	Conclusion	88
6.2	Future Work	89
	<b>Bibliography</b>	<b>92</b>
<b>A</b>	<b>Network Simulator Output</b>	<b>99</b>
<b>B</b>	<b>Source Code</b>	<b>105</b>

# List of Tables

5.1	Simulation Parameters . . . . .	45
5.2	Rate Performance for Adaptive Discrete Rate Over a Two Link Relay Network	60
5.3	Achievable Rate Figures for a Two Link Relay Network . . . . .	60
5.4	Optimal Power Allocation Figures for a Two Link Relay Network . . . . .	61
5.5	Optimal Power Allocation Figures for a Three Link Relay Network . . . . .	61
5.6	Optimal Switching Levels for Adaptive Discrete Rate Modulation over a Rician Fading Environment . . . . .	77
A.1	Point-to-Point Rate Performance for Adaptive Discrete Rate . . . . .	100
A.2	Point-to-Point Rate Performance for TIFR-32QAM . . . . .	101
A.3	Point-to-Point Rate Performance for TIFR-16QAM . . . . .	102
A.4	Point-to-Point Rate Performance for TIFR-4QAM . . . . .	103
A.5	Point-to-Point Rate Performance for CIFR-4QAM . . . . .	104

# List of Figures

1.1	Multi-Hop Communication Scenario for Habitat Monitoring . . . . .	5
1.2	Communication Scenario for an Environmental Monitoring Application . .	6
1.3	Generalized Multi-Hop Communication in a Wireless Sensor Network . . .	8
2.1	System Model for a Digital Communication System . . . . .	12
2.2	Wireless Fading Channels . . . . .	16
2.3	PDF of Received SNR for Rician and Rayleigh Distributions . . . . .	18
3.1	Adaptive Feedback System Model . . . . .	25
3.2	Waterfilling Power Adaptation Policy . . . . .	27
3.3	Spectral Efficiency of Channel Inversion Fixed Rate for a Rician Fading Channel	30
3.4	Spectral Efficiency for Truncated Channel Inversion Fixed Rate for a Rician Fading Channel with $\gamma_0 = 11.82\text{dB}$ (4QAM Cut-Off) . . . . .	31
3.5	Outage Probability for Truncated Channel Inversion Fixed Rate for a Rician Fading Channel with $\gamma_0 = 11.82\text{dB}$ (4QAM Cut-Off) . . . . .	32
3.6	Constellation Assignment for Continuous And Discrete-Rate Adaptation: with $M = 4, 16, 32, 64$ and a Target BER of $10^{-4}$ . . . . .	33
3.7	Capacity per Unit Bandwidth Comparison I . . . . .	36
3.8	Capacity per Unit Bandwidth Comparison II . . . . .	37
4.1	Linear Relay Network with 1 Relay Node . . . . .	41
4.2	Linear Relay Network with N Nodes . . . . .	43
5.1	Network Simulator Components . . . . .	48
5.2	Adaptive Feedback System Model . . . . .	50
5.3	Simulator Flowchart for One Communication Session . . . . .	51
5.4	Simulator Output . . . . .	53
5.5	Received SNR that can be maintained for Channel Inversion Fixed Rate . .	54
5.6	$E_{\gamma_0}$ behavior and Cut-Offs for Truncated Inversion Fixed Rate . . . . .	55
5.7	$p_{\text{out}}$ and Cut-Off Relationship for Truncated Inversion Fixed Rate . . . . .	56
5.8	Outage Probability and Achievable SNR for Truncated Inversion Fixed Rate	57
5.9	Power Adaptation Policy for Channel Inversion Fixed Rate-4QAM . . . . .	58
5.10	Power Adaptation Policy for Truncated Inversion Fixed Rate-4QAM . . . .	59

5.11	Channel Inversion Fixed Rate-4QAM: Achievable Rate For a Two Link Linear Relay Network with Variable Power Constraints . . . . .	62
5.12	Channel Inversion Fixed Rate-4QAM: Optimal Power Allocation Values for a Two Link Linear Relay Network with Variable Power Constraints . . . . .	63
5.13	Channel Inversion Fixed Rate-4QAM: Optimal Power Allocation Values for a Three Link Linear Relay Network with Variable Power Constraints . . . . .	64
5.14	Truncated Inversion Fixed Rate-4QAM: Achievable Rate for a Two Link Linear Relay Network with Variable Power Constraints . . . . .	65
5.15	Truncated Inversion Fixed Rate-4QAM: Optimal Power Allocation Values for a Two Link Linear Relay Network with Variable Power Constraints . . . . .	66
5.16	Truncated Inversion Fixed Rate-4QAM: Optimal Power Allocation Values for a Three Link Linear Relay Network with Variable Power Constraints . . . . .	67
5.17	Truncated Inversion Fixed Rate-16QAM: Achievable Rate for a Two Link Linear Relay Network with Variable Power Constraints . . . . .	68
5.18	Truncated Inversion Fixed Rate-16QAM: Optimal Power Allocation Values for a Two Link Linear Relay Network with Variable Power Constraints . . . . .	69
5.19	Truncated Inversion Fixed Rate-16QAM: Optimal Power Allocation Values for a Three Link Linear Relay Network with Variable Power Constraints . . . . .	70
5.20	Truncated Inversion Fixed Rate-32QAM: Achievable Rate for a Two Link Linear Relay Network with Variable Power Constraints . . . . .	71
5.21	Truncated Inversion Fixed Rate-32QAM: Optimal Power Allocation Values for a Two Link Linear Relay Network with Variable Power Constraints . . . . .	72
5.22	Truncated Inversion Fixed Rate-32QAM: Optimal Power Allocation Values For a Three Link Linear Relay Network with Variable Power Constraints . . . . .	73
5.23	Numerically Obtained Values for $\rho$ . . . . .	76
5.25	Power Adaptation Policies for Rician Fading Channels . . . . .	77
5.24	Power Adaptation Policy for a Rician Fading Channel $K=0$ dB . . . . .	78
5.26	Adaptive Discrete Rate: Achievable Rate for a Two Link Linear Relay Network with Variable Power Constraints . . . . .	79
5.27	Adaptive Discrete Rate: Optimal Power Allocation Values For a Two Link Linear Relay Network with Variable Power Constraints . . . . .	80
5.28	Adaptive Discrete Rate: Optimal Power Allocation Values For a Three Link Linear Relay Network with Variable Power Constraints . . . . .	81
5.29	Maximum effective rate for a two-link relay network, $K_1 = 0$ dB . . . . .	82
5.30	Maximum Effective Rate For a Two Link Relay Network, $K_1 = 10$ dB . . . . .	83
5.31	Maximum Effective Rate For a Two Link Relay Network, $K_1 = 20$ dB . . . . .	83
5.32	Maximum Effective Rate For a Three Link Relay Network . . . . .	84
5.33	Maximum Effective Rate For a Three Link Relay Network . . . . .	85

# List of Acronyms

**ADR** - Adaptive Discrete Rate  
**ARQ** - Automatic Repeat Query  
**AWGN** - Additive White Gaussian Noise  
**BER** - Bit Error Rate  
**CIFR** - Channel Inversion Fixed Rate  
**CSI** - Channel State Information  
**LAN** - Local Area Network  
**LOS** - Line of Sight  
**MAN** - Metropolitan Area Network  
**MAC** - Multiple Access Control  
**PAP** - Power Adaptation Policy  
**PDF** - Probability Density Function  
**PSD** - Power Spectral Density  
**QAM** - Quadrature Amplitude Modulation  
**QoS** - Quality of Service  
**SNR** - Signal to Noise Ratio  
**TDMA** - Time Division Multiple Access  
**TIFR** - Truncated Inversion Fixed Rate  
**WSN** - Wireless Sensor Network

# Chapter 1

## Introduction

This thesis investigates power allocation amongst nodes in an energy constrained relay network in order to maximize the overall achievable rate using link adaptive transmission protocols. We show that link adaptation is an effective means of increasing spectral efficiency.

This thesis focuses on physical layer characteristics and implementation issues of link adaptation for energy constrained relay networks. We outline and discuss, in detail, the main components of a bit-level simulator needed to accurately model the rate performance of such a system.

We calculate optimal power allocation values, power adaptation policies, and switching levels for several link adaptive policies over a broad class of Rician fading channels. The maximum achievable rate for two and three link relay networks using our bit-level simulator and optimal power allocation values for collocated channel distributions is simulated. Furthermore, an overall achievable rate comparison between several link adaptive protocols is investigated.

Finally, we show that adaptive discrete rate continuous power adaptation is a superior candidate to other link adaptive protocols and that an appropriate design facilitates the incorporation of discrete rate adaptation as a link adaptive protocol for energy constrained

relay networks.

## 1.1 Background and Motivation

Recent advances in research have led to the development of new communication technologies and paradigms. The sophistication of contemporary hardware and computing technology has led to the emergence of small low-power devices with limited onboard computing and wireless communication capabilities. These battery-operated devices are equipped with a wireless transceiver, a low-power signal processor, and a sensing unit. The sensing unit itself may be outfitted with a wide array of sensors, often tailored to the requirements of the application for which they are being used. By using peer-to-peer communication protocols these nodes may form an ad hoc Wireless Sensor Network (WSN) in order to achieve some objective goal.

Many of applications for which wireless sensor networks are naturally suited preclude a reliance on established infrastructure (due to remoteness or inhospitableness). If ground access is not a feasible means of installing the network then nodes may be dispersed over a predetermined geographic area via aerial scattering. Given that the topology of the network may not be known *a priori* it is incumbent upon the network itself to perform all of the necessary tasks of a traditional wireless communication network. The lack of available infrastructure necessitates the implementation of robust communication protocols that facilitate peer-to-peer communication and are impervious to a potentially dynamic network topology [6]. However, as the nodes only have a limited amount of battery power that can be used for sensing, data processing, and communication, understanding the trade-off between battery life, signal processing and wireless communication is of paramount importance. This principle of low-power consumption must be kept in mind when designing the sensor nodes; every aspect of their design must strive towards minimizing the energy footprint of the sensing, processing and communication equipment on the node. Furthermore,

all of the instituted control and communication algorithms must also take into account the limited energy supply of the nodes.

Despite a number of constraints WSNs offer the promise of comprehensive, inexpensive, and reliable monitoring for a host of applications. There are also a number of other attractive features which highlight the importance of sensor networks:

- **Cost-effective** - Given decreasing hardware costs, it is often desirable to replace costly human-based data gathering with a system that operates autonomously.
- **Higher resolution** - Dense deployment and high temporal sampling allow researchers to gather data at previously unattainable resolutions.
- **Placed in remote or hazardous environments** - Many applications require the placement of sensor nodes in environments that are not suitable to human data gathering.
- **Monitor disturbance effects** - It is no longer required for researchers to go out into the field to perform invasive data collection. This allows researchers to gather data from organisms in their natural environment .
- **Network retasking** - Parameters of merit (such as data collection frequency) can be adapted to the requirements of the study after the network has already been deployed. This affords the researchers a tremendous amount of flexibility and may help increase the efficacy of the sensor network.

It is because of their flexible, robust, and autonomous nature that WSNs have been envisioned as an indispensable aid in several areas such as military, health care, industrial manufacturing, security, agriculture, and environmental and habitat monitoring.

Much of the work conducted in this thesis has been inspired by the requirements of environmental and habitat monitoring studies.

Applications such as habitat monitoring, where the objective function is to observe animal species, the added complexity of tracking mobile agents whose range may traverse large geographical areas, with vastly different vegetation, requires a design which takes into account a dynamic network topology and knowledge of the wireless propagation environments.

Radio modeling in densely forested environments is challenging due to their great complexity. Physical and geometric parameters of the trees are highly variable, so it is difficult to find models to represent them. The signal propagation model in a forest depends on the density of trees, their distribution and genus [1].

### 1.1.1 The Role of Relay Nodes in Sensor Networks

In environmental and habitat monitoring it is often unfeasible for mobile agents to transmit directly (single-hop) to a local on-site computing center. A more efficient means of communication would be to communicate in a multi-hop fashion where relay nodes or other mobile agents may act as intermediaries that forward received data from the source to its ultimate destination. This point serves as our impetus to focus on the relay component of our sensor network.

We can see a typical communication scenario for habitat monitoring in Figure 1.1. Sensor nodes attached to the mobile agents gather data according to some schedule that is determined *a priori*. Once the device is in range of a relay node the data is offloaded and then transmitted in a multi-hop fashion to an on-site data center which may perform some basic signal processing. Once the data is processed it is then forwarded to the end-user where more complex computational tasks may be performed.

The objective goal for many habitat monitoring applications is to identify how these mobile agents interact with their environment. Often researchers seek to develop mobility models for the agents; to do so and in order to effectively capture the dynamics of a complex environment the network must be operational and capable of gathering *in situ* data for



**Figure 1.1:** Multi-Hop Communication Scenario for Habitat Monitoring

extended periods of time. It is often required for the lifetime of the network, for these applications, to be measured in years. Given the scarcity of available and expendable energy we can see the need to minimize the energy consumption of the nodes and control algorithms which facilitate the operation of this network.

Until now, research in sensor networks has often assumed that the communication links in the network are affected by identically distributed collocated channels. However, in our analysis we assume that the quality of channels may be very different. This is a common scenario in environmental and habitat monitoring. Signals transmitted by nodes placed in densely populated closed-forests may undergo much more severe attenuation than those placed in sparsely populated environments with low-lying vegetation [1] (see Figure 1.1). Even nodes located within close proximity may be subjected to very different propagation

characteristics - signals transmitted above the forest canopy will be affected very differently from those in the understory.

Environmental monitoring applications also evince the aforementioned caveats; looking at Figure 1.2 we can see that the transmitting sensor node is in a densely forested environment (corresponding to poor channel conditions). However, the two relays are situated on either side of a river which we may assume corresponds to a much stronger channel. Due to poor channel conditions, in order for the transmitting sensor node to be able to satisfy the applications QoS requirements, it may be necessary for the sensor to transmit at a much higher power than the relays.

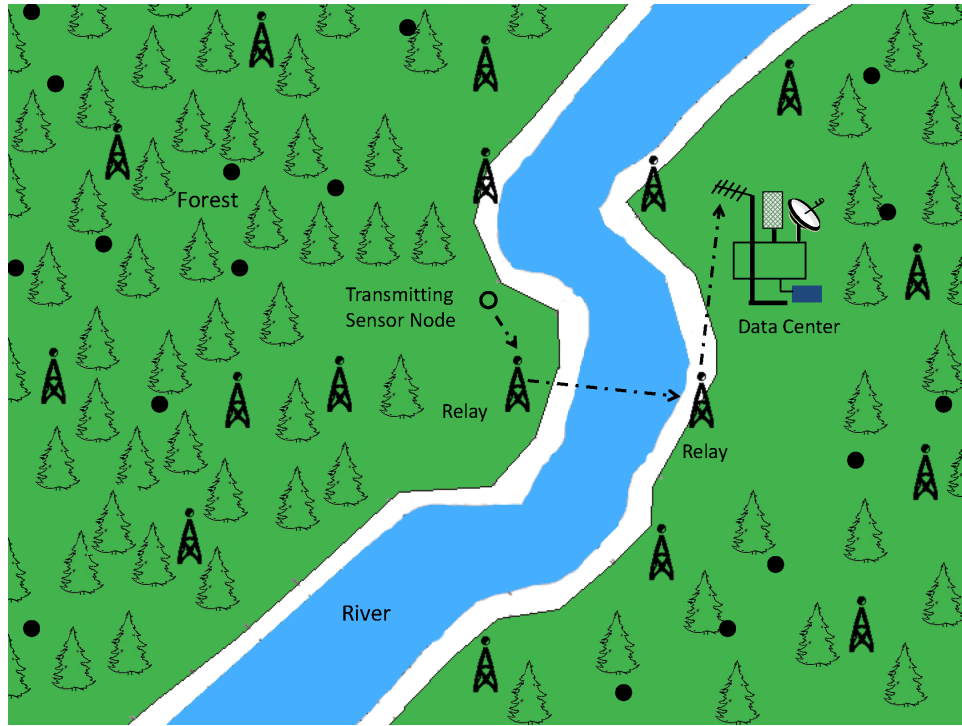


Figure 1.2: Communication Scenario for an Environmental Monitoring Application

In the example presented in Figure 1.2 the transmitting sensor node may need to increase its transmit power, due to the rich scattering environment in the dense forest, while the

relay nodes may decrease their average transmit power. Given the limited energy supply of the sensor nodes any savings in energy may help to extend the networks operational lifetime.

If we assume the same distribution for the channels then we face a scenario where the source (transmitting sensor node) and relay nodes transmit at power levels regardless of the fidelity of the channel. This in turn will result in an inefficient use of resources and will severely tax the energy-budget of the sensor nodes. Allowing each node to independently gauge the required transmit power level significantly complicates the calculation of the expected lifetime of the network. Furthermore, without an operational knowledge of the dynamic propagation environment the sensor network must be designed for a worst-case scenario; resulting in a needless waste of the scarce energy resources.

In order to minimize the energy consumption of nodes along a communication path, we propose to impose a total average transmit power constraint in order to judiciously allocate power in response to channel conditions. Furthermore, the imposition of a total energy constraint allows the network designer to place an upper-bound the aggregate energy consumption of all of the nodes in a communication path. This upper-bound will help to simplify the calculation of the expected lifetime of the network. Thus, if we can obtain an accurate picture of the propagation environment we may be able to fine tune transmission parameters to meet a host of QoS and energy requirements.

It should be noted that the aforementioned issues are not limited to only environmental and habitat monitoring applications. The problem of power allocation amongst nodes in a sensor network can be extended and applied to almost any scenario where links in the network are affected by independent channel fading distributions. As an example we present (Figure 1.3) a simplified communication scenario which helps to highlight the applicability of the research conducted herein.

In this light we now look at some innovative research which helps to establish the merit of the work presented in this thesis. We specifically look at works which give us insight into

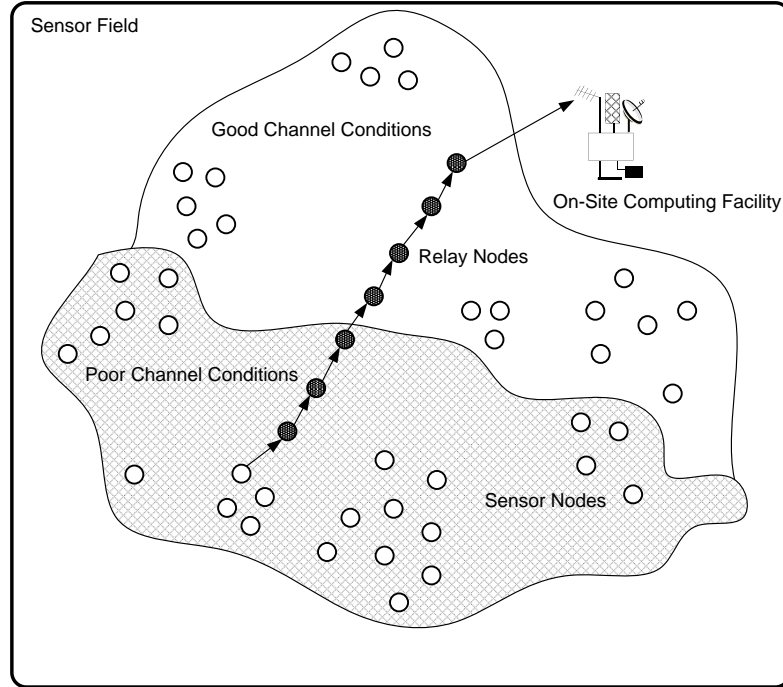


**Figure 1.3:** Generalized Multi-Hop Communication in a Wireless Sensor Network

the problem of power allocation amongst nodes in an energy constrained network.

Recently, there has been a focus in research on how to effectively route information from a source node to its ultimate destination while operating within a fixed energy budget [4], [29], [32]. Researchers have shown that in order to achieve the optimal lifetime of a sensor network it is necessary to include nodal energy information as part of the routing metric in choosing the forwarding path from source to destination [2], [21], [48].

The problem of dynamic routing and power allocation in power constrained networks with time varying channels has received much attention from academia as of late. Of particular interest to us are analyses which consider the problem of resource allocation where a total power constraint is considered as part of the optimization problem [13], [31], [56]. The work by Cui et al. [13], demonstrated that including nodal energy consumption

along the entire communication path, from source to destination, is essential in choosing the optimal forwarding route.

## 1.2 Thesis Contributions

The primary contributions of this thesis are summarized as follows:

- We develop a bit-level simulator to simulate the rate performance, across multiple hops, of an energy constrained relay network
- We extend the work of Goldsmith et al., in order to perform multi-hop link adaptation where a total average transmit power constraint is placed on all nodes in a communication path
- We simulate optimal power allocation values for different link adaptive transmission protocols over a broad class of Rician fading channels
- We simulate the achievable rate for two and three link relay networks employing a number of different link adaptive transmission protocols

## 1.3 Thesis Overview

- In Chapter 2 the analytical framework for this thesis is presented. Pertinent parameters are presented in order to establish the accuracy and repeatability of the simulations. The necessity to incorporate energy consumption along an entire transmission link is presented; and a communication strategy is investigated which exploits channel-distribution information amongst communication links in a wireless network.
- In Chapter 3 adaptive feedback communication for single-hop energy constrained networks is investigated. Specifically, we study several link adaptive protocols and discuss

salient trends and parameters of interest. We investigate several optimal and sub-optimal adaptation strategies and compare their theoretical performance in wireless fading environments.

- Chapter 4 presents our extension to the work discussed in Chapter 3. Specifically, we extend the work of Goldsmith et al., to include the possibility of performing link adaptation across a multi-hop relay network. In this chapter we outline and formulate our principal objectives.
- Chapter 5 presents our simulation results. Based on the framework established in Chapters 2-5 salient figures are presented. In this light we present our simulated rate comparison of a number of different link adaptation policies for energy constrained linear relay networks.
- Chapter 6 presents concluding remarks and highlights some areas for future work.

## Chapter 2

# Analytical Framework

### 2.1 Introduction

In this chapter the mathematical and analytical framework for this thesis is presented. All simulations presented henceforth are based on the work presented herein. Pertinent parameters are derived and presented in order to establish the accuracy and repeatability of the simulations. The necessity to incorporate energy consumption along an entire transmission link is presented; and a communication strategy that exploits channel distribution information amongst communication links in a wireless network is investigated. In this light, components which are germane to the development of a bit-level Physical Layer simulator are presented.

### 2.2 System Architecture

Here we give an overview of the main Physical Layer components of interest in this thesis (see Figure 2.1).

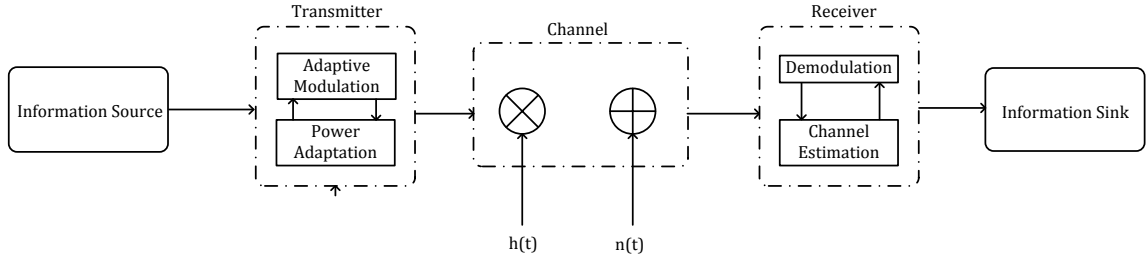


**Figure 2.1:** System Model for a Digital Communication System

### 2.2.1 Information Source

Data generated by the information source is uniformly distributed over the alphabet  $A_j$ ,  $A_j = 0, 1, \dots, M_j - 1$ . The decision as to which value of  $M_j$  to use will be discussed in detail in Section 3.2. It is assumed that data is generated at a fixed symbol rate  $R_s$ . This assumption is made because it is easier to implement in practice and variable symbol rate schemes lead to a variable signal bandwidth, which may, complicate upper-layer processing [22]. Assuming ideal Nyquist pulses we then get that  $B \approx 1/T_S = R_s$ . Where  $B$  is the bandwidth of the communication system.

### 2.2.2 Transmitter

The transmitter is responsible for three main tasks:

- **Transmission:** of data over a wireless channel - generated information is transmitted over the wireless link based on a modulation scheme that is determined *a priori*.
- **Adaptive Modulation:** given an adaptive transmission scheme the optimal constellation size is chosen based on certain QoS criteria. In this thesis we assume that an instantaneous BER (Bit Error Rate) requirement needs to be met.
- **Adaptive Power Control:** given a certain Power Adaptation Policy (PAP) an optimal transmit power level is chosen based on feedback provided by the receiver.

### 2.2.3 Receiver

The receiver is responsible for data reception and demodulation of received data. Once the data has been demodulated, an estimate of the power gain or received SNR is then fed back to the transmitter via the feedback channel. It is assumed that the channel is estimated perfectly and that the feedback channel introduces a negligible amount of delay. If a robust coding scheme is employed we can further assume that the feedback channel introduces no error into the channel estimates.

### 2.2.4 Additive Noise Channels

Thermal noise is present at all levels in all electronic systems. Therefore, we would be remiss if a reasonably accurate model for additive noise was not formulated and included in our analysis. If we let  $x$  denote the input of the additive noise channel,  $y$  its output, an expression relating  $y, x$  is given by:

$$y = h \cdot x + z \tag{2.1}$$

where  $z$  is the sampled noise process and  $h$  is the channel gain. It is assumed that the samples from  $z$  are taken from a zero-mean Gaussian random variable with a PSD (Power Spectral Density) equal to  $\frac{N_0}{2}$ .

### 2.2.5 Wireless Fading Channel: Small Scale Fading

The main phenomena that are responsible for small scale fading are: reflection, diffraction, and scattering by an object or objects [47]. Signals that are affected by these processes may experience attenuation in power, delay in time, and a shift in frequency/phase [46].

We first discuss the statistical simulation model used to simulate Rician and Rayleigh fading environments. The statistical fading model used throughout this thesis is a modified form of Clarke's fading model [10] (see Section 2.3).

### 2.2.6 Wireless Fading Channel: Large Scale Fading

Another important factor in wireless communication is the effect of large scale fading. The statistical simulators presented in Sections 2.3.1 and 2.3.2 model the effects of a wireless propagation environment over small distances (on the order of wavelengths); however, to be able to fully encapsulate the behavior of a wireless channel we must also study the effects of absorption, reflection, scattering and diffraction - collectively termed as large-scale propagation effects. Given the large number of processes that affect a wireless environment, finding a simple yet accurate model that fully describes the aforementioned processes is not a simple task.

We thus endeavor to use a relatively simple model that provides a reasonable level of accuracy in describing a host of wireless environments. The simplified path-loss model is given by:

$$\frac{P_r}{P_t} = \kappa \left[ \frac{d_0}{d} \right]^n \quad (2.2)$$

where  $P_t$  and  $P_r$  are the transmit power and received power, respectively;  $\kappa$  is a unitless constant that depends on the antenna characteristics and average channel attenuation,  $d_0$  is a known received power reference point, and  $n$  is the path-loss exponent [22]. We can express the above equation in dB attenuation as

$$P_r \text{ dBm} = P_t \text{ dBm} + \kappa \text{ dB} + 10n \log_{10} \left[ \frac{d_0}{d} \right] \quad (2.3)$$

The value of  $n$  is highly dependent on the propagation environment; it typically takes on a range of values between [2 – 5] (we assume that  $n = 3$ ). Often, when using this model,  $\kappa$  is set to the free space path gain at the reference point  $d_0$

$$\kappa \text{ dB} = 20 \log_{10} \frac{\lambda}{4\pi d_0}, \quad (2.4)$$

where  $\lambda$  is the wavelength of the transmitted signal [39].

### 2.3 Clarke's Rayleigh and Rician Fading Model

Using a finite number of sinusoids, this model was developed as to provide a more accurate representation of the higher order fading statistics while keeping computational complexity to a reasonable level [55], [37]. We can express the baseband signal of the normalized Clarke's Rayleigh fading model as

$$g(t) = \frac{1}{\sqrt{N_p}} \sum_{n=1}^{N_p} e^{j(2\pi f_d t \cos \alpha_n + \phi_n)}, \quad (2.5)$$

where  $N_p$  is the number of propagation paths,  $f_d$  is the maximum Doppler frequency, and  $\alpha_n$  and  $\phi_n$  are, the angle of arrival and initial phase, respectively. It is assumed that for each of the  $N_p$  paths both  $\alpha_n$  and  $\phi_n$  are *iid* and uniformly distributed over  $[-\pi, \pi)$ .

#### 2.3.1 Rayleigh Fading Channel Simulator

The improved statistical Rayleigh fading model is expressed as

$$\begin{aligned} Y(t) &= Y_c(t) + jY_s(t) \\ Y_c(t) &= \frac{1}{\sqrt{N_p}} \sum_{n=1}^{N_p} \cos(2\pi f_d t \cos \alpha_n + \phi_n) \\ Y_s(t) &= \frac{1}{\sqrt{N_p}} \sum_{n=1}^{N_p} \sin(2\pi f_d t \cos \alpha_n + \phi_n) \end{aligned} \quad (2.6)$$

where  $Y(t)$  is the time varying Rayleigh fading process,  $\alpha_n = \frac{2\pi n + \theta_n}{N_p}$ ,  $n = 1, 2, \dots, N_p$ , and  $\phi_n, \theta_n$  are statistically independent and uniformly distributed over  $[-\pi, \pi)$ .

#### 2.3.2 Rician Fading Channel Simulator

The fading process of the Rician fading channel simulator is quite similar to that presented in the above section, with the addition of a specular LOS (Line of Sight) component. Similar assumptions are made about the angle of arrival, initial phase, and mutual statistical

independence among the  $N_p$  paths (we have chosen  $N_p = 8$  in our simulations). The statistical fading model is given by

$$\begin{aligned} Z(t) &= Z_c(t) + jZ_s(t) \\ Z_c(t) &= [Y_c(t) + \sqrt{K} \cos(2\pi f_d t \cos \theta_0 + \phi_0)] / \sqrt{1 + K} \\ Z_s(t) &= [Y_s(t) + \sqrt{K} \sin(2\pi f_d t \cos \theta_0 + \phi_0)] / \sqrt{1 + K} \end{aligned} \quad (2.7)$$

where  $Z(t)$  is the time varying Rician fading process,  $K$  is defined as the ratio of signal power in the dominant LOS component over the (local-mean) scattered power;  $\phi_0$  and  $\theta_0$  are the initial phase and the angle of arrival of the specular component. It is further assumed that  $\phi_0, \theta_0$  is uniformly distributed over  $[-\pi, \pi)$ . Figure 2.2 was created using (2.6) and (2.7).

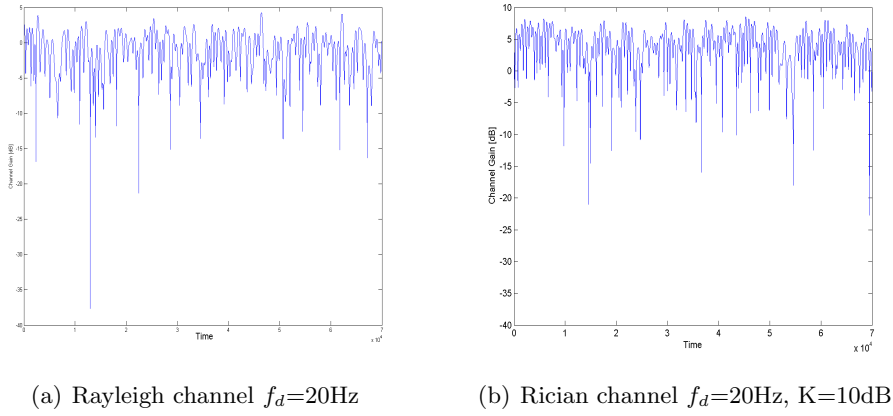


**Figure 2.2:** Wireless Fading Channels

## 2.4 Probability Distributions for Rayleigh and Rician Fading Channels

The subsequent analysis assumes that the probability distribution of the wireless channel gain over which data transmission is to occur is known beforehand. For a Rayleigh fading environment the distribution of the channel fading amplitude,  $P_R(r)$ , and distribution of

the received SNR ,  $P_{\Gamma}(\gamma)$ , are respectively [45]:

$$P_R(r) = \frac{2r}{\Omega} e^{-\frac{r^2}{\Omega}}, r \geq 0 \quad (2.8)$$

where  $\Omega = E(r^2)$ . With a simple transformation of variables (letting  $\gamma = |r|^2$ ) the distribution of the received SNR is:

$$P_{\Gamma}(\gamma) = \frac{1}{\bar{\gamma}} e^{-\frac{\gamma}{\bar{\gamma}}}, \gamma \geq 0 \quad (2.9)$$

where  $\bar{\gamma}$  is the average SNR per symbol. For a Rician fading environment the distribution of the channel fading amplitude,  $P_R(r)$ , and distribution of the received SNR,  $P_{\Gamma}(\gamma)$ , are respectively:

$$P_R(r) = \frac{(1+K)r}{\bar{\gamma}} e^{-K-\frac{(1+K)r^2}{\bar{\gamma}}} I_0\left(2r\sqrt{\frac{K(K+1)}{\bar{\gamma}}}\right), r \geq 0 \quad (2.10)$$

where  $\bar{\gamma}$  is defined as above, K is the Rician K-factor, and  $I_0(\cdot)$  is the zeroth order modified Bessel function of the first kind [45]. Using the same variable transformation as mentioned above, we get the distribution of the received SNR:

$$P_{\Gamma}(\gamma) = \frac{(1+K)}{\bar{\gamma}} e^{-K-\frac{(1+K)\gamma}{\bar{\gamma}}} I_0\left(2\sqrt{\frac{K(1+K)\gamma}{\bar{\gamma}}}\right), \gamma \geq 0. \quad (2.11)$$

## 2.5 Capacity of Wireless Fading Channels

In this section the capacity of a single user flat fading channel under different transmission strategies will be examined.

The mathematical framework used to explain the concept of capacity was developed by Claude Shannon in the late 1940s [12], [43]. The Shannon capacity places theoretical

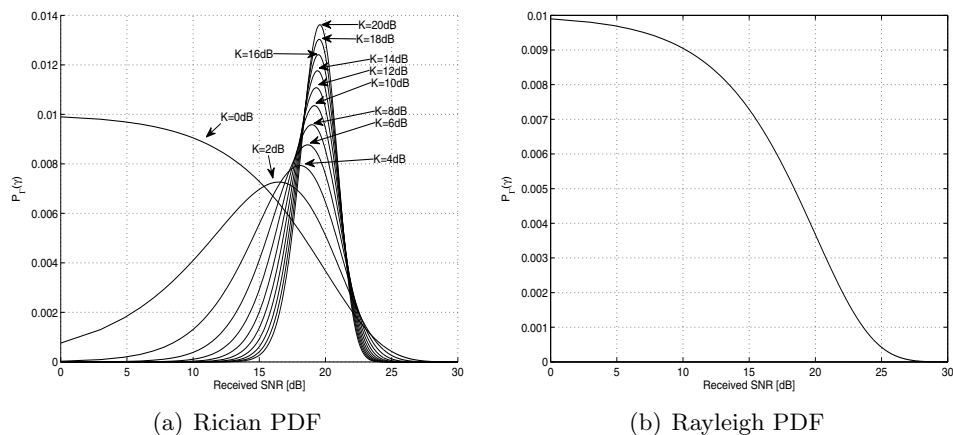


**Figure 2.3:** PDF of Received SNR for Rician and Rayleigh Distributions

bounds on the amount of information a wireless channel can bear with an arbitrarily small probability of error. Transmission rates above this capacity have error probabilities that are bounded away from zero. It should be noted that the Shannon capacity places no restrictions on encoding or decoding complexity or delay requirements; and thus it serves as an upper bound for practical communication systems [45].

We will now look at the formulation of the capacity of both time-invariant and time-varying channels. The capacity for time-varying channels depends on what the transmitter and receiver know about the current state of the channel.

The capacity of a time-invariant additive white Gaussian noise (AWGN) channel is given in [43] as:

$$C_{\text{AWGN}} = B \log_2(1 + \gamma) \tag{2.12}$$

where  $\gamma$  is the received SNR, and  $C_{\text{AWGN}}$  is measured in bits per second (bps).

In a wireless flat-fading environment we must include the effects of the time varying gain of the channel. The capacity of a wireless channel depends on the knowledge of the fading statistics at the transmitter and receiver. We consider the scenario where both the receiver and transmitter are aware of the channel conditions at all times. This is equivalent to saying that they both have full knowledge of the channel state information (CSI). If the

CSI is known to both the transmitter and receiver they are able to adapt both power and rate in response to  $h_i$  (the instantaneous gain of the channel).

The capacity of a wireless channel when CSI is available to both the transmitter and receiver was first investigated by Wolfowitz [53]. Let  $s$  be a stationary and ergodic stochastic process representing the channel state and  $C_s$  its capacity. If  $s$  is chosen from a finite set  $\mathbf{S}$  of discrete memoryless channels and denote  $p(s)$  as the probability of selecting the channel from  $\mathbf{S}$  then the time-varying capacity of this channel is then [53]:

$$C_{\text{Wolf}} = \sum_{s \in \mathbf{S}} C_s p(s) \quad (2.13)$$

This work was extended by Goldsmith and Varaiya in [20] to include selecting  $s$  from an infinite number of channels. We therefore present, without proof, the capacity of a flat-fading channel with CSI available at both the transmitter and receiver:

$$C_{\text{Gold}} = \max_{S(\gamma): \int S(\gamma)p(\gamma)d\gamma = \bar{S}} \int_0^{\infty} B \log_2 \left( 1 + \gamma \frac{S(\gamma)}{\bar{S}} \right) p(\gamma) d\gamma. \quad (2.14)$$

For further information the reader is encouraged to refer to [20] and [22]. The capacity formula above applies to any power adaptation policy ( $\frac{S(\gamma)}{\bar{S}}$ ) so long as the average power constraint

$$\int_0^{\infty} S(\gamma)p(\gamma)d\gamma \leq \bar{S}, \quad (2.15)$$

is satisfied. We thus get:

$$C_{\text{Gold}} = \int_0^{\infty} B \log_2 \left( 1 + \gamma \frac{S(\gamma)}{\bar{S}} \right) p(\gamma) d\gamma. \quad (2.16)$$

## 2.6 Link Adaptation

Link adaptation entails adjusting various transmission parameters according to the time-varying channel characteristics. The basic idea is the incorporation of a feedback channel that enables the communication system to effectively adjust transmission parameters to better suit the channel in order to maintain a QoS constraint.

Parameters which may be adjusted in response to the channel conditions are: the symbol rate [8], transmit power and error probability [25], data rate [7], [9], [19], [52], or other coding parameters [18], [23], [40], [51]. It should be noted that these parameters can be varied individually or jointly as per the requirements of the application. In this analysis we consider joint rate and power adaptation; we also assume that transmission parameters remain constant over the length of a frame (see Table 5.1 for the list of parameters).

The idea behind adapting transmission parameters in accordance with channel variations was first studied by Hayes [25] and Cavers [8]. Although their analyses yielded promising results, link adaptation was deemed to be unfeasible due to hardware limitations and difficulty in accurate estimation of channel fluctuations [22]; thus, until the significant hardware improvements were made link adaptation was relegated to an afterthought. With advances in technology the originally insurmountable constraints became less prohibitive resulting in a revived interest and incorporation of adaptive modulation into 3G and 4G cellular networks [11], [16], [33], [35], [50] and wireless LANs/MANs [17], [30], [36], [54].

Considering a fixed modulation strategy, in order to ensure that QoS requirements are met, the system must be designed with a worst case scenario in mind. The main reason for this is the existence of a fixed link margin that is needed to maintain acceptable performance even in unfavorable conditions. In the presence of fading channels, where deep fades are not uncommon, this design constraint leads to extremely poor utilization of the channel. However, with link adaptive protocols this unfavorable scenario is avoided. Spectral efficiency is increased by transmitting at high speeds under favorable channel

conditions and decreasing the data rate in poor ones.

It must be noted that there exist a number of practical constraints that could potentially limit the efficacy of an adaptive modulation scheme. The most important requirement is the existence of a reliable feedback channel. If the time varying channel gain cannot be estimated and fed back to the transmitter then link adaptation is not possible. Furthermore, the delay associated with the feedback channel is also a parameter of merit; since estimates of the channel gain are only valid for a short time duration it is imperative that the system be able to estimate the channel gain and relay this information within a deadline. In general the feedback channel may use robust channel codes and is thus assumed to be error free (incorporation of a Hybrid ARQ (Automatic Repeat Query) scheme may also be used).

Hardware considerations may also place restrictions on the rate at which information can be updated or estimated. Finally, for a class of applications, especially real time, the delay introduced via link adaptation may compromise their QoS requirements. However, with an appropriate design, adaptive modulation can work for almost any class of application.

## 2.7 Energy Constrained Networks

An energy constrained network is any type of network in which nodes must operate with a finite fixed energy budget (WSNs and ad hoc networks being two examples). Wireless sensor networks are comprised of a variable number of autonomous electronic devices that have the capability of remote sensing, signal processing and communication in an ad hoc fashion [5]. One feature that is common to both network types is the lack of available infrastructure, necessitating the implementation of robust control algorithms to facilitate reliable end-to-end communication [28], [32], [44].

In any constrained system there are certain inherent and unavoidable trade offs. For a wide class of sensor network applications nodes in the network will only have a finite amount of battery power that can be used for sensing, signal processing, routing, and

communication. Understanding the trade off between battery life, signal processing and wireless communication is of paramount importance [5].

One avenue of research which has garnered a significant amount of interest, particularly in energy constrained sensor networks, is how to effectively route information from the source node to its destination [2], [29], [48]. In many instances, particularly when nodes are densely deployed, it is often prudent for nodes to route information in a multi-hop fashion. This is mainly due to the fact that the energy required to transmit data directly from the source to the destination would severely tax the node's energy budget. In multi-hop sensor networks, the nodes may fill the role of generating data to be forwarded and relaying data generated by other nodes [3].

Recent work in the field of sensor networks has shown that in order to achieve the optimal lifetime of a sensor network it is necessary to include nodal energy information as part of the routing metric [2]–[4], [14], [21], [27], [41], [49]. Recently there has been a concerted effort to investigate the problem of dynamic routing and power allocation in power constrained networks with time varying channels [24], [26], [34], [42]. Of particular interest to us are analyses which consider the problem of resource allocation where a total power constraint is considered as part of the optimization problem [13], [31], [56]. The work by Cui et al. [13], demonstrated that including nodal energy consumption along the entire communication path, from source to destination, is essential in choosing the optimal forwarding route.

We can thus see the need to minimize the transmission power of all of the forwarding nodes along the transmitting and receiving paths. The basic concept behind this thesis is that in certain sensor network applications, especially for environmental and habitat monitoring, the area that is to be monitored can be divided into disjoint wireless environments. If the nodes are stationary then we can often assume that the wireless propagation environment experienced by transmitted signals in that area remains constant for long enough that it can be estimated or known *a priori*.

## 2.8 Conclusion

In this chapter we have detailed the conceptual framework that provides a basis for further analysis in the following chapters. The system architecture of a wireless communication system was presented; and its main components were discussed. An improved Rayleigh and Rician fading channel simulator, based on Clarke's fading model, was examined; and Rayleigh and Rician probability distributions, which form an integral part of the analysis in subsequent chapters, were examined. The concept of capacity for a wireless fading channel was introduced in order to help corroborate the results presented in Chapter 5. The concept of link adaptation in wireless fading environments was presented and the problem of resource allocation for energy constrained networks was also discussed. It is hoped that this chapter will provide the necessary groundwork to establish the necessity and pertinence of the problems to be investigated in subsequent chapters.

## Chapter 3

# Adaptive Feedback Communication

### 3.1 Introduction

With the ever increasing scarcity of available radio spectrum, the development of spectrally efficient forms of communication is an important endeavor. Spectral efficiency is the ability of a system to accommodate data within a fixed bandwidth [22]. Use of adaptive M-ary QAM (Quadrature Amplitude Modulation) is one approach that promises to fulfill the need for robust and spectrally-efficient communication schemes.

In this chapter we investigate adaptive feedback communication for single-hop energy constrained networks where. We present the findings of Goldsmith et al. which serves as a basis for our analysis.

### 3.2 Adaptive Feedback Communication

We now present a point-to-point link adaptive modulation technique and extend it to include multi-hopping scenarios where transmission links between nodes are affected by collocated channels with independent fading distributions. The basic feedback system model that is employed in this analysis is presented in Figure 3.1. For a complete description of the figure

please refer to Section 5.3.1.

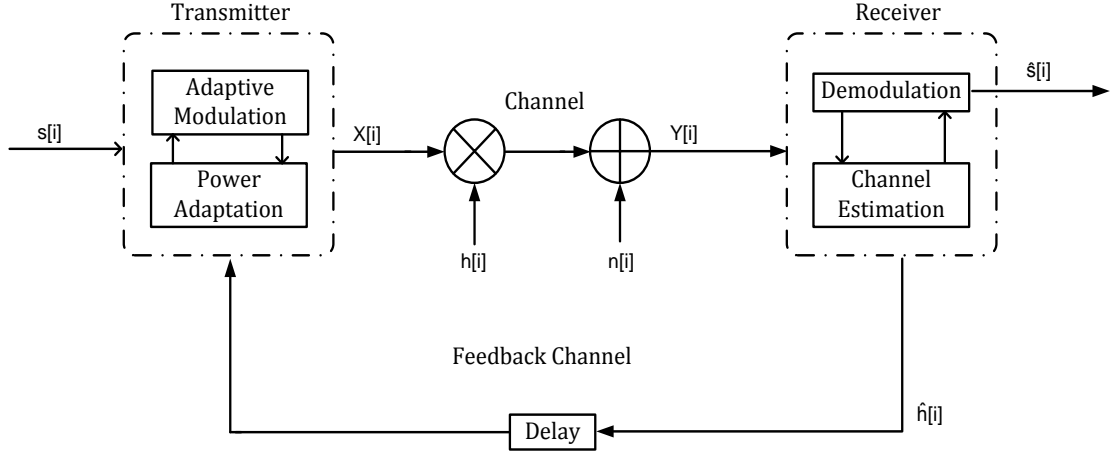


Figure 3.1: Adaptive Feedback System Model

### 3.2.1 Single Hop Continuous Rate Continuous Power Adaptation

With joint power and rate adaptation we seek to maximize spectral efficiency while adapting transmit power and modulation levels in response to channel conditions to meet a QoS requirement. This analysis presumes that our communication system must maintain a fixed and instantaneous BER target. If we assume ideal Nyquist pulses, an average channel gain equal to unity,  $\bar{S}$  as the average transmit power, a noise PSD,  $\frac{N_0}{2}$ , and a bandwidth B, we get that our average received SNR is:

$$\bar{\gamma} = \frac{\bar{S}|\bar{h}|}{N_0B} = \frac{\bar{S}}{N_0B} = \frac{\bar{S}T_s}{N_0} = \frac{\bar{E}_s}{N_0}. \quad (3.1)$$

Using an easily invertible, with respect to rate and power, BER (Bit Error Rate) approximation for M-QAM over AWGN simplifies our analysis considerably. More accurate approximations for M-QAM performance over AWGN are available; however, they often do not lend themselves easily to analysis in this regard [38], [22]. An accurate approximation

(to within 1dB) for M-QAM over AWGN with  $M \geq 4, 0 \leq \gamma \leq 30\text{dB}$ , is:

$$P_b(\gamma) \leq 0.2 \exp \left[ \frac{-1.5}{M-1} \frac{\gamma S(\gamma)}{\bar{S}} \right]. \quad (3.2)$$

Letting  $\Phi = \frac{-1.5}{\ln(5P_b)}$  and rearranging the above in terms of  $M$  we get an expression for the instantaneous constellation size as a function of the received SNR,  $\gamma$  (3.3). It should be noted that this analysis assumes that non-integer values for the constellation size are allowed; while this is possible it is somewhat impractical [15]; however, it provides a foundation for more detailed analysis.

$$M(\gamma) = 1 + \Phi \frac{S(\gamma)}{\bar{S}} \quad (3.3)$$

We wish to maximize the spectral efficiency, with respect to the distribution of the received SNR,  $\gamma$ . Recall the relation between constellation size,  $M$ , for M-QAM and its instantaneous rate [22]:

$$k(\gamma) = \log_2 (M(\gamma)) \quad (3.4)$$

Maximizing (3.4)

$$E[k(\gamma)] = \int_0^{\infty} \left[ 1 + \Phi \frac{S(\gamma)}{\bar{S}} \right] p(\gamma) d\gamma \quad (3.5)$$

with respect to the power constraint

$$\int_0^{\infty} S(\gamma) p(\gamma) d\gamma \leq \bar{S}. \quad (3.6)$$

yields an optimal PAP that is waterfilling in power [9] (3.7). When the channel conditions are poor little to no power is used to compensate for the fading; as the channel quality increases more power is then allocated. This is in contrast to inverse waterfilling where less

power is allocated to the channel when its quality increases. Optimal waterfilling power adaptation can be seen in Figure 3.2.

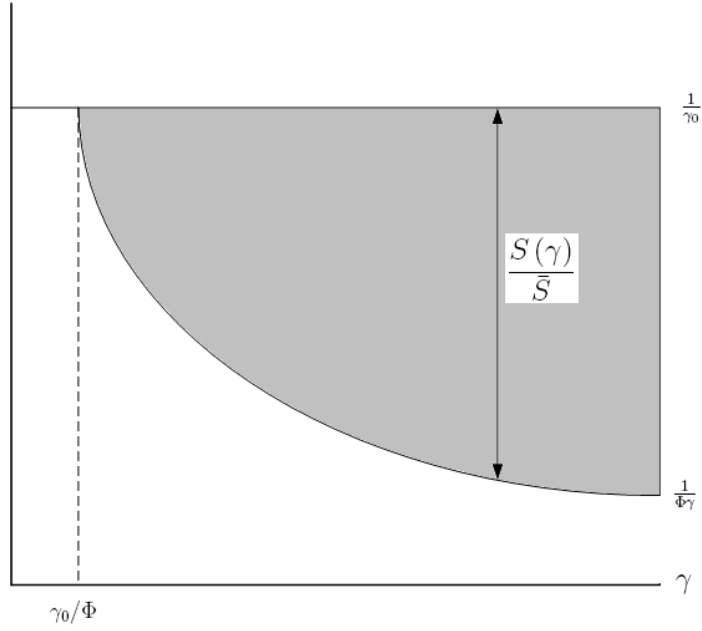


**Figure 3.2:** Waterfilling Power Adaptation Policy

$$\frac{S(\gamma)}{\bar{S}} = \begin{cases} \frac{1}{\gamma_0} - \frac{1}{\Phi\gamma}, & \gamma \geq \gamma_0/\Phi \\ 0, & \gamma < \gamma_0/\Phi \end{cases} \quad (3.7)$$

If we define  $\gamma_\Phi \triangleq \gamma_0/\Phi$  (the cutoff value below which no transmission occurs) we can write the maximum achievable instantaneous rate as:

$$k(\gamma) = \log_2 \left( \frac{\gamma}{\gamma_\Phi} \right), \gamma > \gamma_\Phi. \quad (3.8)$$

The maximum achievable spectral efficiency is then calculated as [22]:

$$\eta = \int_{\gamma_{\Phi}}^{\infty} \log_2 \left( \frac{\gamma}{\gamma_{\Phi}} \right) p(\gamma) d\gamma, \quad (3.9)$$

by substituting Equation (3.7) into (3.6) we can finally obtain the power constraint in terms of  $\gamma_{\Phi}$ :

$$\Phi = \int_{\gamma_{\Phi}}^{\infty} \left( \frac{1}{\gamma_{\Phi}} - \frac{1}{\gamma} \right) p(\gamma) d\gamma. \quad (3.10)$$

As was stated in Section 3.2.1, the analysis in this section presumes that modulators with non-integer values of  $M$  can be developed. However, if instead the value of  $M$  is taken from a set of discrete values we then perform discrete-rate adaptation (please refer to Section 3.2.4).

### 3.2.2 Single Hop Fixed Rate Channel Inversion

By inverting the channel fading alone, giving the appearance to both the transmitter and receiver of a time invariant AWGN channel, we perform channel inversion by the following power adaptation policy

$$\frac{S(\gamma)}{\bar{S}} = \frac{\sigma_{\text{CIFR}}^{\text{SH}}}{\gamma}, \quad (3.11)$$

where  $\sigma_{\text{CIFR}}^{\text{SH}}$  is the single-hop received SNR that can be maintained given the average transmit power constraint in Equation (3.6) using a CIFR (Channel Inversion Fixed Rate) transmission policy [22]. Substituting equation (3.11) into (3.6) and assuming equality we get

$$\int_0^{\infty} \frac{\sigma_{\text{CIFR}}^{\text{SH}}}{\gamma} p(\gamma) d\gamma = 1, \quad (3.12)$$

and thus:

$$\sigma_{\text{CIFR}}^{\text{SH}} = \text{E} \left( \frac{1}{\gamma} \right)^{-1} \quad (3.13)$$

where  $E(\cdot)$  denotes mathematical expectation. We can see that this policy inverts the channel fading for all channel states, regardless of channel conditions (see Figure 3.3). It is because of this reason that channel inversion suffers a large capacity penalty in relation to the Shannon capacity. Because this approach always allows the communication system to transmit information, regardless of the fidelity of the channel this is termed zero-outage capacity [22].

The capacity of channel inversion is [22]

$$C_{\text{CIFR}} = B \log_2 (1 + \sigma_{\text{CIFR}}^{\text{SH}}) = B \log_2 \left[ 1 + \frac{1}{E\left(\frac{1}{\gamma}\right)} \right]. \quad (3.14)$$

### 3.2.3 Single Hop Fixed Rate Truncated Channel Inversion

If we instead endeavor to invert the channel fading only above a certain threshold,  $\gamma_0$ , our new power adaptation policy becomes

$$\frac{S(\gamma)}{\bar{S}} = \begin{cases} \frac{\sigma_{\text{TIFR}}^{\text{SH}}}{\gamma}, & \gamma \geq \gamma_0 \\ 0 & \gamma < \gamma_0 \end{cases}. \quad (3.15)$$

Since transmission occurs only when the received SNR is above a threshold this power adaptation policy is termed TIFR (Truncated Inversion Fixed Rate) [22]. Thus, there exists a distinct probability of outage, i.e. the probability that the received SNR falls below this threshold and no data is transmitted (see Figure 3.5). Given that we know the distribution of the received SNR we can calculate the outage probability as

$$p_{\text{out}} = p(\gamma \leq \gamma_0) = \int_0^{\gamma_0} p(\gamma) d\gamma. \quad (3.16)$$

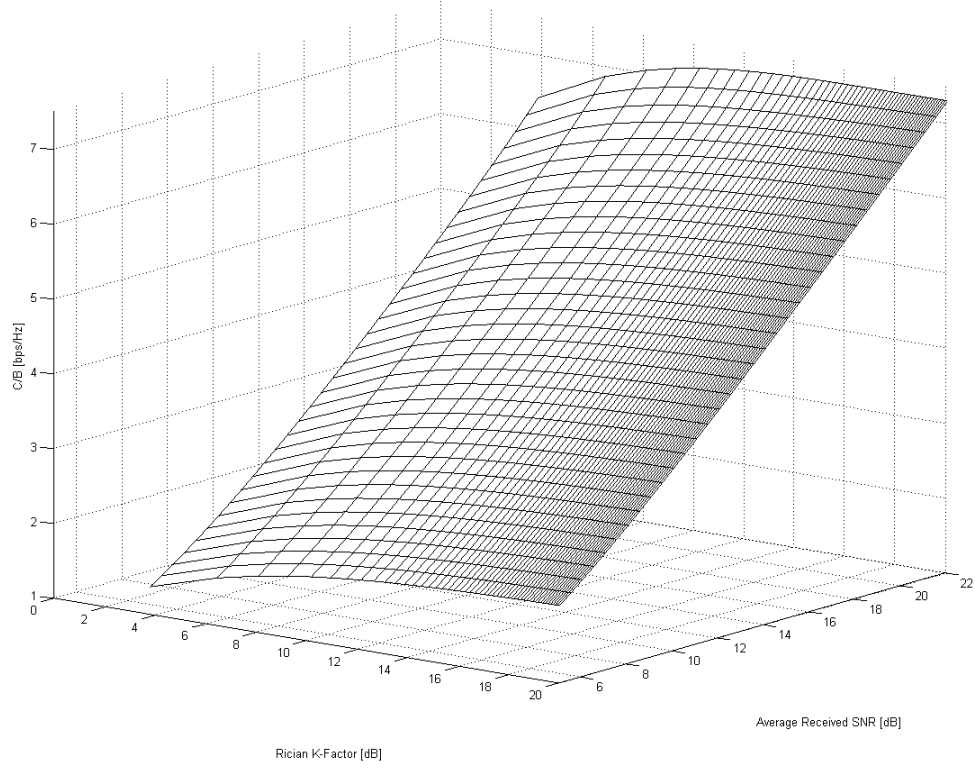


**Figure 3.3:** Spectral Efficiency of Channel Inversion Fixed Rate for a Rician Fading Channel

The outage capacity for a given  $p_{\text{out}}$  and cutoff value,  $\gamma_0$  is

$$C_{\text{out}} = C_{\text{TIFR}} = B \log_2 \left( 1 + \frac{1}{E_{\gamma_0} \left( \frac{1}{\gamma} \right)} \right) (1 - p_{\text{out}}), \quad (3.17)$$

where

$$E_{\gamma_0} \left[ \frac{1}{\gamma} \right] \triangleq \int_{\gamma_0}^{\infty} \frac{1}{\gamma} p(\gamma) d\gamma. \quad (3.18)$$

Although the outage capacity will be less than the Shannon capacity, it is easier to implement and in general has lower complexity [22]. With truncated channel inversion, as it is not necessary to distribute power amongst all of the channel fading states (see Figures 3.4

and 3.5), it is further expected that truncated inversion, will, in general lead to a larger capacity than total channel inversion.

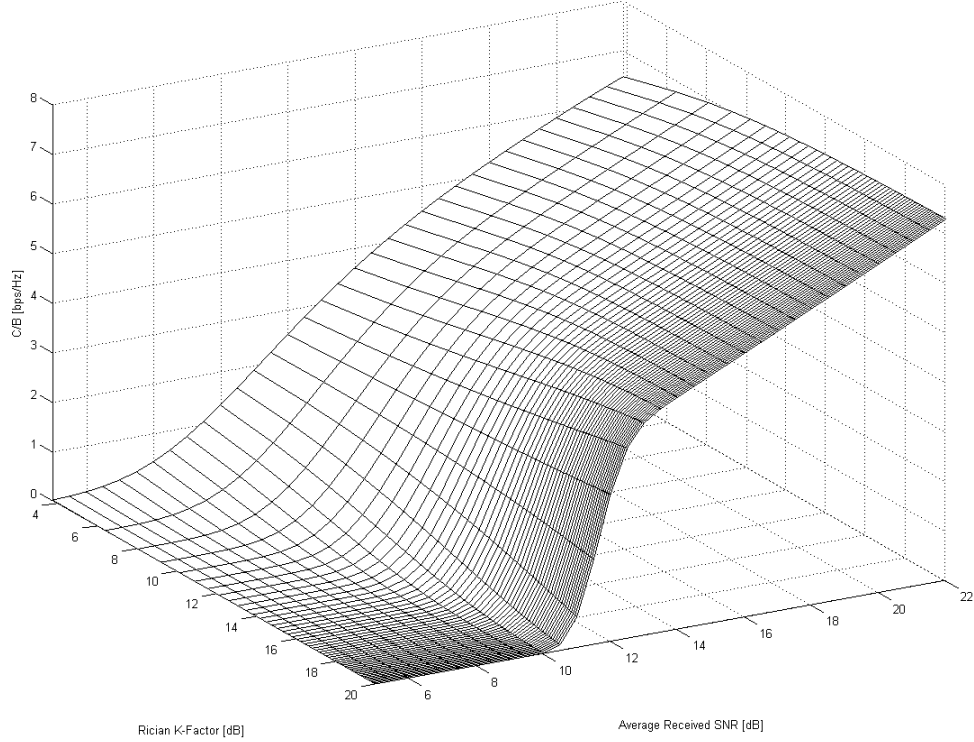


**Figure 3.4:** Spectral Efficiency for Truncated Channel Inversion Fixed Rate for a Rician Fading Channel with  $\gamma_0 = 11.82\text{dB}$  (4QAM Cut-Off)

### 3.2.4 Single Hop Discrete Rate Continuous Power Adaptation

In this case instead of allowing  $M(\gamma)$  to vary over a continuous set, we restrict  $M$  to be chosen from a limited set of constellations  $\mathbf{M}$ . Based on feedback information provided to the transmitter from the receiver, a discrete constellation is chosen from the set  $\mathbf{M} = \{M_j\}_{j=0}^{N-1}$ . When  $M_j = 0$  no data is transmitted for the length of the frame. Discrete rate adaptation partitions the entire SNR range into  $N + 1$  discrete fading regions; and each region is

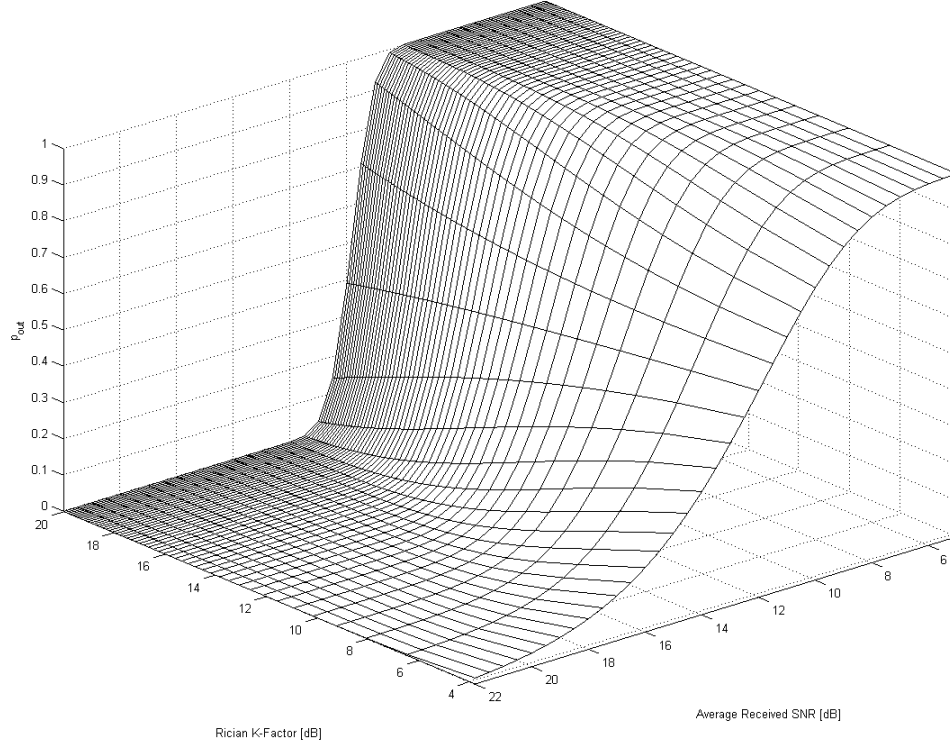


**Figure 3.5:** Outage Probability for Truncated Channel Inversion Fixed Rate for a Rician Fading Channel with  $\gamma_0 = 11.82\text{dB}$  (4QAM Cut-Off)

allocated a constellation of size  $M_j$  [7]. The region assignment that is used in this thesis can be seen in Figure 3.6.

We can calculate the rate associated with each region as  $k_j = \log_2 M_j$ ,  $j = 1, \dots, N - 1$ ,  $k_0 = 0$ . This is similar to mapping particular values of the received SNR to discrete regions  $\Gamma_j = [\gamma_{j-1}, \gamma_j)$ ,  $j = 0, \dots, N - 1$  [9]. It should be noted that, by convention,  $\gamma_{-1} = 0$  and  $\gamma_{N-1} = \infty$ . When the received SNR falls within a given region, the associated signal constellation is used to modulate the transmitted data. If the received SNR falls below a certain threshold ( $\gamma \leq \gamma_0$ ) then no data is transmitted. What remains to be investigated is how these switching thresholds ( $\{\gamma_j\}_{j=0}^{N-2}$ ) are calculated. Rearranging (3.2), and setting

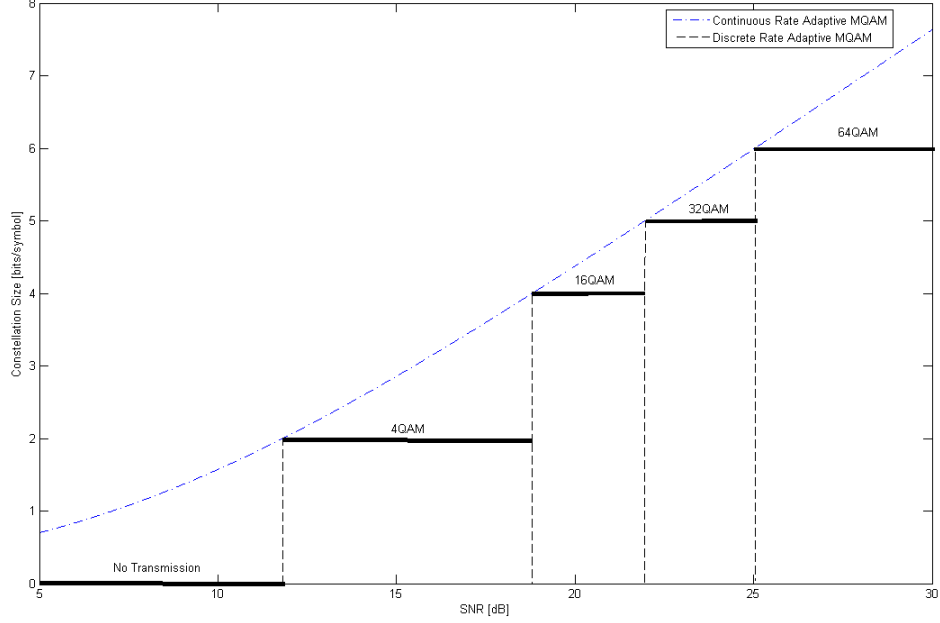


**Figure 3.6:** Constellation Assignment for Continuous And Discrete-Rate Adaptation: with  $M = 4, 16, 32, 64$  and a Target BER of  $10^{-4}$ .

$S(\gamma) = \bar{S}$ , we get an expression for the switching thresholds as a function of the constellation size  $M$ :

$$\gamma_j = \frac{M_j - 1}{\Phi}, j = 0, 1, \dots, N - 2. \quad (3.19)$$

We obtain an expression for the maximum constellation size for a given BER requirement  $P_b$ , as

$$M(\gamma) = \left\lfloor 1 + \Phi \gamma \frac{S(\gamma)}{\bar{S}} \right\rfloor_M \quad (3.20)$$

where  $\lfloor x \rfloor_M$  denotes the largest element in the set  $M$  less than or equal to  $x$ . We can further

express the parameterized spectral efficiency as

$$\eta = \sum_{j=0}^{N-1} k_j \int_{\gamma_j}^{\gamma_{j+1}} p(\gamma) d\gamma. \quad (3.21)$$

In Figures 3.6 and 3.7 we can see the performance of adaptive continuous and discrete modulation as a function of the average received SNR for different wireless environments. We can see that as we increase the number of modulation levels the performance of discrete rate adaptation can come quite close to that of continuous adaptation. Despite a decrease in achievable rate the ease of hardware implementation and lower complexity of discrete adaptation makes it an attractive alternative to continuous adaptation. If we assume an instantaneous BER requirement, and the set of discrete rates  $M$ , we get that the optimal power adaptation policy is given by

$$\frac{S(\gamma)}{\bar{S}} = \frac{h(k_j)}{\gamma}, \gamma_{j-1} \leq \gamma \leq \gamma_j, \quad (3.22)$$

where  $h(k_j) = \frac{2^{k_j}-1}{\Phi}$ . Now we can calculate the optimal switching levels  $\gamma_0^*, \gamma_1^*, \dots$ , and  $\gamma_{N-2}^*$  that maximize the spectral efficiency using the Lagrange equation [9]

$$J(\gamma_0^*, \gamma_1^*, \dots, \gamma_{N-2}^*) = \sum_{j=1}^{N-1} k_j \int_{\gamma_{j-1}^*}^{\gamma_j^*} p(\gamma) d\gamma + \lambda \left( \sum_{j=1}^{N-1} \int_{\gamma_{j-1}^*}^{\gamma_j^*} \frac{h(k_j)}{\gamma} p(\gamma) d\gamma - 1 \right) \quad (3.23)$$

We obtain the optimal region boundaries by successively solving the following equation for  $\gamma_j^*$

$$\frac{\partial J}{\partial \gamma_j^*} = 0, 0 \leq j \leq N-2. \quad (3.24)$$

We thus get that

$$\gamma_0^* = \frac{h(k_1)}{k_1} \rho \quad (3.25)$$

and

$$\gamma_j^* = \frac{h(k_{j+1}) - h(k_j)}{k_{j+1} - k_j} \rho, \quad 1 \leq j \leq N - 2. \quad (3.26)$$

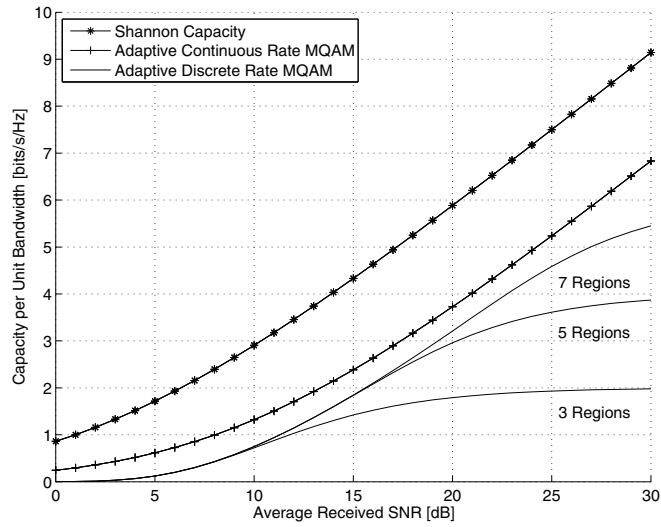
the value for  $\rho$  is determined by the average power constraint, yielding:

$$\sum_{j=1}^{N-1} \int_{\gamma_{j-1}^*}^{\gamma_j^*} \frac{h(k_j)}{\gamma} p(\gamma) d\gamma = 1. \quad (3.27)$$

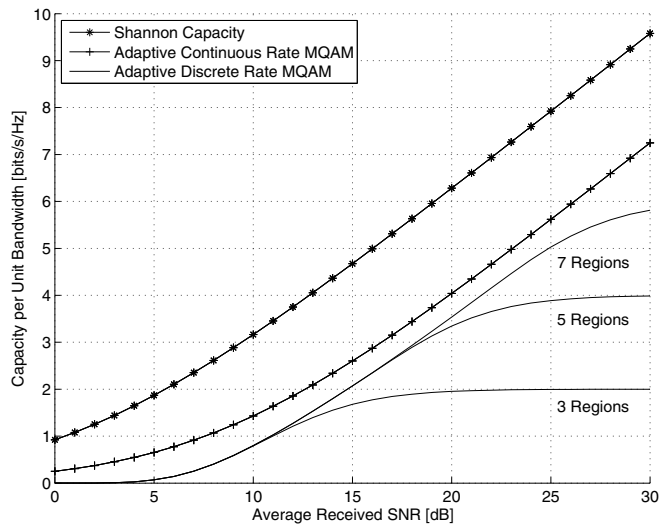
### 3.3 Conclusion

In this chapter we provided the analytical and mathematical framework to enable us to formulate our problem description. The main components of an adaptive communication system were discussed in detail; and their roles in communicating over a wireless fading environment.

With this in mind we will now formulate our problem description which we hope to answer via simulations, in the next chapter.

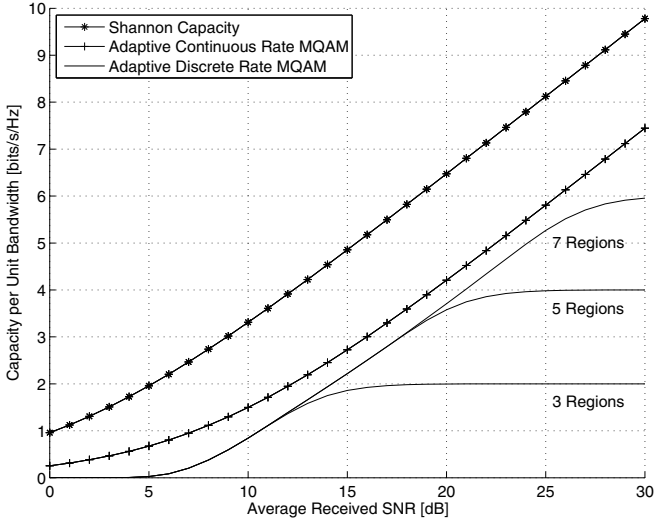


(a)  $P_b = 10^{-4}$ ,  $K = 0$  (Rayleigh)

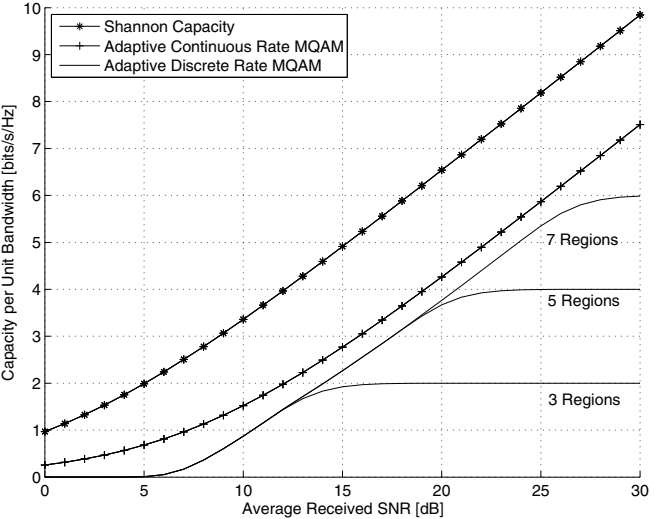


(b)  $P_b = 10^{-4}$ ,  $K = 0$  dB

Figure 3.7: Capacity per Unit Bandwidth Comparison I



(a)  $P_b = 10^{-4}, K = 8\text{dB}$



(b)  $P_b = 10^{-4}, K = 10\text{dB}$

Figure 3.8: Capacity per Unit Bandwidth Comparison II

## Chapter 4

# Link Adaptation for Energy Constrained Networks

### 4.1 Introduction

Work by Goldsmith et al. [20], has established the superiority of adaptive modulation over a fixed communication strategy. However, most of their analysis, especially the work on adaptive modulation focused on point-to-point links; this thesis is an extension of their work to multi-hopping scenarios.

In this chapter we extend Goldsmith's work to encompass scenarios where link adaptation is to be performed in a multi-hopping environment where nodes in the network have stringent energy consumption constraints. We outline in detail the calculation of new power adaptation policies and switching levels for the link adaptive transmission protocols discussed in Chapter 3. With these parameters firmly established we then develop our problem statement which we hope to simulate in the following chapters.

## 4.2 Multi-hop Discrete Rate Continuous Power Adaptation

We are interested in investigating the behavior of multi-hop link adaptation where communication occurs between nodes in a sensor network. In order to control the aggregate power consumption of nodes along the communication path, a total average transmit power constraint,  $\bar{S}$ , is imposed.

Extending the work of Section 3.2.4, specifically, equation (3.27), we introduce a term  $\alpha$  that is parameterized by  $\bar{S}$  (4.1).

$$J(\gamma_0^*, \gamma_1^*, \dots, \gamma_{N-2}^*) = \sum_{j=1}^{N-1} k_j \int_{\gamma_{j-1}^*}^{\gamma_j^*} p(\gamma) d\gamma + \lambda \left( \sum_{j=1}^{N-1} \int_{\gamma_{j-1}^*}^{\gamma_j^*} \frac{h(k_j)}{\gamma} p(\gamma) d\gamma - \alpha \right). \quad (4.1)$$

The value  $\alpha$  is simply the percentage of the total aggregate transmit power that is allocated to a transmitting node (thus  $0 \leq \alpha \leq 1$ ). In this thesis we presume that  $\bar{S} = 1$ . As we will see later, this value may be changed to better suit the needs of the network. The power adaptation policies are dependent on the average transmit power constraint.

For a fixed  $\bar{S}$ , increasing the number of transmitting devices in a communication path will decrease the available transmit power to the incremental nodes. In order to avoid this unfavorable scenario we can further increase the total average transmit power constraint  $\bar{S}$  to a new value:

$$\bar{S}' = \beta \bar{S}, \quad \beta \geq 1. \quad (4.2)$$

By allowing the total average transmit power to vary we are afforded a new degree of freedom with which we our simulation parameters can be varied. Once a new value for the total average transmit power has been selected it is necessary to recalculate the power adaptation policies according to the equations presented in Chapter 3. For the remainder of this thesis we will assume that  $\beta$  and  $\bar{S}$  are set to unity.

Once the total average transmit power constraint has been set we can calculate the

switching levels using the same procedure described by equations (3.24-3.27). This procedure will be explained briefly, below.

If we look at (3.27), modify it using the relation in (3.22), and insert our new parameter  $\alpha$  we get

$$\sum_{j=1}^{N-1} \int_{\gamma_{j-1}^*}^{\gamma_j^*} \frac{S(\gamma)}{\alpha \bar{S}} p(\gamma) d\gamma = 1 \quad (4.3)$$

Rearranging (4.3) and using (3.22) we get

$$\sum_{j=1}^{N-1} \int_{\gamma_{j-1}^*}^{\gamma_j^*} \frac{h(k_j)}{\gamma} p(\gamma) d\gamma = \alpha. \quad (4.4)$$

### 4.3 Multi-hop Fixed Rate Channel and Truncated Inversion

Extending the equations presented in Section 3.2.2, a similar procedure to Section 4.2 is performed; whereby the introduction of  $\alpha$ , a variable parameterized by the average transmit power constraint  $\bar{S}$  facilitates the analysis of multi-hop (MH) fixed-rate channel inversion. Specifically, looking at equations (3.11) and (3.12), by introducing  $\alpha$  we get an expression involving the modified transmit power constraint:

$$\int_0^\infty \frac{S(\gamma)}{\alpha \bar{S}} p(\gamma) d\gamma = 1, \quad (4.5)$$

which is equivalent to:

$$\int_0^\infty \frac{\sigma_{\text{CIFR}}^{\text{MH}}}{\gamma} p(\gamma) d\gamma = \alpha. \quad (4.6)$$

Rearranging the above equation, we get:

$$\sigma_{\text{CIFR}}^{\text{MH}} = \frac{\alpha}{\text{E}\left(\frac{1}{\gamma}\right)}, \quad (4.7)$$

$$\sigma_{\text{CIFR}}^{\text{MH}} = \alpha \sigma_{\text{CIFR}}^{\text{SH}}. \quad (4.8)$$

As the analysis for both of these fixed transmit-power policies are very similar, for the sake of brevity, they will be analyzed together. The analogue of equation (4.7) for truncated inversion is:

$$\sigma_{\text{TIFR}}^{\text{MH}} = \frac{\alpha}{\mathbb{E}_{\gamma_0} \left( \frac{1}{\gamma} \right)}, \quad (4.9)$$

$$\sigma_{\text{TIFR}}^{\text{MH}} = \alpha \sigma_{\text{TIFR}}^{\text{SH}}. \quad (4.10)$$

#### 4.4 Problem Formulation

For the sake of simplicity we start with a relatively simple network that consists of a source, relay, and destination (Figure 4.1). It is further assumed that the channel between the source and relay is different from that of the relay and destination. It is assumed that the relay node has no information of its own to add and that it simply forwards the information that it receives from the source to the destination.

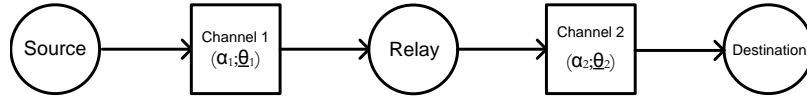


**Figure 4.1:** Linear Relay Network with 1 Relay Node

The achievable rate for this line network is constrained by the poorest link. If we denote  $\bar{r}_{1,2}(\alpha_1; \underline{\theta}_1)$  as the achievable rate between the nodes 1 and 2 we get:

$$\bar{r}_{1,3}(\alpha; \underline{\theta}) = \min\{\bar{r}_{1,2}(\alpha_1; \underline{\theta}_1), \bar{r}_{2,3}(\alpha_2; \underline{\theta}_2)\}, \quad (4.11)$$

where nodes 1, 2 and 3 represent the source, relay, and destination, respectively, and  $\underline{\theta}$  is a vector of parameters known to the  $i$ th transmitter and corresponding receiver. For a general

relay network, consisting of  $N$  nodes in the communication path, we define  $\underline{\theta}$  as:

$$\underline{\theta}_i = \{K_i, P_t^i, f_d^i, P_b\}, \quad 1 \leq i \leq N - 1, \quad (4.12)$$

where  $K_i$  is the Rician K-factor between nodes  $i$  and  $i + 1$ ,  $P_t^i$  is the instantaneous transmit power of node  $i$ ,  $f_d^i$  is the Doppler frequency perceived by the receiver node ( $i + 1$ ), and  $P_b$  is our instantaneous bit-error requirement.

Looking at Figure 4.1, the problem lies in choosing the optimal values for  $\alpha_1$  in order to maximize  $\bar{r}_{1,3}$  (since  $\alpha_2$  will be uniquely determined by  $\alpha_1$  in this case). The optimal values for  $\alpha_1$  and  $\alpha_2$  will be based on the collocated channel distributions and out bit-error requirement. A total average transmit power constraint over the whole network can be ensured by appropriate selection of  $\alpha_1, \alpha_2$ , i.e.,

$$\sum_{i=1}^2 \alpha_i = \bar{S}. \quad (4.13)$$

#### 4.4.1 Problem Definition

We now formulate our problem for a more general linear relay network consisting of  $N$  nodes:

**Find**  $\{\alpha_i\}_{i=1}^{N-1}$  that maximizes  $\bar{r}_{1,N}$  such that  $\sum_{i=1}^{N-1} \alpha_i = \bar{S}$ . More succinctly:

$$\{\alpha_i^*\}_{i=1}^{N-1} = \arg \max_{\alpha_i \in \mathbb{R}, \sum_i \alpha_i = 1} \Psi(\alpha; \underline{\theta}) \quad (4.14)$$

we define  $\Psi(\cdot; \cdot)$  as

$$\Psi(\alpha; \underline{\theta}) = \min \{\bar{r}_{1,2}(\alpha_1; \underline{\theta}_1), \bar{r}_{2,3}(\alpha_2; \underline{\theta}_2), \dots, \bar{r}_{i-1,i}(\alpha_i; \underline{\theta}_i), \dots, \bar{r}_{N-1,N}(\alpha_N; \underline{\theta}_N)\} \quad (4.15)$$

where  $\underline{\theta}$  is defined as above,  $\bar{r}_{1,2}(\alpha_1; \underline{\theta}_1)$  is the rate between nodes 1, and 2 with transmit power  $\alpha_1$ . This problem amounts to finding the  $(N - 1)$ -tuple that maximizes  $\bar{r}_{1,N}$ . This is

akin to selecting the optimal power distribution among the collocated channels.

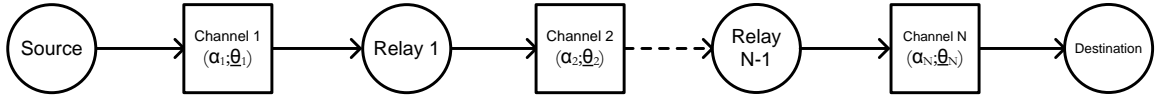


Figure 4.2: Linear Relay Network with N Nodes

## 4.5 Conclusion

In this chapter we extended the seminal works of Goldsmith et al., specifically the work on link adaptation, to include multi-hopping scenarios where we place a total average transmit power constraint on all of the nodes in a communication path. This extension allows us to simulate the rate performance and investigate the problem power allocation amongst relay terminals in a relay network. In this light we were able to formulate the problems which we hope to address and elucidate in the following chapters.

In the next chapter we will outline and discuss in detail the simulation framework that we have utilized in this thesis. Furthermore, the main components of a bit-level simulator used to model the rate performance of several rate adaptive protocols over an energy constrained relay network will be investigated.

## Chapter 5

# Simulation Results

### 5.1 Introduction

In this chapter we present our simulation results. Our simulation methodology is presented and pertinent simulation parameters and caveats are discussed. We further present a flowchart of our simulator in order to clarify and establish the validity of our simulation assumptions. Based on the framework established in Chapters 2 and 3 we produce the salient parameters and figures presented therein. In this light we finally present a comparison between a number of different link-adaptation policies for energy constrained linear relay networks.

### 5.2 Simulation Objectives

Our objective was to see how energy constrained link adaptation performs in a wireless sensor network. Specifically we wanted to investigate the behavior of a sensor network when power is distributed optimally, based on *a priori* knowledge of the channel distributions. To this effect a bit-level simulator was developed as a means of testing the efficacy and performance of joint rate and power adaptation for energy constrained wireless networks.

### 5.2.1 Simulation Parameters

We now discuss the parameters which we have included in our simulator. As there are a number different types of wireless sensor networks, a significant challenge lies in choosing a realistic set of parameters for our system. Table 5.1 lists the main parameters of interest.

**Table 5.1:** Simulation Parameters

Parameter	Description	Value
$f_d$	Doppler Frequency	0-10 Hz
$n$	Path-Loss Exponent	3
$K$	Rician K-Factor	0-20 dB
$N_0$	Noise PSD	$10^{-9}$ W/Hz
$B$	Bandwidth of System	250 kHz
$T_s$	Symbol Time	$4 \mu\text{s}$
$P_t$	Transmit Power	10-25 mW
$P_b$	QoS BER requirement	$10^{-4}$
$\bar{\gamma}$	Average SNR per symbol	20 dB
$M$	Set of MQAM Constellations	{4,16,32,64}
$\{\gamma_4, \gamma_{16}, \gamma_{32}, \gamma_{64}\}$ QAM	MQAM Switching Levels	{11.82,18.81,21.96,25.04} dB
$L$	Symbols per Frame	100
$N_F$	Number of Frames	$1.0 \times 10^4$
$N_{it}$	Number of Simulation Iterations	50
$N_r$	Number of Relays	1-2

### 5.2.2 Simulation Assumptions

As with any simulation environment there is an inherent tradeoff between accuracy and complexity. Our objective is to model the communication system as accurately as possible while minimizing the number of communication blocks necessary to yield accurate results.

The following is a list of assumptions we have made about our system:

- There is an estimation delay between the receiver and transmitter of one frame
- The transmitter and receiver both have perfect knowledge of the CSI
- Ideal coherent detection is performed at the receiver

- The feedback channel introduces no error in relaying information to the transmitter
- We place a BER requirement on a per link basis, thus ignoring the effect of error propagation amongst relay nodes in the network
- During the duration of a communication session between two nodes the relative distance they move is small in comparison to the distance between the nodes
- TDMA (Time Division Multiple Access) MAC scheme was used for all nodes at all levels in the network
- There is perfect time synchronization amongst the nodes which facilitates conflict-free medium access
- Packets are generated at an appropriate rate for reliable transmission and their arrival process is independent for each user
- Nodes are aware of the locations of other nodes in the network at all times

### 5.3 Simulation Model, Methodology, and Metrics

In this section we detail the simulation model used to evaluate the performance of multi-hop link adaptation in a relay network. MATLAB was used to conduct all of the simulations in this thesis.

The simulator was responsible for:

- Physical Layer Communication:
  1. Generation of data to be transmitted
  2. Modulation and power adaptation
  3. Bit-level transmission of modulated data
  4. Demodulation of transmitted data

- Multiple Access Control:
  1. Coordinating and ensuring fair access to the medium
  2. Time synchronization

The simulator was developed to afford these two layers a certain amount of transparency. Thus the MAC scheme could be developed independently and in a modular fashion. As the objective of this study mainly focused on Physical Layer behavior, it was deemed sufficient to develop a rather simple medium access protocol in order to test our simulations in a multiple-access environment.

### 5.3.1 Methodology

To establish the veracity of the work presented in this thesis we now outline how our simulator was used to produce the results that are presented in this chapter. We will first take a brief look at the main components in our network simulator and their functions (Figure 5.1).

Before we can communicate using any form of link adaptive protocol, there are a number of parameters which must be calculated beforehand. This is the main function of the **Parameter Preprocessor** in Figure 5.1. For a given transmission policy, the **Parameter Preprocessor** accepts a vector of parameters, determined by the application's QoS requirements, which it then uses to calculate the switching levels and corresponding power adaptation policies. Our thesis simulates the rate performance of the following transmission protocols:

- Adaptive Discrete Rate Continuous Power (Sections 3.2.4 and 4.2)
  - **Switching Levels** - determined by (3.26)
  - **Power Adaptation Policy** - determined by (3.22 and 4.2)
- Truncated Inversion Fixed Rate  $\{4,16,32\}$ QAM (Sections 3.2.3 and 4.3)

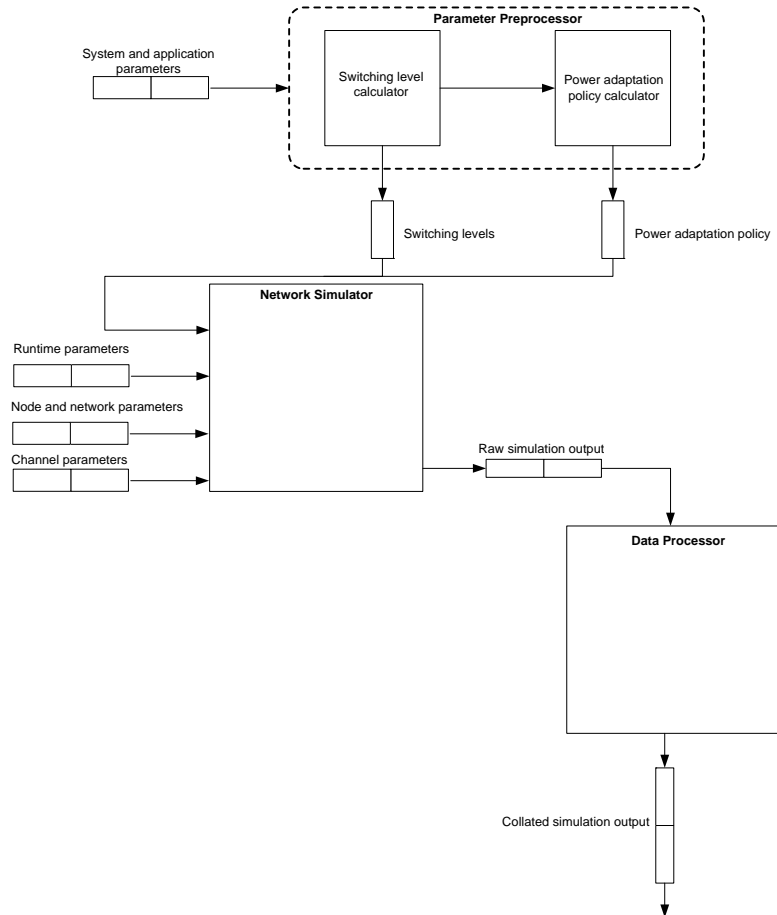


Figure 5.1: Network Simulator Components

- **Switching Levels** - determined by (3.19)
- **Power Adaptation Policy** - determined by (3.15 and 4.9)
- Channel Inversion Fixed Rate 4QAM (Sections 3.2.2 and 4.3)
  - **Switching Levels** - determined by (3.19)
  - **Power Adaptation Policy** - determined by (3.11 and 4.7)

The Parameter Preprocessor accepts the following vector of parameters:

**System and application parameters** =  $\{p(\gamma), \bar{\gamma}, M, P_b\}$ .

Once the switching levels and power adaptation policies have been calculated we can now simulate the wireless transmission of data. The **Network Simulator** is responsible for simulating the transmission of data over the network. It has a number of different inputs which we will now clarify. A flowchart, outlining the main functions of the **Network Simulator** is given in Figure 5.3.

The **Runtime Parameters** is a set of values which determine the characteristics of a typical communication session and the duration of a simulation session:

**Runtime parameters** =  $\{L, N_f, N_{it}\}$ . The **Node and network parameters** input tells the **Network Simulator** the number of nodes (source, relays, destination) in the network. It accepts, as inputs:

**Node and network parameters** =  $\{P_t, N_r, B\}$ . The **Channel parameters** input determines the characteristics of the wireless channel over which data is to be transmitted. It accepts, as inputs:

**Channel parameters** =  $\{K, f_d, n, N_0, d, d_0, \kappa\}$ .

We will discuss the function of the **Data Processor** in Section 5.3.2.

### Simulation of the Physical Layer

Referring to our system model (Figure 5.2) in conjunction with the simulator flowchart (Figure 5.3) gives an overview of the main steps involved in a link-adaptive communication session.

- The source generates data symbols  $s[i]$  at a constant rate of  $R_s$  from a uniform distribution. Once the data has been generated it is then packaged into a frame of  $L$  symbols. This frame of symbols is then passed on to the modulator which transforms the signal into an appropriate representation for transmission. Modulation is performed on a per-symbol basis; given our set of constellations  $M$  (please refer to

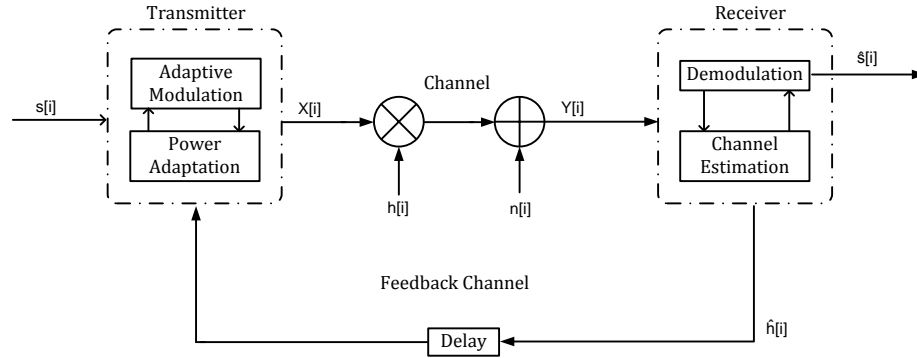


Figure 5.2: Adaptive Feedback System Model

Table 5.1 for a list of simulation parameters) each frame can contain anywhere from 200-600 bits. The decision as to which modulation level to use and at what power the signal should be transmitted is based on the communication strategy employed by the system.

- Once the data has been modulated, based on the fading estimate from the previous frame, an appropriate power level is then selected in accordance with (2.2). The threshold calculations and Power Adaptation Policy (PAP) generation for the different transmission schemes discussed in will be discussed in further detail in Sections 5.4.1 and 5.5.1.
- The wireless channel introduces large and small-scale fading effects as well as additive noise to the transmitted signal  $X[i]$ . Each block of  $L$  symbols sees the channel as flat-fading. The time-varying channel gain was simulated using the model presented in Section 2.2.5. Each QAM symbol in a frame was multiplied by its corresponding block-fading coefficient, after which additive noise was superimposed on a per-symbol basis.
- Once the data  $Y[i]$  is received it is demodulated and the channel gain estimate  $\hat{h}[i]$  is

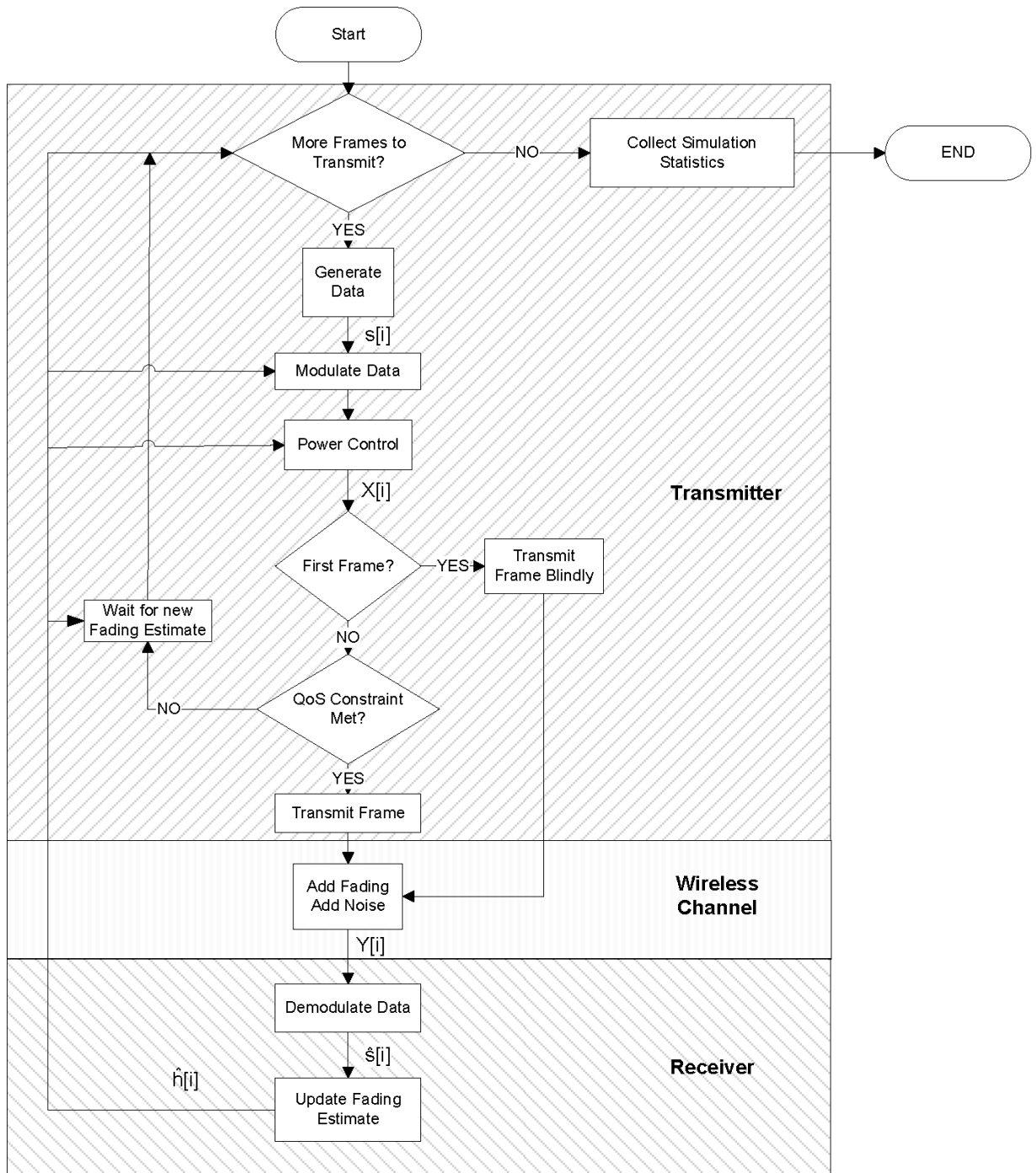


Figure 5.3: Simulator Flowchart for One Communication Session

then fed back to the transmitter so that it can adapt its transmission parameters in accordance with the behavior of the channel over the previous frame.

### 5.3.2 Effective Rate and Simulation Output

The main metric we used to compute the performance of each link-adaptive scheme is effective rate. For a given set of QAM constellations,  $\mathbf{M} = \{M_j\}_{j=0}^{N-1}$ , a total number of transmitted frames,  $N_{total} > N_F$  (referring to Table 5.1), and that for one communication session we use each modulation level  $N_{M_j}, j = 0, 1, \dots, N - 1$ , times we can calculate the effective rate between two transmitting nodes pairs  $(i, i + 1)$  as:

$$\bar{r}_{i,i+1} = \frac{1}{N_{total}} \sum_{j=0}^{N-1} N_{M_j} \log_2 M_j, \quad (5.1)$$

where  $N_{total} = \sum_{j=0}^{N-1} N_{M_j}$ . It should be noted that for this thesis, the effective rate,  $\bar{r}$ , is calculated numerically. We also have included our simulation output in Appendix A. The values stored in each of the tables represent the averaged simulation output for a point-to-point communication using the link adaptive transmission protocols described in Chapter 3.

We can then calculate the achievable rate for a multi-hop network by selecting values from the tables such that  $\sum_i \alpha_i = \bar{S}$  (recall that  $\bar{S} = 1$  as per Section 4.2). The tables in Appendix A serve as inputs to our **Data Processor** (as look-up tables) which enable it to perform rate calculations and to obtain the power allocation values for our relay network.

Figure 5.4 is a sample output after an adaptive discrete rate continuous power communication session. We can see that the modulation levels closely track the channel SNR.

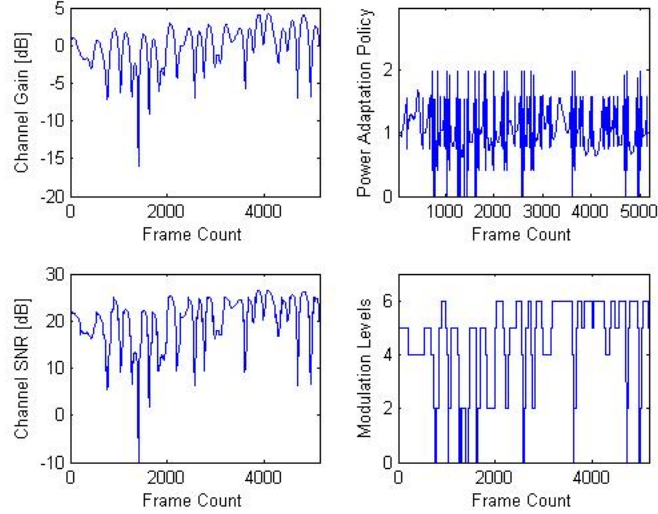


Figure 5.4: Simulator Output

## 5.4 Fixed Rate and Truncated Channel Inversion

Before we simulated a communication scenario using the communication strategies herein it was first necessary to generate the power adaptation policies and switching levels in accordance with Sections 3.2 and 4.1.

### 5.4.1 Received SNR and Switching Levels for Fixed Rate and Truncated Channel Inversion

#### Channel Inversion Fixed Rate

Recall that  $\sigma_{\text{CIFR}}^{\text{SH}}$  is the received SNR that can be maintained given (3.6). Integrating over the PDF of the received SNR for a Rician channel, we obtain:

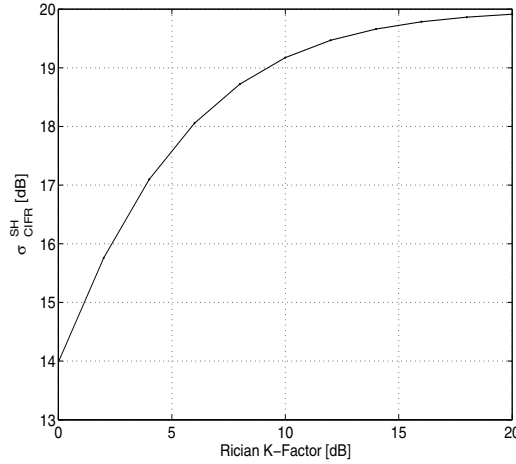


**Figure 5.5:** Received SNR that can be maintained for Channel Inversion Fixed Rate

We can see from Figure 5.5 in conjunction with the cutoff values in Table 5.1 that if we transmit using only 4QAM we can ensure that our QoS requirement is met for all possible values of the Rician K-factor. However, if we choose to use 16QAM we can only transmit reliably if the K-factor is greater than or equal to 10dB. Given that the cutoffs for both 32 and 64QAM are greater than the received SNR that can be provided using channel inversion fixed rate (CIFR) we can not transmit information reliably using these transmission strategies.

Although it was stated in Section 3.2.2 that CIFR inverts the channel fading in all states, regardless of the fidelity of the channel, for our simulations it was necessary to introduce a cut-off value to ensure that our BER QoS requirement was met. This is due to the fact that the analysis presumes that we are always transmitting at the maximum available power; however, when we decrease the transmit power we also increase the probability that transmitted information will be received in error, thus compelling us to introduce the cut-off.

Truncated Inversion Fixed Rate

The received SNRs that can be maintained for this policy are plotted in Figure 5.8 next to their respective outage probabilities. For TIFR-4/32QAM the received SNR is positively correlated to the Rician K-factor. However, this situation is reversed for TIFR-16QAM. The aforementioned behavior is highly dependent on the cut-offs and the behavior of the PDF of the received SNR. Referring to Figure 5.7 we can see that for a given cut-off in the [0-19] dB range the outage probability decreases as the Rician K-factor increases. However, when the threshold is in the [20-25] dB range the outage probability increases as the K-factor increases. Recalling that truncated inversion fixed rate inverts the channel fading only above a given threshold we can see how, in general, a larger cut-off leads to an increase in the received SNR that can be maintained. A larger cut-off means that this inversion policy can distribute its available power more favorably among fewer fading states. Looking at Figure 5.6(a) we see that as the Rician K-Factor increases, the variance of  $E_{\gamma_0}$  decreases significantly - meaning the power is more densely distributed around its mean.

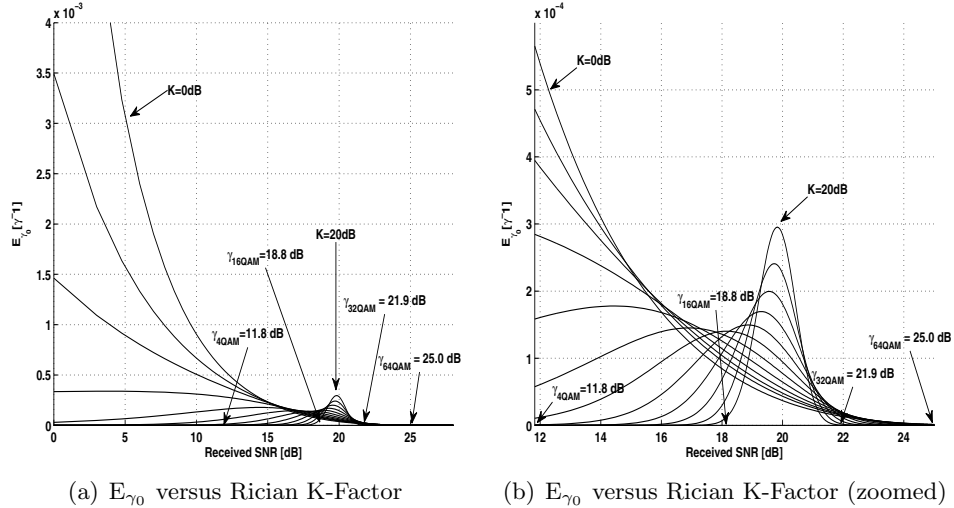


**Figure 5.6:**  $E_{\gamma_0}$  behavior and Switching Levels for Truncated Inversion Fixed Rate

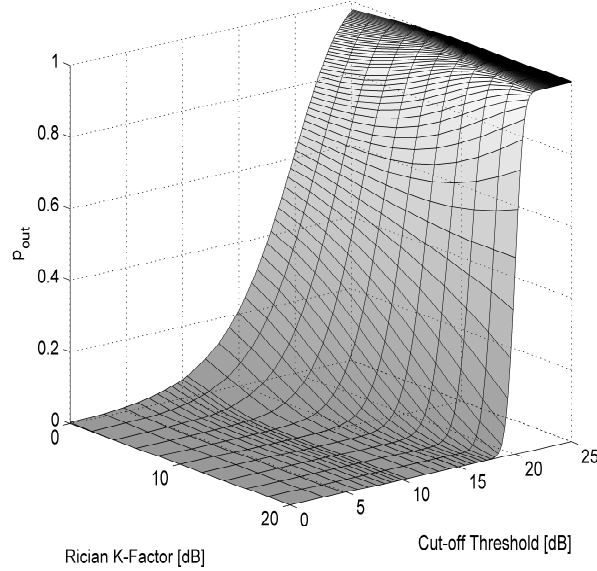


**Figure 5.7:**  $p_{out}$  and Cut-Off Relationship for Truncated Inversion Fixed Rate

Looking at the cut-off for TIFR-16QAM ( $\gamma_{16QAM}$ ), in Figure 5.6(a), we can see that when the K-factor is small the the received SNR is more evenly distributed among the fading states; given the relatively large SNR required for TIFR-16QAM, in poor channels the percentage of time the received SNR is above this threshold is small. However, as the channel quality increases more power must be distributed to a larger number of fading states which results in a decrease in the received SNR that can be maintained using this inversion policy. We thus expect to see a decrease in performance for TIFR-16QAM as the channel quality increases.

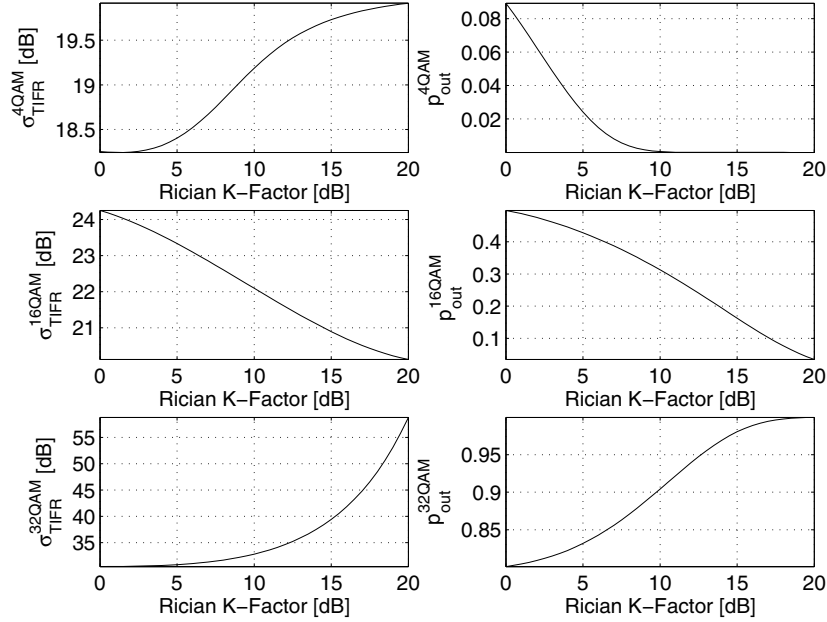


Figure 5.8: Outage Probability and Achievable SNR for Truncated Inversion Fixed Rate

#### 5.4.2 Power Adaptation Policies for Fixed Rate and Truncated Channel Inversion

Once the values for the received SNR have been calculated the next step is to generate the power adaptation policies. Using the equations presented in Section 4.3 we created power adaptation policies for different Rician channels (Figures 5.9 and 5.10).

#### 5.4.3 Effective Rate and Optimal Power Allocation for Fixed Rate and Truncated Channel Inversion over a Linear Relay Network

We now present the results of the problem description detailed in Section 4.4. To ensure the accuracy of the results each simulation was run 50 times, each communication session required the transmission of  $10^4$  frames each at varying power levels. Our average transmit power was varied from  $0.1\bar{S} - 0.9\bar{S}$  at a step-size of  $0.025\bar{S}$ . After all the data was generated it was then averaged to yield our final results.

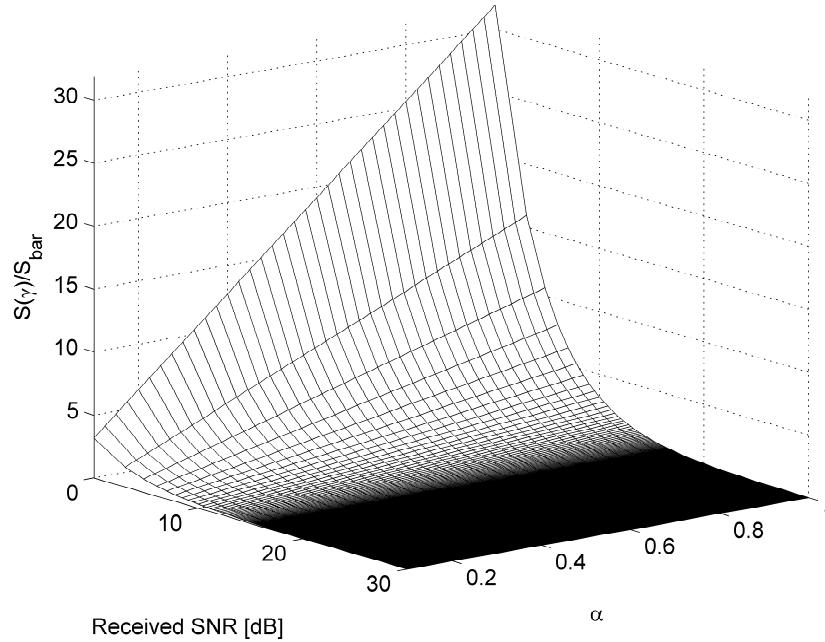


Figure 5.9: Power Adaptation Policy for Channel Inversion Fixed Rate-4QAM

### Figure Descriptions

Before we present our results we will take a moment to explain them.

### Achievable rate for a two link relay network

These figures were generated as follows:

Given a transmission protocol (TIFR-4QAM, CIFR-4QAM, ADR, etc.) we fixed the K-factor of the first channel, the K-factor of the second channel was taken from the set  $K_2 = \{0, 10, 20\}$ dB. A matrix of power allocation values that satisfy (4.14) was generated and populated with the corresponding rate values taken from the tables in Appendix A. The overall achievable rate of the relay network was then calculated as the minimum of the two rates. An example of this procedure is given in Table 5.2. In this example, we are transmitting using adaptive discrete rate modulation and the K-factors of the two channels

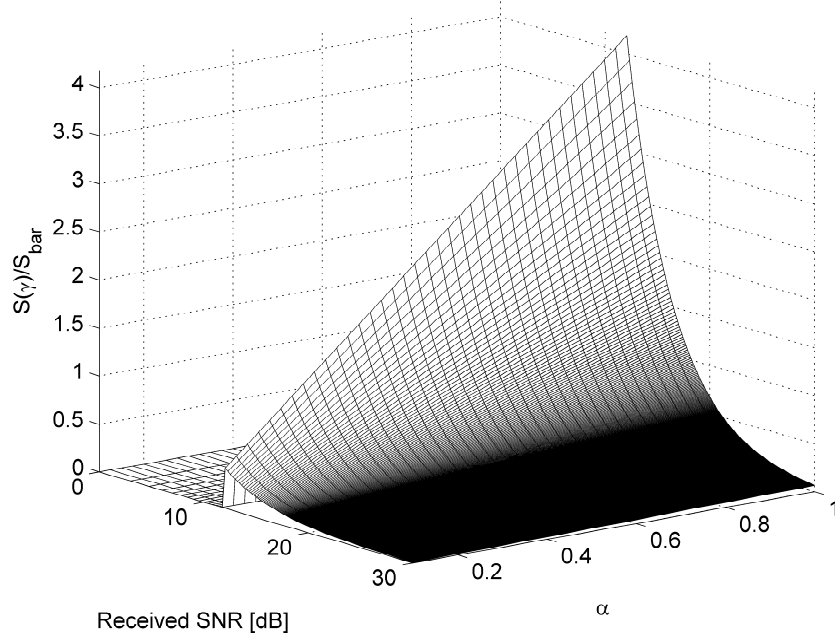


Figure 5.10: Power Adaptation Policy for Truncated Inversion Fixed Rate-4QAM

are (0dB,20dB), respectively. After this was done, the K-factor of the first channel was then changed and this procedure was repeated.

Given the large number of figures generated in this thesis we now provide a table that helps to reference the figures in question.

### Optimal Power Allocation for a Two Link Relay Network

In these figures, we allowed the K-factor of the second channel to vary (while keeping the first K-factor fixed) over the set  $K_2 = [0 - 20]$ dB with a step size of 2dB. A matrix of power allocation values was generated and rate data from Appendix A was used in order to calculate the power allocation values  $(\alpha_1, \alpha_2)$ . These values were calculated by following a similar procedure used to generate the aforementioned achievable rate data. Given the K-factors of the two channels and a transmission protocol we are able to uniquely identify the power allocation values that maximize the overall rate of the network. Each point in

**Table 5.2:** Rate Performance for Adaptive Discrete Rate Over a Two Link Relay Network

$\alpha_1$	$\alpha_2$	$K_1=0\text{dB}$	$K_2=20\text{dB}$	min. Rate
<b>0.100</b>	<b>0.900</b>	1.710	4.474	1.710
<b>0.125</b>	<b>0.875</b>	1.804	4.425	1.804
<b>0.150</b>	<b>0.850</b>	1.891	4.374	1.891
<b>0.175</b>	<b>0.825</b>	1.975	4.332	1.975
<b>0.200</b>	<b>0.800</b>	2.031	4.281	2.031
<b>0.225</b>	<b>0.775</b>	2.109	4.237	2.109
...	...	...	...	...
<b>0.775</b>	<b>0.225</b>	3.478	3.579	3.478
<b>0.800</b>	<b>0.200</b>	3.480	3.568	3.480
<b>0.825</b>	<b>0.175</b>	3.485	3.558	3.485
<b>0.850</b>	<b>0.150</b>	3.523	3.519	3.519
<b>0.875</b>	<b>0.125</b>	3.558	3.505	3.505
<b>0.900</b>	<b>0.100</b>	3.593	3.463	3.463

**Table 5.3:** Achievable Rate Figures for a Two Link Relay Network

Transmission Protocol	Applicable Figures
CIFR-4QAM	5.11
TIFR-4QAM	5.14
TIFR-16QAM	5.17
TIFR-32QAM	5.20
ADR	5.26

the graphs represent the optimal power allocation values between the two channels.

In order to clarify our data analysis, we've provided the **MATLAB** source code of the algorithm used to calculate the optimal power allocation for a two link relay network (please refer to Appendix B).

### **Optimal Power Allocation for a Three Link Relay Network**

In these figures, we fixed the K-factors of all three channels and looked at the rate performance when an extra node was added to the network. Each of the sub-figures correspond to a specific set of channel distributions. The optimal power allocation values for the three channels can be determined from the figure. The minimum effective rate for power allocation values which do not satisfy the average transmit power constraint are set to zero.

**Table 5.4:** Optimal Power Allocation Figures for a Two Link Relay Network

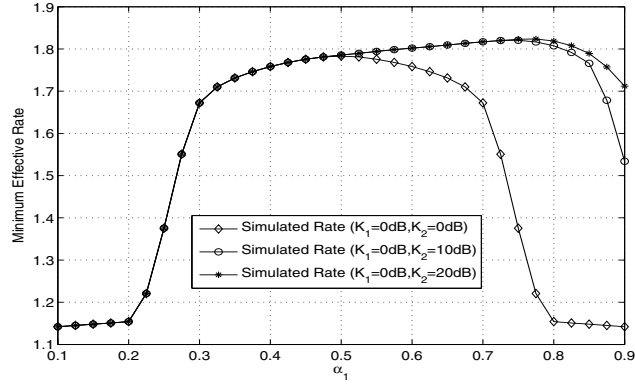
Transmission Protocol	Applicable Figures
CIFR-4QAM	5.12
TIFR-4QAM	5.15
TIFR-16QAM	5.18
TIFR-32QAM	5.21
ADR	5.27

The algorithm used to calculate the optimal power allocation for a three link relay network is provided in Appendix B.

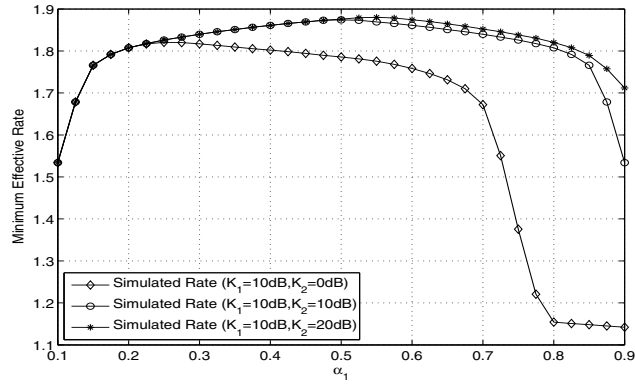
**Table 5.5:** Optimal Power Allocation Figures for a Three Link Relay Network

Transmission Protocol	Applicable Figures
CIFR-4QAM	5.13
TIFR-4QAM	5.14
TIFR-16QAM	5.19
TIFR-32QAM	5.22
ADR	5.27

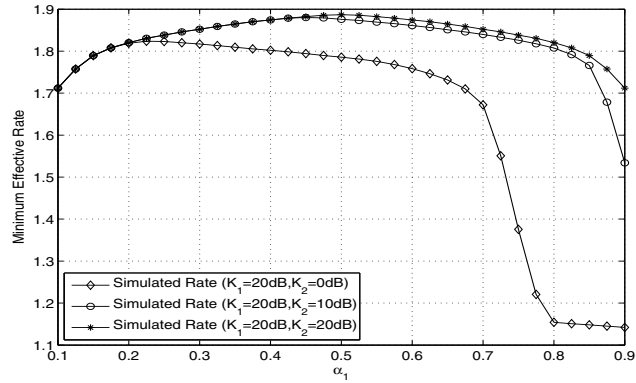
## Chapter 5. Simulation Results



(a) Rician Channels:  $K_1 = 0\text{dB}$ ,  $K_2 \in \{0, 10, 20\}\text{dB}$



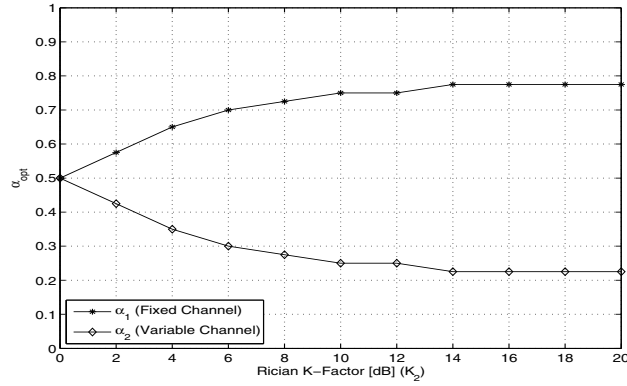
(b) Rician Channels:  $K_1 = 10\text{dB}$ ,  $K_2 \in \{0, 10, 20\}\text{dB}$



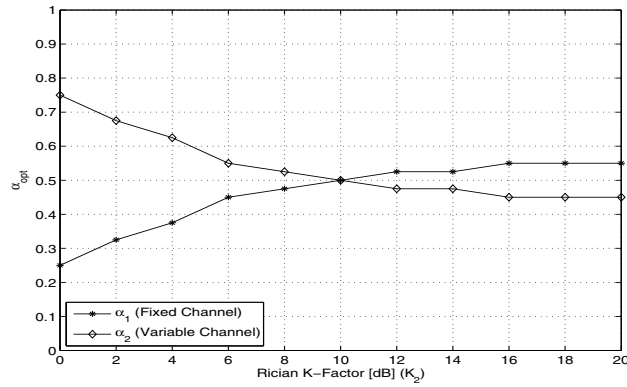
(c) Rician Channels:  $K_1 = 20\text{dB}$ ,  $K_2 \in \{0, 10, 20\}\text{dB}$

**Figure 5.11:** Channel Inversion Fixed Rate-4QAM: Achievable Rate For a Two Link Linear Relay Network with Variable Power Constraints

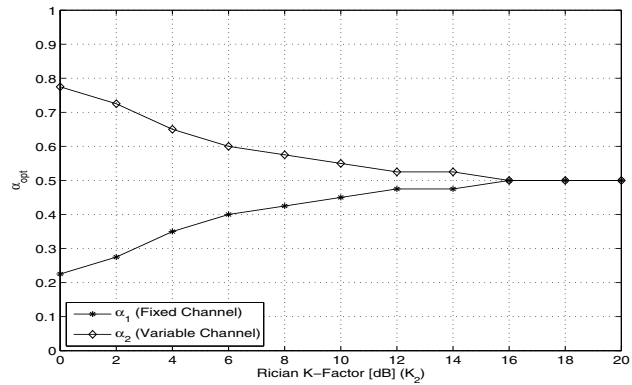
## Chapter 5. Simulation Results



(a) Rician Channels:  $K_1 = 0\text{dB}$ ,  $K_2 \in [0 - 20]\text{dB}$

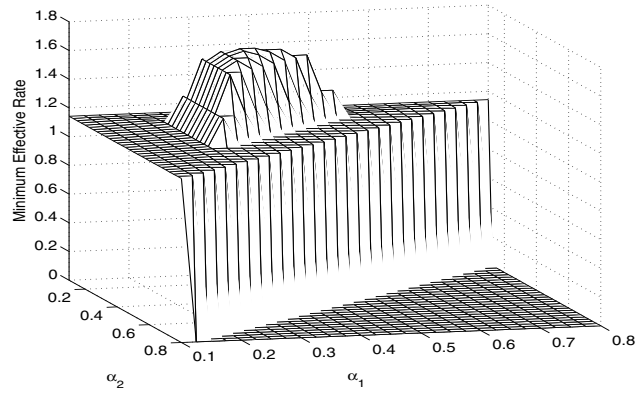


(b) Rician Channels:  $K_1 = 10\text{dB}$ ,  $K_2 \in [0 - 20]\text{dB}$

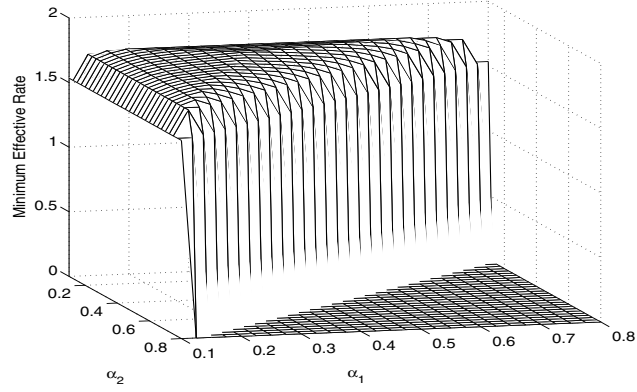


(c) Rician Channels:  $K_1 = 20\text{dB}$ ,  $K_2 \in [0 - 20]\text{dB}$

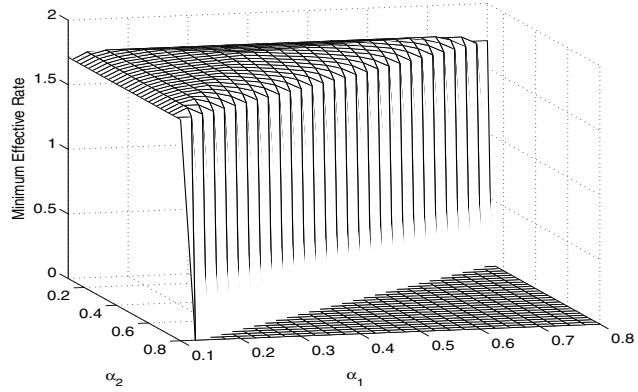
**Figure 5.12:** Channel Inversion Fixed Rate-4QAM: Optimal power allocation values for a two-link linear relay network with variable power constraints



(a) Rician Channels:  $K_1 = 0\text{dB}, K_2 = 0\text{dB}, K_3 = 0\text{dB}$



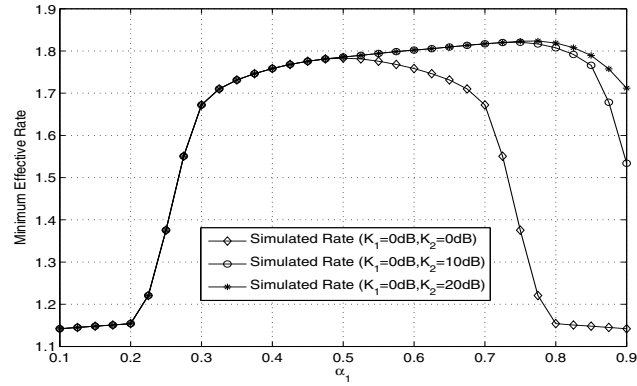
(b) Rician Channels:  $K_1 = 10\text{dB}, K_2 = 10\text{dB}, K_3 = 10\text{dB}$



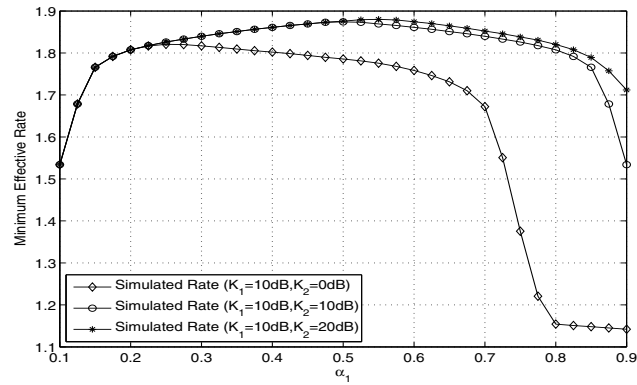
(c) Rician Channels:  $K_1 = 20\text{dB}, K_2 = 20\text{dB}, K_3 = 20\text{dB}$

**Figure 5.13:** Channel Inversion Fixed Rate-4QAM: Optimal Power Allocation Values for a Three Link Linear Relay Network with Variable Power Constraints

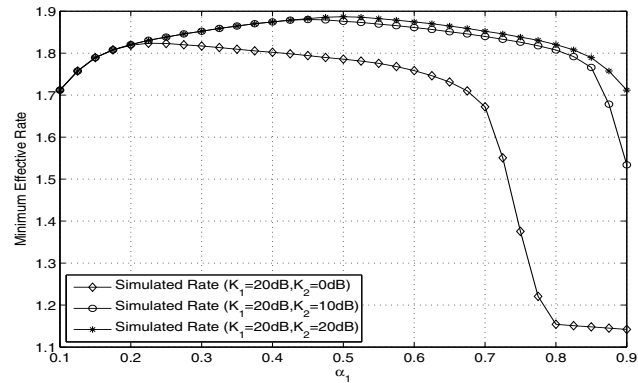
## Chapter 5. Simulation Results



(a) Rician Channels:  $K_1 = 0\text{dB}, K_2 \in \{0, 10, 20\}\text{dB}$



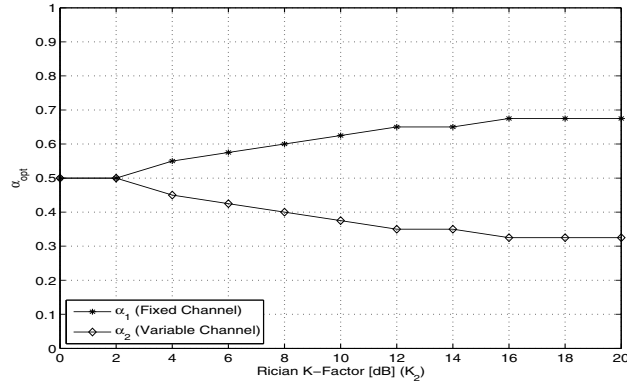
(b) Rician Channels:  $K_1 = 10\text{dB}, K_2 \in \{0, 10, 20\}\text{dB}$



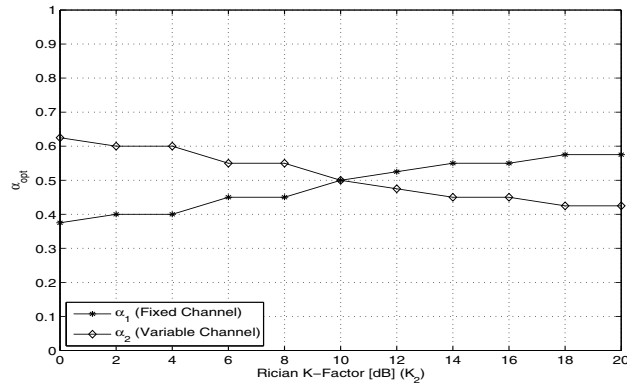
(c) Rician Channels:  $K_1 = 20\text{dB}, K_2 \in \{0, 10, 20\}\text{dB}$

**Figure 5.14:** Truncated Inversion Fixed Rate-4QAM: Achievable Rate for a Two Link Linear Relay Network with Variable Power Constraints

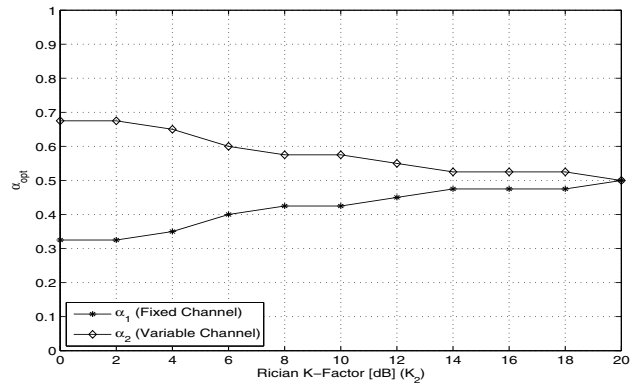
## Chapter 5. Simulation Results



(a) Rician Channels:  $K_1 = 0\text{dB}, K_2 \in [0 - 20]\text{dB}$

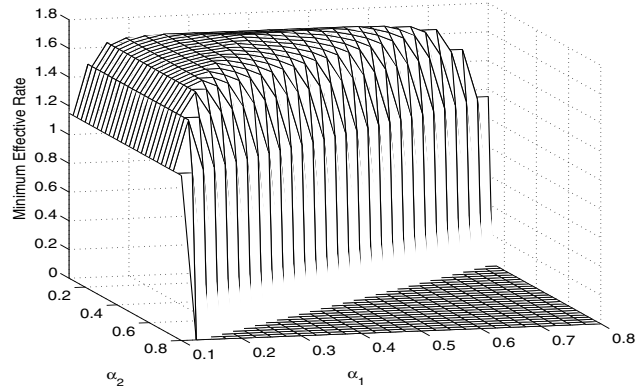


(b) Rician Channels:  $K_1 = 10\text{dB}, K_2 \in [0 - 20]\text{dB}$

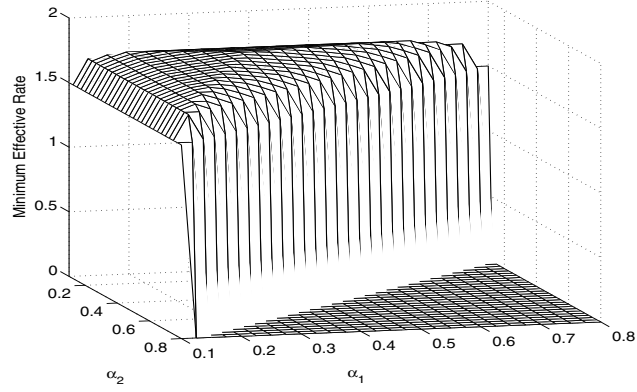


(c) Rician Channels:  $K_1 = 20\text{dB}, K_2 \in [0 - 20]\text{dB}$

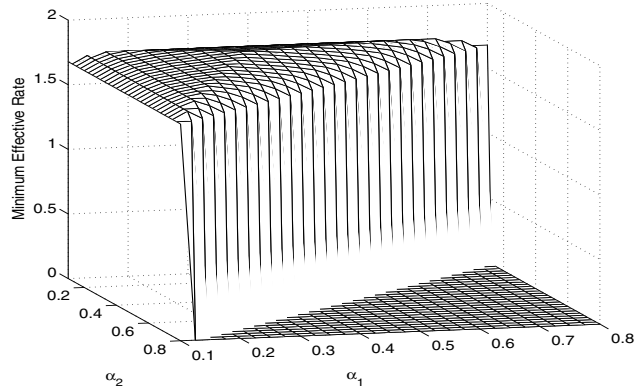
**Figure 5.15:** Truncated Inversion Fixed Rate-4QAM: Optimal Power Allocation Values for a Two Link Linear Relay Network with Variable Power Constraints



(a) Rician Channels:  $K_1 = 0\text{dB}, K_2 = 0\text{dB}, K_3 = 0\text{dB}$



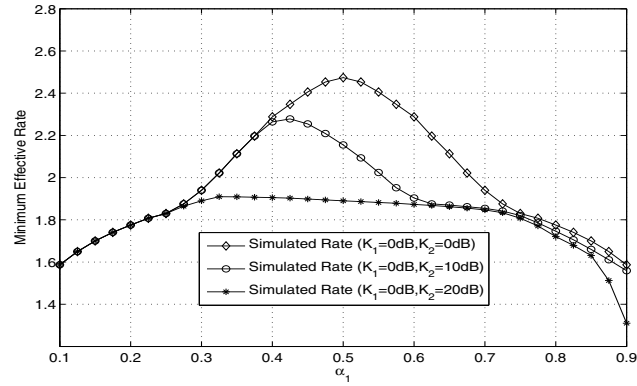
(b) Rician Channels:  $K_1 = 10\text{dB}, K_2 = 10\text{dB}, K_3 = 10\text{dB}$



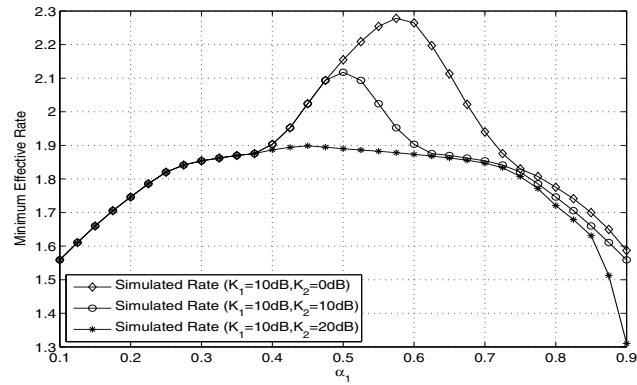
(c) Rician Channels:  $K_1 = 20\text{dB}, K_2 = 20\text{dB}, K_3 = 20\text{dB}$

**Figure 5.16:** Truncated Inversion Fixed Rate-4QAM: Optimal Power Allocation Values for a Three Link Linear Relay Network with Variable Power Constraints

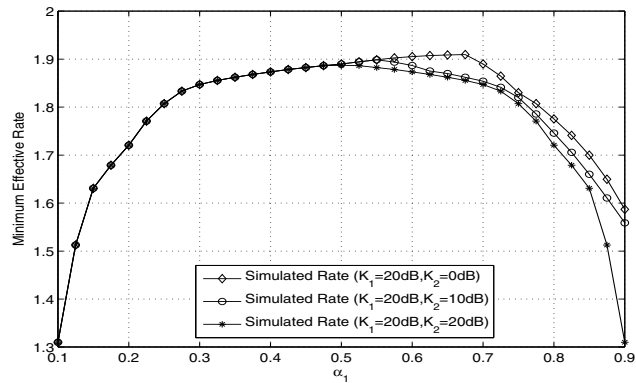
## Chapter 5. Simulation Results



(a) Rician Channels:  $K_1 = 0\text{dB}$ ,  $K_2 \in \{0, 10, 20\}\text{dB}$



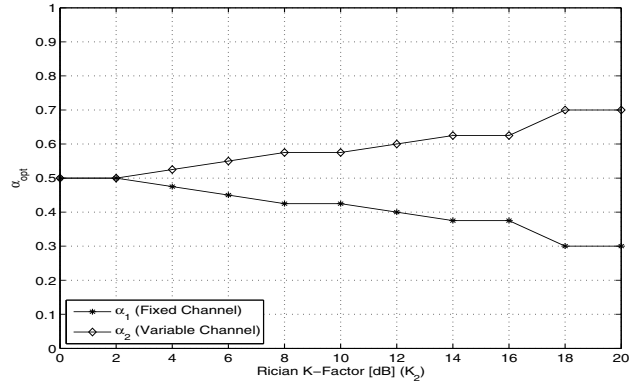
(b) Rician Channels:  $K_1 = 10\text{dB}$ ,  $K_2 \in \{0, 10, 20\}\text{dB}$



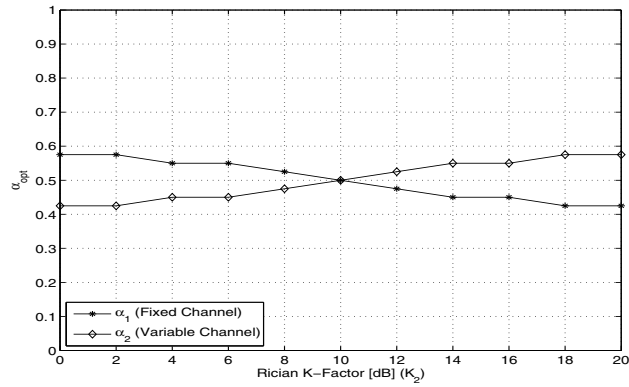
(c) Rician Channels:  $K_1 = 20\text{dB}$ ,  $K_2 \in \{0, 10, 20\}\text{dB}$

**Figure 5.17:** Truncated Inversion Fixed Rate-16QAM: Achievable Rate for a Two Link Linear Relay Network with Variable Power Constraints

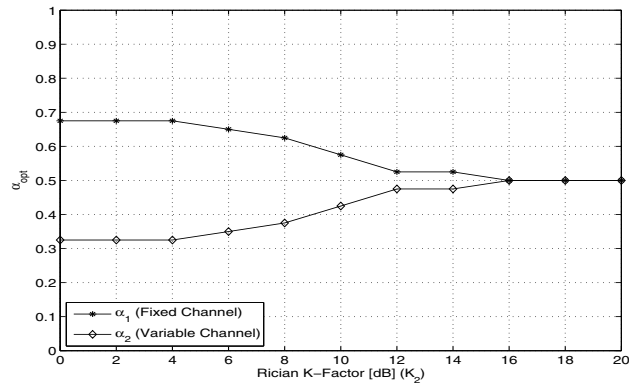
## Chapter 5. Simulation Results



(a) Rician Channels:  $K_1 = 0\text{dB}$ ,  $K_2 \in [0 - 20]\text{dB}$

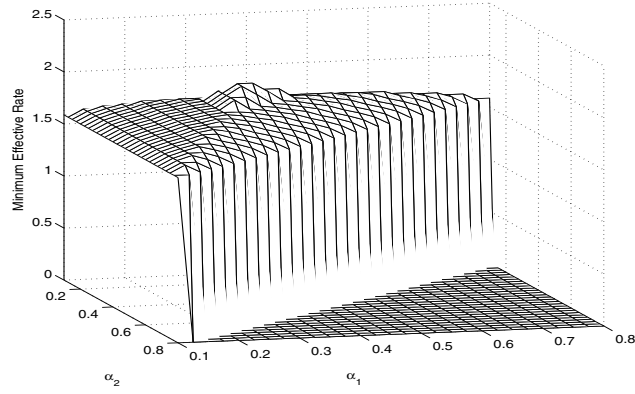


(b) Rician Channels:  $K_1 = 10\text{dB}$ ,  $K_2 \in [0 - 20]\text{dB}$

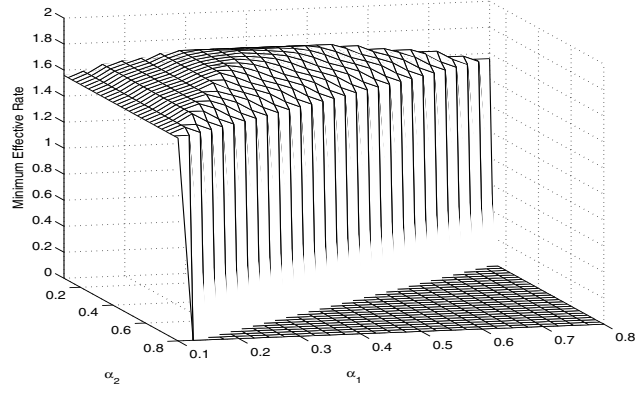


(c) Rician Channels:  $K_1 = 20\text{dB}$ ,  $K_2 \in [0 - 20]\text{dB}$

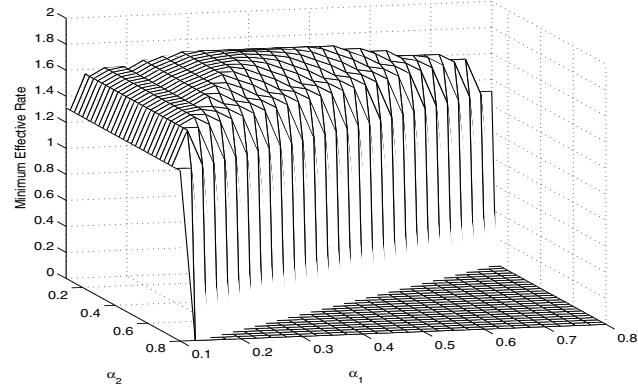
**Figure 5.18:** Truncated Inversion Fixed Rate-16QAM: Optimal Power Allocation Values for a Two Link Linear Relay Network with Variable Power Constraints



(a) Rician Channels:  $K_1 = 0\text{dB}, K_2 = 0\text{dB}, K_3 = 0\text{dB}$



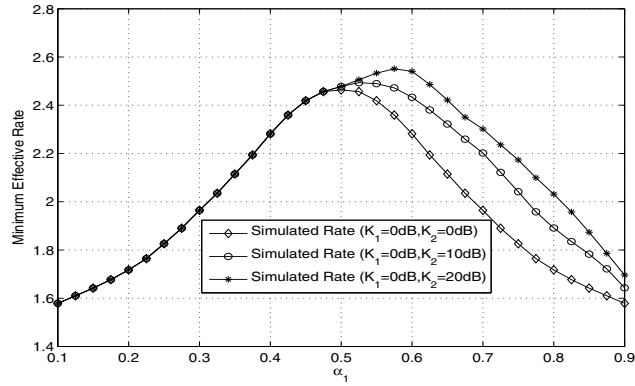
(b) Rician Channels:  $K_1 = 10\text{dB}, K_2 = 10\text{dB}, K_3 = 10\text{dB}$



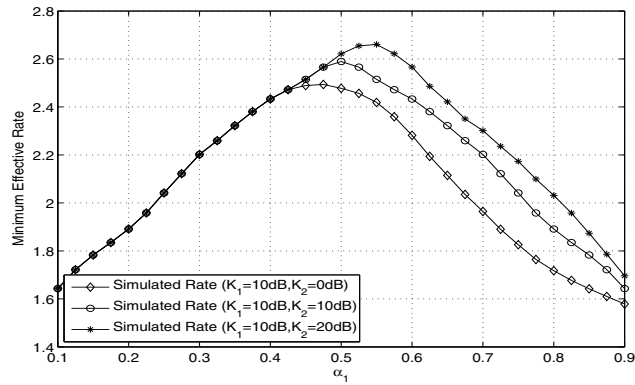
(c) Rician Channels:  $K_1 = 20\text{dB}, K_2 = 20\text{dB}, K_3 = 20\text{dB}$

**Figure 5.19:** Truncated Inversion Fixed Rate-16QAM: Optimal Power Allocation Values for a Three Link Linear Relay Network with Variable Power Constraints

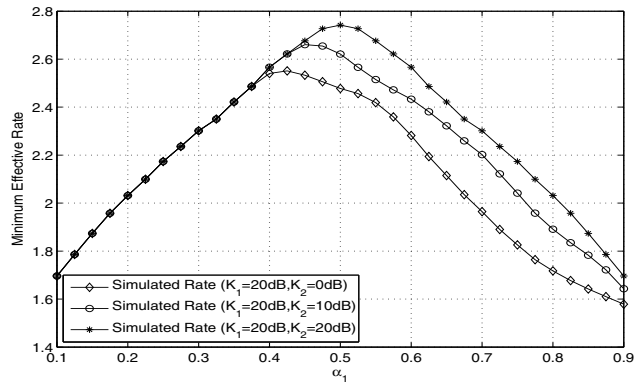
## Chapter 5. Simulation Results



(a) Rician Channels:  $K_1 = 0\text{dB}, K_2 \in \{0, 10, 20\}\text{dB}$



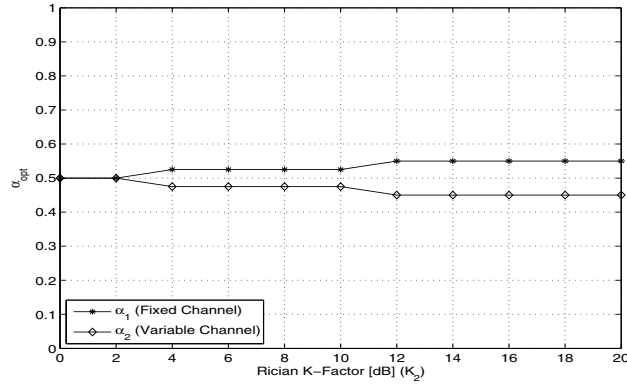
(b) Rician Channels:  $K_1 = 10\text{dB}, K_2 \in \{0, 10, 20\}\text{dB}$



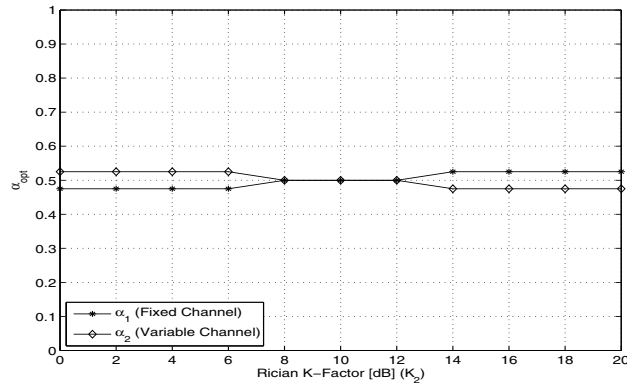
(c) Rician Channels:  $K_1 = 20\text{dB}, K_2 \in \{0, 10, 20\}\text{dB}$

**Figure 5.20:** Truncated Inversion Fixed Rate-32QAM: Achievable Rate for a Two Link Linear Relay Network with Variable Power Constraints

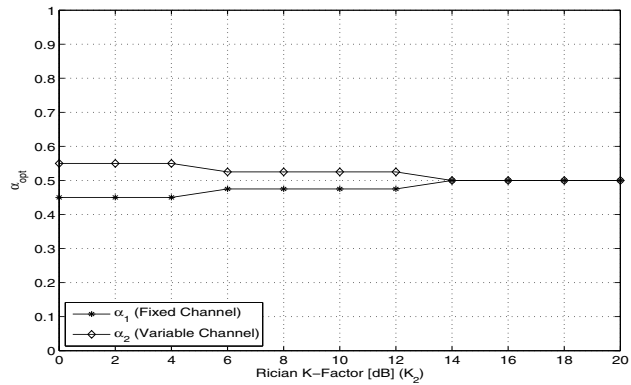
## Chapter 5. Simulation Results



(a) Rician Channels:  $K_1 = 0\text{dB}, K_2 \in [0 - 20]\text{dB}$

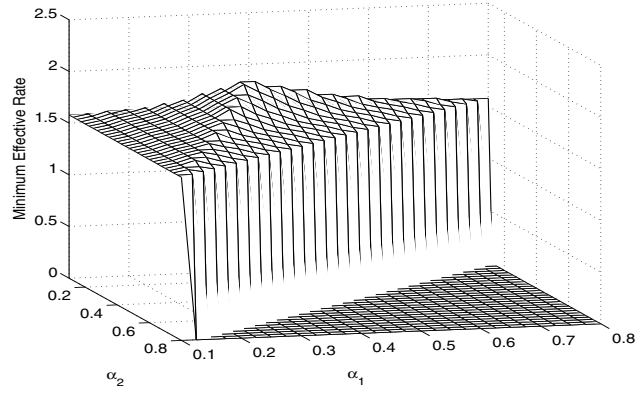


(b) Rician Channels:  $K_1 = 10\text{dB}, K_2 \in [0 - 20]\text{dB}$

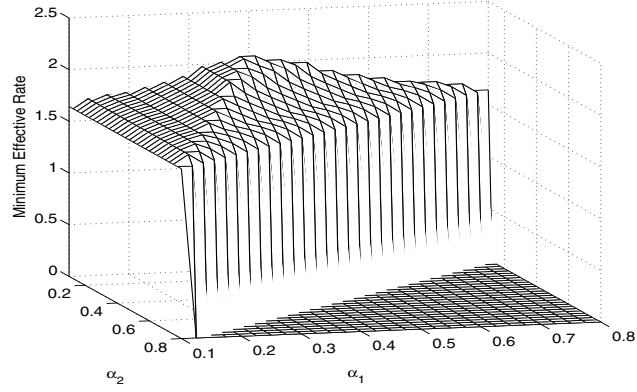


(c) Rician Channels:  $K_1 = 20\text{dB}, K_2 \in [0 - 20]\text{dB}$

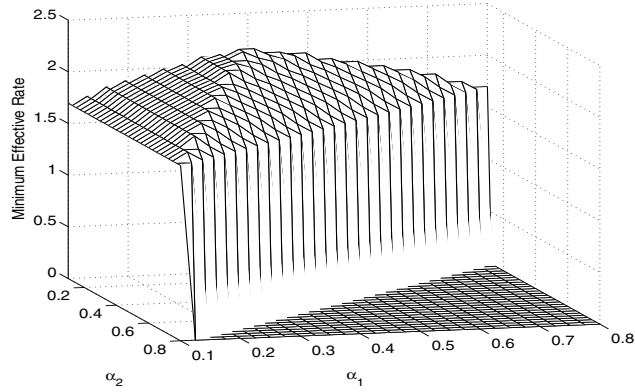
**Figure 5.21:** Truncated Inversion Fixed Rate-32QAM: Optimal Power Allocation Values for a Two Link Linear Relay Network with Variable Power Constraints



(a) Rician Channels:  $K_1 = 0\text{dB}, K_2 = 0\text{dB}, K_3 = 0\text{dB}$



(b) Rician Channels:  $K_1 = 10\text{dB}, K_2 = 10\text{dB}, K_3 = 10\text{dB}$



(c) Rician Channels:  $K_1 = 20\text{dB}, K_2 = 20\text{dB}, K_3 = 20\text{dB}$

**Figure 5.22:** Truncated Inversion Fixed Rate-32QAM: Optimal Power Allocation Values For a Three Link Linear Relay Network with Variable Power Constraints

#### 5.4.4 Discussion: Results for Truncated and Channel Inversion Fixed Rate

Looking at Figures 5.11 and 5.14 we can see that there is a positive correlation between the quality of the second channel and the achievable rate over the source to destination path. However, the achievable rate for these two policies is relatively insensitive to the power allocated to each channel. This is mainly due to the fact that the required transmit SNR is relatively small, and thus even in poor channel conditions we are able to sustain the required power to ensure that we meet our BER constraint.

Comparing the achievable rate for these two policies when there is a significant difference in the quality of the two channels ( $K_1 = 0\text{dB}, K_2 = 20\text{dB}$ ) and when the two channels are identically distributed ( $K_1 = 20\text{dB}, K_2 = 20\text{dB}$ ) yields only a marginal increase in the effective rate ( $\sim 3\%$  increase for CIFR-4QAM,  $< 2\%$  increase for TIFR-4QAM). Thus even when a significant amount of power is allocated to the poorer channel we see only a modest increase in the achievable rate. We can see evidence of this general trend in Figures 5.12 and 5.15, as the quality of the second link increases, we allocate more power to the poorer link.

Extending the relay network to include three possible links, and fixing the distribution of the three channels we get Figures 5.13 and 5.16. Like the two-link relay case, increasing the K-factor from 0dB to 20dB for all three channels doesn't significantly increase the overall achievable rate. The reason for this is similar to that of the two-link relay case. However, as was discussed in Section 4.2, for a fixed average transmit power constraint, the inclusion of an extra transmitting node in the communication path leads to an overall decrease in achievable rate. However, we can increase the overall achievable rate of this network by increasing our average transmit power constraint to some new value  $\bar{S}' > \bar{S}$ ; this new value  $\bar{S}'$  must be determined numerically. By dynamically adjusting this parameter in relation to the number of transmitting nodes in a communication path we can maintain the overall achievable rate of the relay network.

When all three channels are identically distributed we expect that the optimal power

allocation strategy is to divide the available transmit power evenly amongst all three channels. This is indeed the case for these link-adaptation policies, we can see that the maximum achievable rate for the three-link relay network peaks when  $\alpha_1 = \alpha_2 = \alpha_3 = \frac{1}{3}$ .

The achievable rate for TIFR-16QAM (Figure 5.17) agrees with the results that were presented in Section 5.4.1 in that as the quality of the second collocated channel increases the achievable rate for the two-link relay network decreases. We further see that as the quality of the two links increase there is a corresponding decrease in the achievable rate for the two-link network. Thus we see a significant difference (a decrease of  $\sim 24\%$ ) in achievable rate when the channels are identically distributed ( $K_1 = 0\text{dB}, K_2 = 0\text{dB}$ ) than when the second channel is much stronger ( $K_1 = 0\text{dB}, K_2 = 20\text{dB}$ ). Thus for TIFR-16QAM the situation is reversed, we allocate more power to the stronger channel and less to the weaker one. When we institute an average transmit power constraint for a three-link relay network using TIFR-16QAM we see that increasing the K-factor also leads to a decrease in overall achievable rate for the network. Although there is a negative correlation between the maximum achievable rate and Rician K-factor for the three-link relay network, the optimal power allocation policy is maximized, for identically distributed collocated channels, when the power is divided equally amongst the channels.

## 5.5 Discrete Rate Adaptation

### 5.5.1 Switching Levels for Discrete Rate Adaptation

Given our set of M-QAM constellations (see Table 5.1) and a BER constraint, we can now calculate the switching levels for discrete rate adaptation. Using (3.25-3.26) we get the following expression in terms of  $\rho$  for the optimal region boundaries:

$$\gamma_{4\text{QAM}}^* = \frac{1.5\rho}{\Phi}, \gamma_{16\text{QAM}}^* = \frac{6\rho}{\Phi}, \gamma_{32\text{QAM}}^* = \frac{16\rho}{\Phi}, \gamma_{64\text{QAM}}^* = \frac{32\rho}{\Phi} \quad (5.2)$$

Inserting the above into (3.27) we can solve for  $\rho$  and in turn the switching levels. It should be noted that, in general, there is no closed form expression for  $\rho$  - its value must be computed numerically. The figure below depicts the behavior of  $\rho$  as a function of the Rician K-factor.

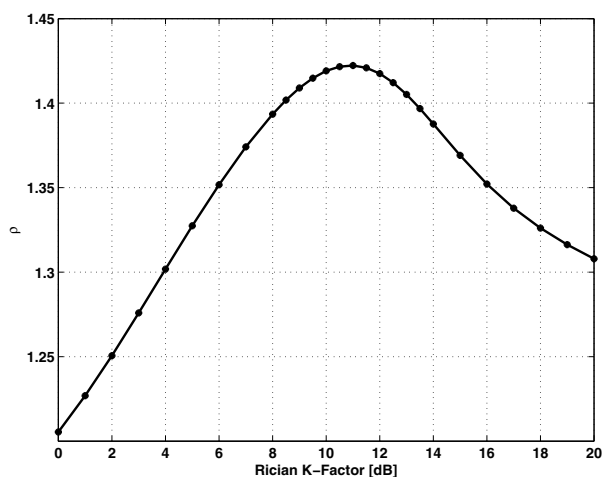


**Figure 5.23:** Numerically Obtained Values for  $\rho$

The optimal switching levels are given in Table 5.6.

### 5.5.2 Power Adaptation Policies for Adaptive Discrete Rate Transmission

Given the optimal region boundaries found in the previous section and using the equations presented in Section 4.3 we can now generate our power policies. We created power-policies for Rician channels with K-factors in the range of 0-20 dB with a step size of 2dB. The following figures are the aforementioned policies for K=0,10, and 20 dB, respectively.

**Table 5.6:** Optimal Switching Levels for Adaptive Discrete Rate Modulation over a Rician Fading Environment

Rician K-Factor [dB]	$\gamma_{4\text{QAM}}^*$ [dB]	$\gamma_{16\text{QAM}}^*$ [dB]	$\gamma_{32\text{QAM}}^*$ [dB]	$\gamma_{64\text{QAM}}^*$ [dB]
0	9.604	15.624	19.884	22.894
2	9.770	15.790	20.050	23.060
4	9.949	15.970	20.230	23.240
6	10.116	16.137	20.397	23.407
8	10.249	16.270	20.530	23.540
10	10.329	16.349	20.609	23.619
12	10.324	16.345	20.604	23.615
14	10.232	16.252	20.512	23.522
16	10.119	16.139	20.399	23.409
18	10.034	16.055	20.315	23.325
20	9.974	15.995	20.255	23.265

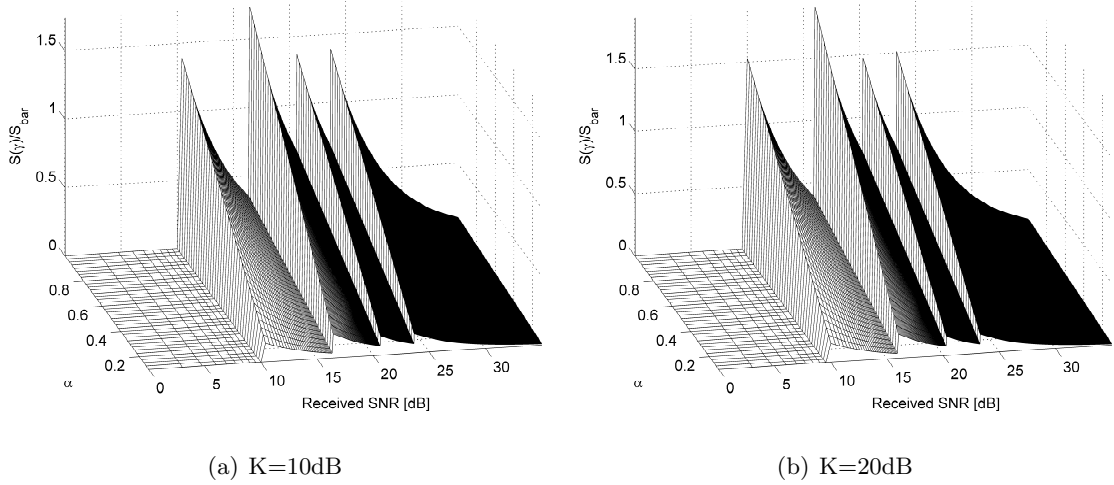


**Figure 5.25:** Power Adaptation Policies for Rician Fading Channels

### 5.5.3 Effective Rate and Optimal Power Allocation for Adaptive Discrete Rate Transmission over a Linear Relay Network

We now present the results of the problem description detailed in Section 4.4. The simulation methodology is identical to that presented in Section 5.4.3.

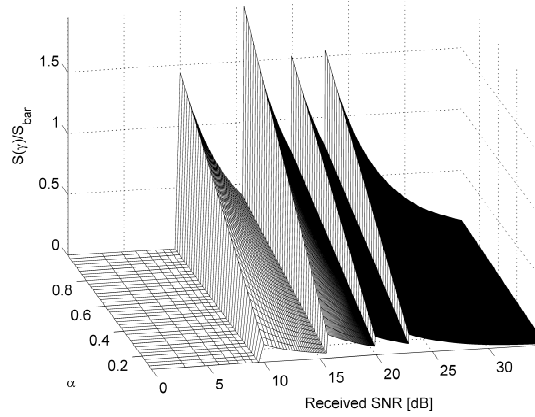
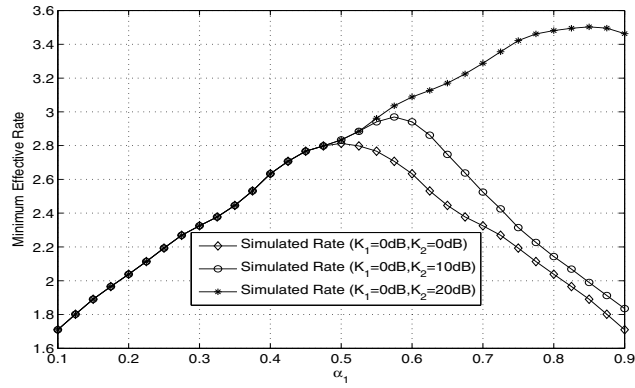


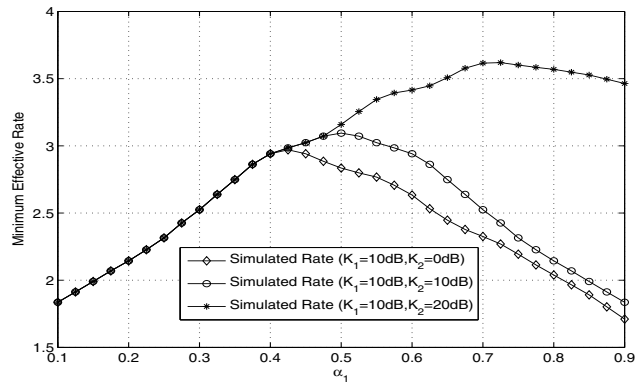
Figure 5.24: Power Adaptation Policy for a Rician Fading Channel  $K=0\text{dB}$

#### 5.5.4 Discussion: Results for Adaptive Discrete Rate Transmission

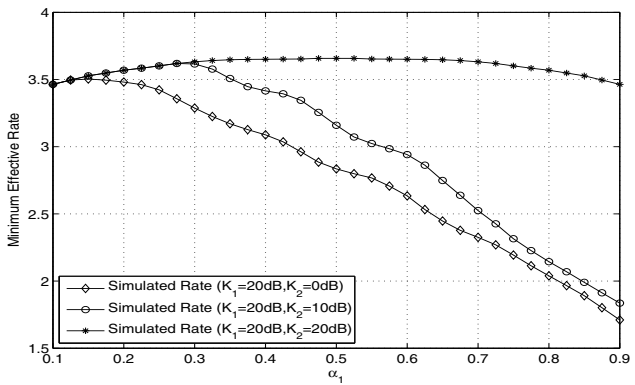
Looking at Figure 5.23 we can see that the achievable rate for adaptive discrete rate transmission is more sensitive to the power allocated between the two channels. Comparing the achievable rate when the two channels are the weakest ( $K_1 = 0\text{dB}, K_2 = 0\text{dB}$ ) and when they are the strongest ( $K_1 = 20\text{dB}, K_2 = 20\text{dB}$ ) we can see a maximum increase of  $\sim 30\%$  between the achievable rate for the relay network. This is due to the fact that in order to maximize the rate over the network we wish to transmit using the highest order modulation scheme available to the transmitter. This is achieved by allocating more power to the weaker channel and less to the stronger one. We can see further evidence of this in the optimal power allocation curves for ADR (see Figure 5.24). Thus we see that when the first channel is poor ( $K_1 = 0\text{dB}$ ) and the second is quite strong ( $K_2 = 20\text{dB}$ ) the maximum rate is achieved by allocating 85% of the total transmit power constraint to the poorer link and 15% to the stronger one.



(a) Rician Channels:  $K_1 = 0\text{dB}, K_2 \in \{0, 10, 20\}\text{dB}$



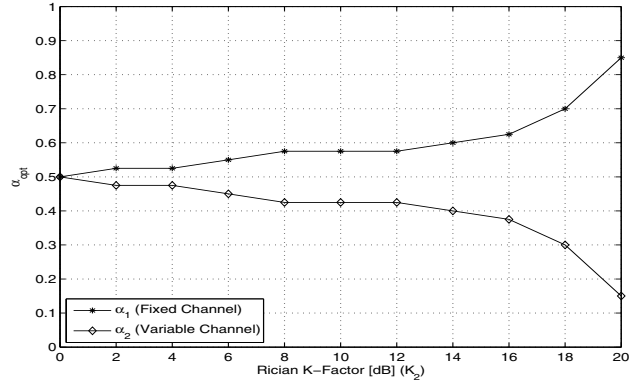
(b) Rician Channels:  $K_1 = 10\text{dB}, K_2 \in \{0, 10, 20\}\text{dB}$



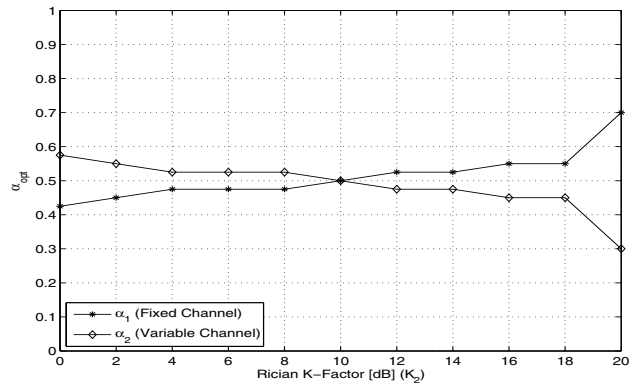
(c) Rician Channels:  $K_1 = 20\text{dB}, K_2 \in \{0, 10, 20\}\text{dB}$

**Figure 5.26:** Adaptive Discrete Rate: Achievable Rate for a Two Link Linear Relay Network with Variable Power Constraints

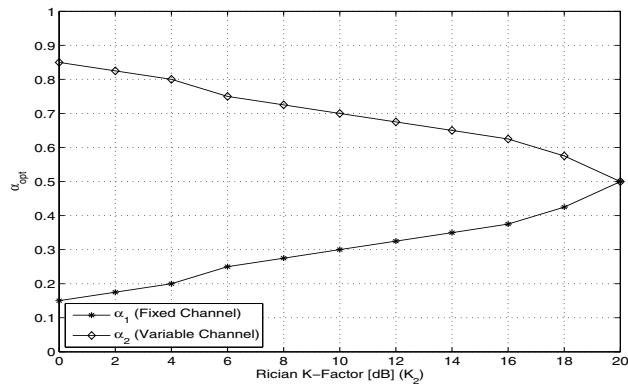
## Chapter 5. Simulation Results



(a) Rician Channels:  $K_1 = 0\text{dB}, K_2 \in [0 - 20]\text{dB}$

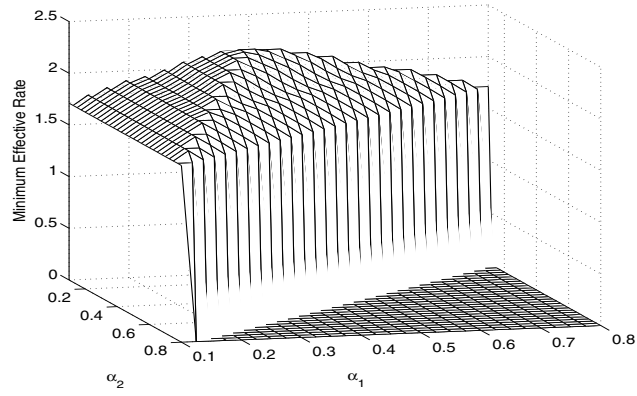


(b) Rician Channels:  $K_1 = 10\text{dB}, K_2 \in [0 - 20]\text{dB}$

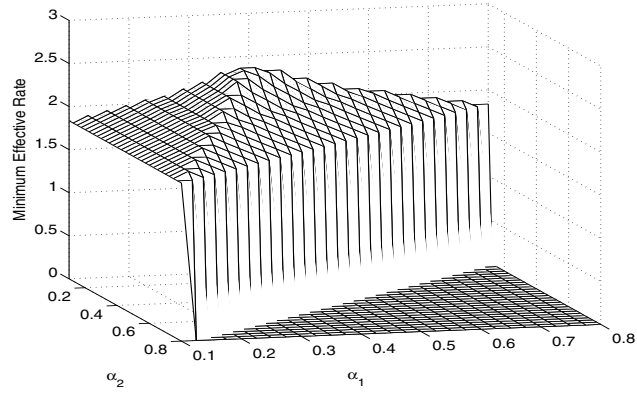


(c) Rician Channels:  $K_1 = 20\text{dB}, K_2 \in [0 - 20]\text{dB}$

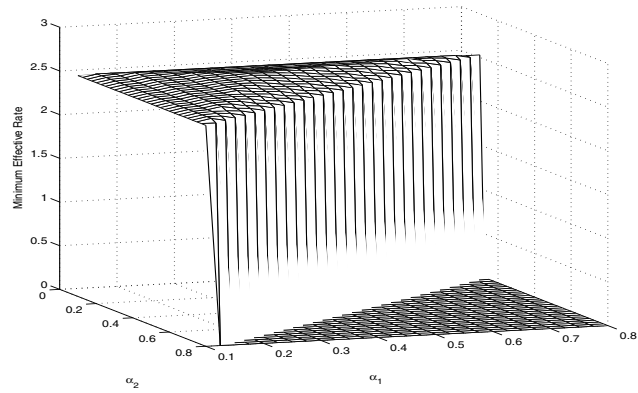
**Figure 5.27:** Adaptive Discrete Rate: Optimal Power Allocation Values For a Two Link Linear Relay Network with Variable Power Constraints



(a) Rician Channels:  $K_1 = 0\text{dB}$ ,  $K_2 = 0\text{dB}$ ,  $K_3 = 0\text{dB}$



(b) Rician Channels:  $K_1 = 10\text{dB}$ ,  $K_2 = 10\text{dB}$ ,  $K_3 = 10\text{dB}$



(c) Rician Channels:  $K_1 = 20\text{dB}$ ,  $K_2 = 20\text{dB}$ ,  $K_3 = 20\text{dB}$

**Figure 5.28:** Adaptive Discrete Rate: Optimal Power Allocation Values For a Three Link Linear Relay Network with Variable Power Constraints

## 5.6 Achievable Rate Comparison between Link Adaptation Policies

We now provide a comparison between the aforementioned communication strategies. Our results unquestionably show the superiority of link-adaptation, especially rate adaptation, for linear relay networks with an average transmit power constraint along the entire communication path. The results were generated by fixing one of the two channels in the communication link, the second channel was then varied. Once the transmissions were complete, using the optimal power allocation values generated in Sections 5.4.3 and 5.5.3, the maximum effective rate was determined. The figures below were generated using the aforementioned steps.

### Two Link Linear Relay Network

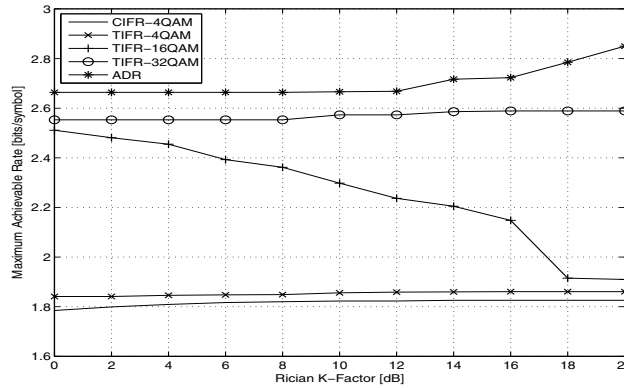


Figure 5.29: Maximum effective rate for a two-link relay network,  $K_1 = 0\text{dB}$

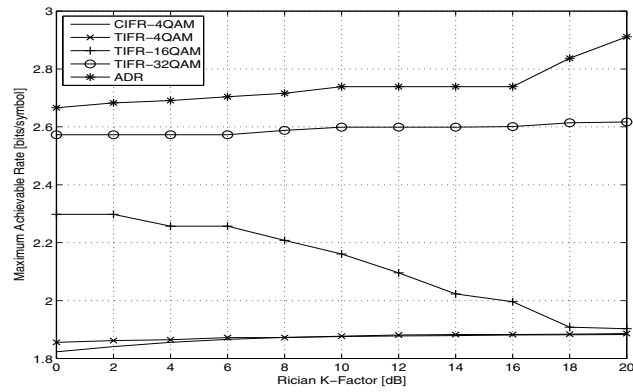


Figure 5.30: Maximum Effective Rate For a Two Link Relay Network,  $K_1 = 10\text{dB}$

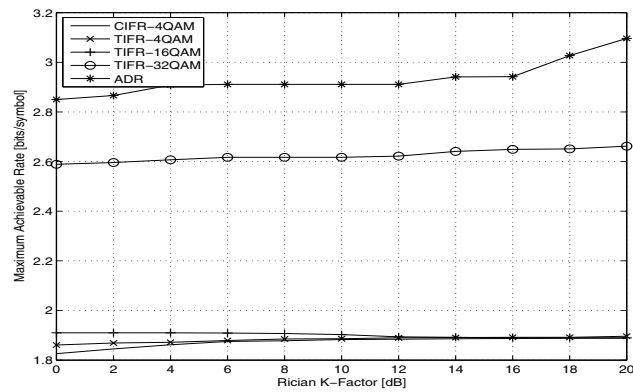
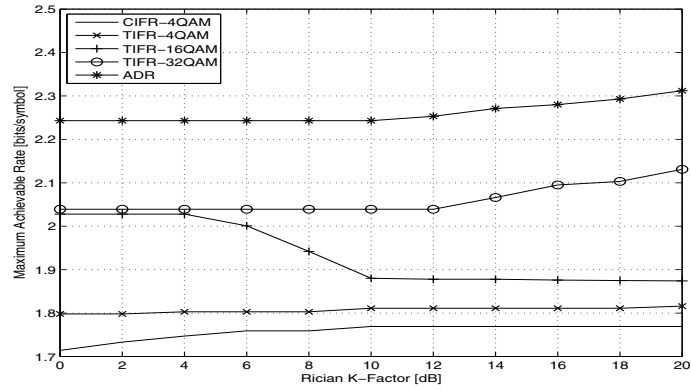


Figure 5.31: Maximum Effective Rate For a Two Link Relay Network,  $K_1 = 20\text{dB}$

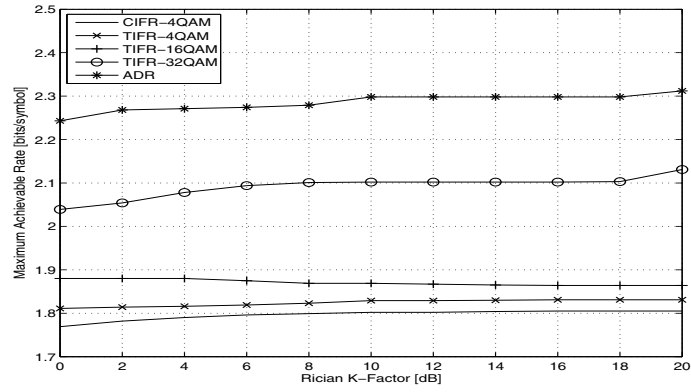
### Three Link Linear Relay Network

In this section we extended the relay network to include three links.

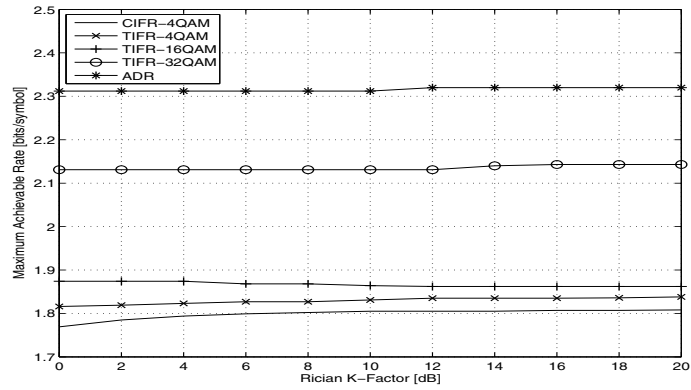
## Chapter 5. Simulation Results



(a) Rician Channels:  $K_1 = 0\text{dB}$ ,  $K_2 = 0\text{dB}$ ,  $K_3 \in [0 - 20]\text{dB}$



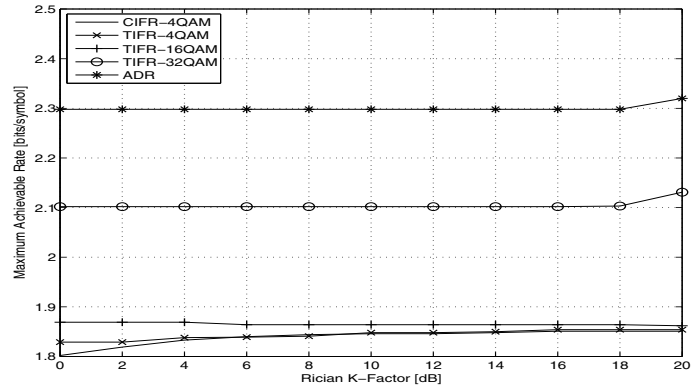
(b) Rician Channels:  $K_1 = 0\text{dB}$ ,  $K_2 = 10\text{dB}$ ,  $K_3 \in [0 - 20]\text{dB}$



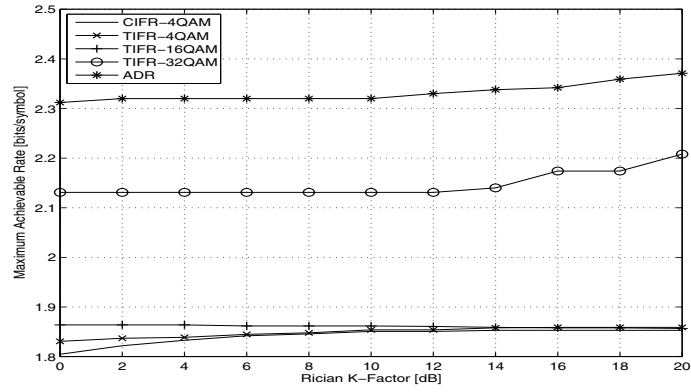
(c) Rician Channels:  $K_1 = 0\text{dB}$ ,  $K_2 = 20\text{dB}$ ,  $K_3 \in [0 - 20]\text{dB}$

**Figure 5.32:** Maximum Effective Rate For a Three Link Relay Network

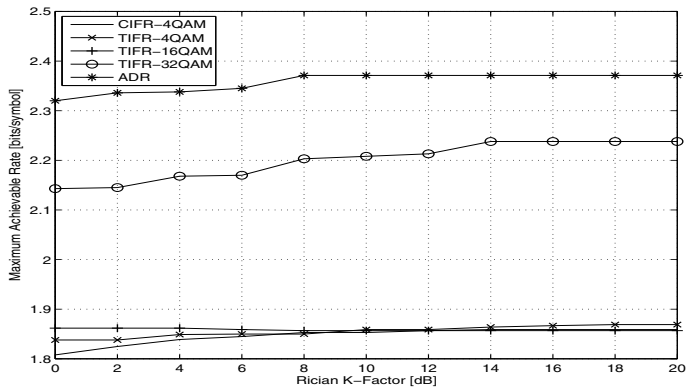
## Chapter 5. Simulation Results



(a) Rician Channels:  $K_1 = 10\text{dB}$ ,  $K_2 = 10\text{dB}$ ,  $K_3 \in [0 - 20]\text{dB}$



(b) Rician Channels:  $K_1 = 10\text{dB}$ ,  $K_2 = 20\text{dB}$ ,  $K_3 \in [0 - 20]\text{dB}$



(c) Rician Channels:  $K_1 = 20\text{dB}$ ,  $K_2 = 20\text{dB}$ ,  $K_3 \in [0 - 20]\text{dB}$

**Figure 5.33:** Maximum Effective Rate For a Three Link Relay Network

### 5.6.1 Discussion: Achievable Rate Comparison Between Adaptation Policies

Comparing the achievable rates of the link adaptation policies we can see that, irrespective of the channel distribution or the number of relay nodes in the networks, adaptive discrete rate transmission outperforms all other schemes.

The performance of TIFR-32QAM for a two-link relay network is close to that of ADR; however, we see that there is a positive correlation between the difference in performance and the channel quality. This is mainly due to the fact that in high SNR environments ADR can make use of higher-order modulation schemes, while TIFR-32QAM can only transmit using a fixed rate.

The performance of TIFR-16QAM closely mirrors the behavior we expected, in that as the channel quality increases (i.e. Rician K-factor) we see a decrease in achievable rate (see Section 5.4). Looking at Figure 5.8 we can see that as the Rician K-factor increases the received SNR that can be provided by TIFR-16QAM approaches that of both TIFR-4QAM and CIFR-4QAM.

Looking at the results for both two and three link relay networks we see that the achievable rate performance agrees with Figure 5.8. As we increase the number of relay nodes, we expect to see a decrease in overall achievable rate; this is due to the fact that we must now allocate power to an extra node, decreasing the available power to other nodes in the network. Given that we must satisfy an overall average transmit power constraint, we can see how the inclusion of an extra node in the communication path from the source to the destination results in a decrease in overall rate for the relay network. It is evident from our results that the overall achievable rate for a two link relay network always serves as an upper-bound to the performance of the three link relay network. The main advantage of using ADR is really evident when the relay network is extended to include three links. This is due to the fact that, at lower transmit powers, ADR can use its available bandwidth more advantageously than other fixed rate policies.

## 5.7 Conclusion

This chapter has provided the simulation results originally discussed in Chapter 3. Simulation assumptions and parameters were presented in order to establish the accuracy and repeatability of the simulations. Our simulation methodology was discussed in detail in order to demonstrate the veracity of our approach. A detailed simulator flowchart was provided to help guide the reader through a single communication session. With this groundwork firmly established we then provided detailed simulation results for two and three-link communication scenarios, using a number of different link-adaptive transmission schemes, and investigated their behavior over Rician fading environments. Optimal power allocation values between the collocated channels and their maximum achievable rates were calculated. Finally we provided a comparison between all of the link-adaptive schemes in order to establish the superiority of link adaptation, specifically discrete-rate continuous-power adaptation, to other transmission schemes.

## Chapter 6

# Conclusions and Future Work

This chapter presents concluding remarks for this thesis and highlights some areas for future work.

### 6.1 Conclusion

In this thesis we have investigated the physical layer characteristics and implementation issues of link adaptation for energy constrained wireless networks. We have outlined and discussed in detail the main components of a bit-level simulator needed to accurately model the rate performance of such a system. Several adaptive rate protocols were simulated; and switching levels and power adaptation policies were calculated for the protocols and were incorporated into our bit-level simulator to effectively gauge their achievable rate performance over a wireless link. The maximum achievable rate for two and three link relay networks was measured using our bit-level simulator and optimal power allocation values for collocated channel distributions were simulated and presented. Furthermore, an overall achievable rate comparison between several link adaptive protocols was investigated. It was shown that adaptive discrete rate continuous power adaptation is a superior candidate to other link adaptive protocols presented herein. The advantages of using discrete rate

adaptation are particularly prevalent in poor channels conditions when the relay network was extended to include three links. This is mainly due to the fact that discrete rate adaptation is capable of making more efficient use of the available bandwidth than other transmission schemes. We have shown that with a thoughtful design discrete rate adaptation is a natural candidate for link adaptive protocols for energy constrained relay networks.

## 6.2 Future Work

This work opens several avenues for future research. While we have endeavored to be as comprehensive as possible in our analysis, there are still many issues that can be investigated which are outside the scope of this thesis:

- One of the main caveats in this thesis is the fact that as we increase the number of communication nodes in the relay network our overall achievable rate decreases. In order to circumvent this problem would be necessary to increase our overall average transmit power constraint; however, our work has presumed that we are operating under a fixed transmit power constraint. Future works may study how to dynamically adjust the transmit power constraint in relation to the number of nodes in the relay network.
- The results presented in this thesis were generated through extensive simulation. In the future we hope to conduct further research on this topic in an analytical fashion.
- Our analysis has included only the use of uncoded rectangular M-QAM constellations. Future work may include the use of lattice, trellis or rate-compatible punctured convolutional codes to bridge the gap between the Shannon capacity and the spectral efficiency of fading channels with transmitter adaptation.
- In our study we assume ideal coherent modulation/demodulation. An interesting extension to this work would be to investigate the effect on overall system performance

of the effects of phase error, quadrature error, and I-Q gain mismatch.

- We have further assumed that we can respond to the rate of channel variation very quickly, thus enabling us to assume that the channel the system experiences slow fading. If we relax this assumption to include the possibility of both fast and slow fading we would be obliged to use a different analytical approach in designing our adaptive communication system.
- One of the main tasks involved in link adaptation is the estimation of the CSI between transmitting links. This could be done by a centralized node with specialized hardware or in a decentralized fashion, whereby each pair of communicating nodes are responsible for this duty. We have assumed that CSI estimation is performed by transmitting node pairs. An interesting problem would be to investigate how to estimate and disseminate CSI information from a centralized node to transmitting node pairs in the network.
- An interesting extension of this thesis would be to study the effects of joint bandwidth and power allocation amongst the nodes. The work in this thesis has assumed that nodes in the network communicate with a fixed bandwidth. The possibility of jointly allocating bandwidth and power is an interesting research topic which may yield interesting and valuable results.
- Our analysis used only a single carrier transmission. The use of multicarrier transmission can significantly increase the performance of a wireless system through either multiplexing or diversity gain. However, multicarrier transmission entails much more complex circuitry than single carrier transmission because separate circuitry is needed for each antenna which can significantly complicate the signal processing algorithms needed at the nodes. Since we are primarily interested in energy constrained networks it is unclear whether multicarrier transmission is a suitable technique for wireless

transmission in such low power environments.

- We have seen that nodal energy information is an important metric used in different layers in the protocol stack. Given that nodes often only have a finite amount of energy with which to perform all of their necessary tasks we can see the incentive of minimizing energy consumption amongst disjoint layers in order to prolong the lifetime of the network. An investigation into cross-layer design for energy constrained networks, using the link adaptive protocols presented in this thesis could yield interesting and beneficial results.

# Bibliography

- [1] S. Akhavan-Astaneh, A. Alemdar, and M. Ibnkahla, “Wireless sensor networks for wildlife monitoring: System architecture design,” in *WoSPA 2008 : 5th International Workshop on Signal Processing and its Applications, 18-20 March, Sharjah, U.A.E.*, 2008.
- [2] K. Akkaya and M. F. Younis, “A survey on routing protocols for wireless sensor networks,” *Ad Hoc Networks*, vol. 3, no. 3, pp. 325–349, 2005.
- [3] I. F. Akyildiz, W. Su, Y. Sankarasubramaniam, and E. Cayirci, “Wireless sensor networks: a survey,” *Computer Networks (Amsterdam, Netherlands: 1999)*, vol. 38, no. 4, pp. 393–422, 2002. [Online]. Available: [citeseer.ist.psu.edu/akyildiz02wireless.html](http://citeseer.ist.psu.edu/akyildiz02wireless.html)
- [4] J. N. Al-Karaki and A. E. Kamal, “Routing techniques in wireless sensor networks: a survey,” *IEEE Wireless Communications*, vol. 11, no. 6, pp. 6–28, 2004. [Online]. Available: [http://ieeexplore.ieee.org/xpls/abs/\\_all.jsp?arnumber=1368893](http://ieeexplore.ieee.org/xpls/abs/_all.jsp?arnumber=1368893)
- [5] A. Alemdar and M. Ibnkahla, “Wireless sensor networks: Applications and challenges,” *9th International Symposium on Signal Processing and Its Applications, 2007. ISSPA 2007.*, pp. 1–6, Feb. 2007.

## *Bibliography*

---

- [6] —, “Wireless Sensor Networks: Technologies, Challenges and Future Trends,” in *Adaptation and Cross-Layer Design in Wireless Networks*, M. Ibnkahla, Ed. Boca Raton, Fl.: CRC Press, 2008.
- [7] M.-S. Alouini and A. J. Goldsmith, “Adaptive modulation over nakagami fading channels,” *Wirel. Pers. Commun.*, vol. 13, no. 1-2, pp. 119–143, 2000.
- [8] J. Cavers, “Variable-rate transmission for rayleigh fading channels,” *IEEE Transactions on Communications [legacy, pre - 1988]*, vol. 20, no. 1, pp. 15–22, Feb 1972.
- [9] S. T. Chung and A. Goldsmith, “Degrees of freedom in adaptive modulation: a unified view,” *IEEE Transactions on Communications*, vol. 49, no. 9, pp. 1561–1571, Sep 2001.
- [10] R. Clarke, “Statistical theory of mobile-radio reception,” *Bell System Technical Journal*, vol. 47, pp. 957–1000, July 1968.
- [11] B. Classon, K. Blankenship, and V. Desai, “Channel coding for 4G systems with adaptive modulation and coding,” *IEEE Wireless Communications*, vol. 9, no. 2, pp. 8–13, April 2002.
- [12] T. M. Cover and J. A. Thomas, *Elements of Information Theory*, 1991.
- [13] S. Cui, A. Goldsmith, and A. Bahai, “Energy-constrained modulation optimization,” *IEEE Transactions on Wireless Communications*, vol. 4, no. 5, pp. 2349–2360, Sept. 2005.
- [14] A. Ephremides, “Energy concerns in wireless networks,” *IEEE Wireless Communications*, vol. 9, no. 4, pp. 48–59, Aug. 2002.
- [15] G. D. Forney Jr., R. G. Gallager, G. Lang, F. M. Longstaff, and S. U. Qureshi, “Efficient modulation for band-limited channels,” *IEEE J. Select. Areas Commun.*, vol. 2, no. 5, pp. 632–646),, Sep 1984.

## *Bibliography*

---

- [16] A. Furuskar, S. Mazur, F. Muller, and H. Olofsson, “EDGE: enhanced data rates for GSM and TDMA/136 evolution,” *IEEE Personal Communications [see also IEEE Wireless Communications]*, vol. 6, no. 3, pp. 56–66, Jun 1999.
- [17] A. Ghosh, D. Wolter, J. Andrews, and R. Chen, “Broadband wireless access with WiMax/802.16: current performance benchmarks and future potential,” *IEEE Communications Magazine*, vol. 43, no. 2, pp. 129–136, Feb. 2005.
- [18] D. L. Goeckel, “Adaptive coded modulation for transmission over fading channels,” in *Signal Processing for Mobile Communications Handbook*, M. Ibnkahla, Ed. New York: CRC Press, 2004, ch. 16, pp. 16.1–16.30.
- [19] A. Goldsmith and S.-G. Chua, “Variable-rate variable-power MQAM for fading channels,” *IEEE Transactions on Communications*, vol. 45, no. 10, pp. 1218–1230, Oct 1997.
- [20] A. Goldsmith and P. Varaiya, “Capacity of fading channels with channel side information,” *IEEE Transactions on Information Theory*, vol. 43, no. 6, pp. 1986–1992, Nov 1997.
- [21] A. Goldsmith and S. Wicker, “Design challenges for energy-constrained ad hoc wireless networks,” *IEEE Wireless Communications*, vol. 9, no. 4, pp. 8–27, Aug. 2002.
- [22] A. Goldsmith, *Wireless Communications*. New York, NY, USA: Cambridge University Press, 2005.
- [23] J. Hagenauer, “Rate-compatible punctured convolutional codes (RCPC codes) and their applications,” *IEEE Transactions on Communications*, vol. 36, no. 4, pp. 389–400, Apr 1988.

## *Bibliography*

---

- [24] M. Hasna and M.-S. Alouini, "Optimal power allocation for relayed transmissions over rayleigh-fading channels," *IEEE Transactions on Wireless Communications*, vol. 3, no. 6, pp. 1999–2004, Nov. 2004.
- [25] J. Hayes, "Adaptive feedback communications," *IEEE Transactions on Communication Technology*, vol. 16, no. 1, pp. 29–34, February 1968.
- [26] Y.-W. Hong, W.-J. Huang, F.-H. Chiu, and C.-C. Kuo, "Cooperative communications in resource-constrained wireless networks," *IEEE Signal Processing Magazine*, vol. 24, no. 3, pp. 47–57, May 2007.
- [27] Y. Hou, Y. Shi, H. Sherali, and S. Midkiff, "On energy provisioning and relay node placement for wireless sensor networks," *IEEE Transactions on Wireless Communications*, vol. 4, no. 5, pp. 2579–2590, Sept. 2005.
- [28] M. Ilyas, I. Mahgoub, and L. Kelly, *Handbook of Sensor Networks: Compact Wireless and Wired Sensing Systems*. Boca Raton, FL, USA: CRC Press, Inc., 2004.
- [29] C. Intanagonwiwat, R. Govindan, and D. Estrin, "Directed diffusion: a scalable and robust communication paradigm for sensor networks," *Mobile Computing and Networking*, pp. 56–67, 2000.
- [30] Q. Liu, S. Zhou, and G. Giannakis, "Cross-layer combining of adaptive modulation and coding with truncated ARQ over wireless links," *IEEE Transactions on Wireless Communications*, vol. 3, no. 5, pp. 1746–1755, Sept. 2004.
- [31] I. Maric and R. Yates, "Bandwidth and power allocation for cooperative strategies in gaussian relay networks," *Conference Record of the Thirty-Eighth Asilomar Conference on Signals, Systems and Computers*, vol. 2, pp. 1907–1911 Vol.2, Nov. 2004.

## *Bibliography*

---

- [32] F. Martincic and L. Schwiebert, “Introduction to wireless sensor networking,” in *Handbook of Sensor Networks: Algorithms and Architectures*, I. Stojmenovic, Ed. John Wiley & Sons, Sep. 2005, pp. 1–41.
- [33] S. Nanda, K. Balachandran, and S. Kumar, “Adaptation techniques in wireless packet data services,” *IEEE Communications Magazine*, vol. 38, no. 1, pp. 54–64, Jan 2000.
- [34] M. Neely, E. Modiano, and C. Rohrs, “Dynamic power allocation and routing for time-varying wireless networks,” *IEEE Journal on Selected Areas in Communications*, vol. 23, no. 1, pp. 89–103, Jan. 2005.
- [35] S. Otsuki, S. Sampei, and N. Morinaga, “Square-QAM adaptive modulation/TDMA/TDD systems using modulation level estimation with walsh function,” *Electronics Letters*, vol. 31, no. 3, pp. 169–171, Feb 1995.
- [36] F. Peng, J. Zhang, and W. Ryan, “Adaptive modulation and coding for IEEE 802.11n,” *Wireless Communications and Networking Conference, 2007. WCNC 2007. IEEE*, pp. 656–661, March 2007.
- [37] M. Pop and N. Beaulieu, “Design of wide-sense stationary sum-of-sinusoids fading channel simulators,” *IEEE International Conference on Communications, 2002. ICC 2002.*, vol. 2, pp. 709–716 vol.2, 2002.
- [38] J. G. Proakis, *Digital Communications*, 4th ed. McGraw-Hill, 2001.
- [39] T. S. Rappaport, *Wireless Communications: Principles and Practice (2nd Edition)*. Prentice Hall PTR, December 2001. [Online]. Available: <http://www.amazon.ca/exec/obidos/redirect?tag=citeulike09-20&path=ASIN/0130422320>
- [40] M. Rice and S. Wicker, “Adaptive error control for slowly varying channels,” *IEEE Transactions on Communications*, vol. 42, no. 234, pp. 917–926, Feb/Mar/Apr 1994.

## *Bibliography*

---

- [41] B. Sadler, “Fundamentals of energy-constrained sensor network systems,” *IEEE Aerospace and Electronic Systems Magazine*, vol. 20, no. 8, pp. 17–35, Aug. 2005.
- [42] S. Serbetli and A. Yener, “Relay assisted F/TDMA ad hoc networks: node classification, power allocation and relaying strategies,” *IEEE Transactions on Communications*, vol. 56, no. 6, pp. 937–947, June 2008.
- [43] C. E. Shannon, “A mathematical theory of communication,” *Bell System Technical Journal*, vol. 27, no. 3, pp. 379–423, 1948, continued in following volume.
- [44] R. Shorey and C. M. Choon, *Mobile, Wireless and Sensor Networks: Technology, Applications and Future Directions*. Wiley-Interscience, 2005.
- [45] M. K. Simon and M.-S. Alouini, *Digital Communication over Fading Channels (Wiley Series in Telecommunications and Signal Processing)*. Wiley-IEEE Press, December 2004. [Online]. Available: <http://www.amazon.ca/exec/obidos/redirect?tag=citeulike09-20&path=ASIN/0471649538>
- [46] B. Sklar, “A structured overview of digital communications—a tutorial review—part ii,” *IEEE Communications Magazine*, vol. 21, no. 5, pp. 4–17, Aug 1983.
- [47] —, “Rayleigh fading channels in mobile digital communication systems .i. characterization,” *IEEE Communications Magazine*, vol. 35, no. 7, pp. 90–100, Jul 1997.
- [48] K. Sohrabi, J. Gao, V. Ailawadhi, and G. Pottie, “Protocols for self-organization of a wireless sensor network,” *IEEE Personal Communications [see also IEEE Wireless Communications]*, vol. 7, no. 5, pp. 16–27, 2000.
- [49] S. Tilak, N. B. Abu-Ghazaleh, and W. Heinzelman, “A taxonomy of wireless micro-sensor network models,” *SIGMOBILE Mob. Comput. Commun. Rev.*, vol. 6, no. 2, pp. 28–36, 2002.

## *Bibliography*

---

- [50] T. Ue, S. Sampei, N. Morinaga, and K. Hamaguchi, "Symbol rate and modulation level-controlled adaptive modulation/TDMA/TDD system for high-bit-rate wireless data transmission," *IEEE Transactions on Vehicular Technology*, vol. 47, no. 4, pp. 1134–1147, Nov 1998.
- [51] B. Vucetic, "An adaptive coding scheme for time-varying channels," *IEEE Transactions on Communications*, vol. 39, no. 5, pp. 653–663, May 1991.
- [52] W. Webb and R. Steele, "Variable rate QAM for mobile radio," *IEEE Transactions on Communications*, vol. 43, no. 7, pp. 2223–2230, Jul 1995.
- [53] J. Wolfowitz, *Coding Theorems of Information Theory*. Secaucus, NJ, USA: Springer-Verlag New York, Inc., 1978.
- [54] J.-L. Wu, H.-H. Liu, and Y.-J. Lung, "An adaptive multirate IEEE 802.11 wireless LAN," *Proceedings. 15th International Conference on Information Networking, 2001.*, pp. 411–418, 2001.
- [55] C. Xiao, Y. R. Zheng, and N. Beaulieu, "Novel sum-of-sinusoids simulation models for rayleigh and rician fading channels," *IEEE Transactions on Wireless Communications*, vol. 5, no. 12, pp. 3667–3679, December 2006.
- [56] Y. Zhao, R. Adve, and T. Lim, "Improving amplify-and-forward relay networks: optimal power allocation versus selection," *IEEE Transactions on Wireless Communications*, vol. 6, no. 8, pp. 3114–3123, August 2007.

Appendix A

## Network Simulator Output

**Appendix A. Network Simulator Output**

**Table A.1:** Point-to-Point Rate Performance for Adaptive Discrete Rate

$\alpha$	Rician K-Factor [dB]										
	0	2	4	6	8	10	12	14	16	18	20
<b>0.100</b>	1.660	1.662	1.664	1.671	1.678	1.684	1.687	1.696	1.700	1.707	1.712
<b>0.125</b>	1.738	1.742	1.747	1.756	1.760	1.760	1.763	1.766	1.770	1.774	1.778
<b>0.150</b>	1.783	1.788	1.789	1.792	1.794	1.794	1.818	1.837	1.852	1.856	1.884
<b>0.175</b>	1.802	1.804	1.807	1.807	1.808	1.826	1.872	1.916	1.931	1.958	1.959
<b>0.200</b>	1.820	1.822	1.832	1.851	1.859	1.891	1.929	1.995	2.002	2.024	2.030
<b>0.225</b>	1.878	1.914	1.917	1.946	1.956	1.997	2.000	2.070	2.077	2.092	2.105
<b>0.250</b>	1.985	1.999	2.010	2.028	2.069	2.084	2.119	2.129	2.140	2.157	2.163
<b>0.275</b>	2.072	2.098	2.105	2.140	2.170	2.180	2.191	2.197	2.214	2.251	2.252
<b>0.300</b>	2.166	2.197	2.198	2.209	2.223	2.231	2.253	2.271	2.280	2.293	2.320
<b>0.325</b>	2.243	2.268	2.271	2.274	2.279	2.298	2.330	2.338	2.342	2.359	2.371
<b>0.350</b>	2.312	2.336	2.338	2.345	2.374	2.390	2.399	2.406	2.425	2.475	2.572
<b>0.375</b>	2.390	2.424	2.426	2.427	2.430	2.442	2.468	2.473	2.507	2.606	2.699
<b>0.400</b>	2.464	2.466	2.483	2.492	2.508	2.509	2.548	2.552	2.553	2.729	2.809
<b>0.425</b>	2.513	2.523	2.540	2.554	2.565	2.581	2.583	2.589	2.640	2.779	2.911
<b>0.450</b>	2.562	2.568	2.576	2.584	2.592	2.611	2.615	2.631	2.673	2.837	2.942
<b>0.475</b>	2.620	2.621	2.636	2.654	2.664	2.666	2.668	2.717	2.723	2.917	3.027
<b>0.500</b>	2.664	2.683	2.691	2.704	2.716	2.739	2.742	2.791	2.808	2.982	3.096
<b>0.525</b>	2.730	2.746	2.750	2.781	2.785	2.823	2.839	2.842	2.892	3.061	3.170
<b>0.550</b>	2.785	2.823	2.824	2.856	2.867	2.869	2.905	2.941	2.986	3.178	3.278
<b>0.575</b>	2.850	2.866	2.908	2.911	2.931	2.955	2.998	3.000	3.062	3.267	3.338
<b>0.600</b>	2.895	2.910	2.962	2.964	2.990	3.025	3.049	3.052	3.119	3.338	3.409
<b>0.625</b>	2.961	2.974	3.024	3.043	3.048	3.082	3.095	3.104	3.179	3.392	3.461
<b>0.650</b>	3.016	3.027	3.076	3.110	3.115	3.123	3.147	3.155	3.240	3.428	3.518
<b>0.675</b>	3.072	3.076	3.116	3.160	3.162	3.168	3.201	3.204	3.290	3.478	3.576
<b>0.700</b>	3.122	3.130	3.135	3.211	3.226	3.242	3.261	3.266	3.334	3.520	3.624
<b>0.725</b>	3.161	3.187	3.187	3.267	3.281	3.284	3.310	3.318	3.389	3.577	3.661
<b>0.750</b>	3.212	3.238	3.255	3.321	3.328	3.340	3.357	3.358	3.464	3.623	3.705
<b>0.775</b>	3.266	3.278	3.320	3.375	3.381	3.397	3.405	3.416	3.514	3.684	3.751
<b>0.800</b>	3.320	3.322	3.381	3.412	3.434	3.447	3.455	3.460	3.550	3.730	3.817
<b>0.825</b>	3.361	3.364	3.420	3.438	3.478	3.482	3.491	3.498	3.594	3.769	3.851
<b>0.850</b>	3.407	3.417	3.463	3.472	3.486	3.532	3.534	3.534	3.646	3.813	3.906
<b>0.875</b>	3.460	3.465	3.486	3.502	3.532	3.563	3.579	3.579	3.681	3.859	3.940
<b>0.900</b>	3.491	3.514	3.518	3.540	3.579	3.605	3.609	3.634	3.722	3.898	3.987

**Appendix A. Network Simulator Output**

**Table A.2:** Point-to-Point Rate Performance for TIFR-32QAM

$\alpha$	Rician K-Factor [dB]										
	<b>0</b>	<b>2</b>	<b>4</b>	<b>6</b>	<b>8</b>	<b>10</b>	<b>12</b>	<b>14</b>	<b>16</b>	<b>18</b>	<b>20</b>
<b>0.100</b>	1.605	1.606	1.608	1.621	1.635	1.640	1.641	1.643	1.651	1.659	1.659
<b>0.125</b>	1.687	1.690	1.696	1.698	1.712	1.719	1.725	1.731	1.731	1.734	1.735
<b>0.150</b>	1.729	1.738	1.740	1.751	1.753	1.758	1.766	1.771	1.772	1.777	1.779
<b>0.175</b>	1.764	1.773	1.779	1.785	1.787	1.791	1.794	1.796	1.796	1.798	1.799
<b>0.200</b>	1.801	1.805	1.808	1.809	1.810	1.810	1.811	1.814	1.816	1.817	1.820
<b>0.225</b>	1.819	1.823	1.823	1.824	1.827	1.827	1.829	1.830	1.831	1.846	1.866
<b>0.250</b>	1.837	1.838	1.838	1.839	1.839	1.843	1.855	1.861	1.897	1.937	1.940
<b>0.275</b>	1.894	1.901	1.903	1.926	1.929	1.932	1.944	1.987	1.990	2.009	2.034
<b>0.300</b>	1.959	1.960	1.996	2.000	2.015	2.017	2.018	2.066	2.095	2.103	2.131
<b>0.325</b>	2.039	2.054	2.078	2.094	2.101	2.102	2.122	2.140	2.174	2.174	2.238
<b>0.350</b>	2.143	2.145	2.168	2.170	2.203	2.208	2.213	2.248	2.250	2.263	2.300
<b>0.375</b>	2.309	2.309	2.318	2.318	2.321	2.341	2.345	2.379	2.382	2.386	2.388
<b>0.400</b>	2.361	2.366	2.376	2.387	2.397	2.404	2.424	2.430	2.437	2.444	2.451
<b>0.425</b>	2.408	2.409	2.419	2.443	2.465	2.469	2.469	2.471	2.477	2.480	2.506
<b>0.450</b>	2.449	2.457	2.487	2.493	2.502	2.503	2.530	2.540	2.547	2.553	2.556
<b>0.475</b>	2.486	2.516	2.526	2.533	2.534	2.573	2.573	2.586	2.601	2.614	2.617
<b>0.500</b>	2.553	2.555	2.556	2.563	2.588	2.599	2.622	2.641	2.649	2.651	2.662
<b>0.525</b>	2.589	2.596	2.607	2.617	2.619	2.638	2.669	2.671	2.692	2.695	2.704
<b>0.550</b>	2.621	2.636	2.639	2.649	2.688	2.691	2.692	2.693	2.726	2.756	2.770
<b>0.575</b>	2.634	2.655	2.665	2.678	2.706	2.712	2.755	2.756	2.775	2.827	2.848
<b>0.600</b>	2.665	2.678	2.690	2.694	2.728	2.734	2.765	2.828	2.856	2.880	2.888
<b>0.625</b>	2.692	2.695	2.704	2.735	2.742	2.757	2.785	2.897	2.914	2.938	2.951
<b>0.650</b>	2.714	2.715	2.719	2.745	2.760	2.769	2.799	2.901	2.973	2.999	3.015
<b>0.675</b>	2.728	2.740	2.742	2.772	2.772	2.783	2.811	2.904	3.036	3.055	3.066
<b>0.700</b>	2.740	2.762	2.768	2.785	2.794	2.810	2.829	2.924	3.087	3.097	3.114
<b>0.725</b>	2.761	2.774	2.784	2.789	2.808	2.828	2.873	2.933	3.142	3.150	3.157
<b>0.750</b>	2.773	2.799	2.800	2.817	2.820	2.849	2.907	2.940	3.157	3.192	3.197
<b>0.775</b>	2.801	2.814	2.815	2.828	2.835	2.871	2.923	2.942	3.162	3.234	3.259
<b>0.800</b>	2.820	2.827	2.836	2.843	2.852	2.884	2.937	2.959	3.164	3.272	3.316
<b>0.825</b>	2.836	2.843	2.849	2.854	2.869	2.894	2.952	2.966	3.165	3.311	3.351
<b>0.850</b>	2.856	2.861	2.865	2.874	2.884	2.913	2.957	2.990	3.166	3.360	3.391
<b>0.875</b>	2.866	2.878	2.889	2.891	2.895	2.923	2.982	2.994	3.193	3.392	3.435
<b>0.900</b>	2.874	2.882	2.894	2.912	2.929	2.938	2.994	2.995	3.197	3.427	3.469

**Appendix A. Network Simulator Output**

---

**Table A.3:** Point-to-Point Rate Performance for TIFR-16QAM

$\alpha$	Rician K-Factor [dB]										
	<b>0</b>	<b>2</b>	<b>4</b>	<b>6</b>	<b>8</b>	<b>10</b>	<b>12</b>	<b>14</b>	<b>16</b>	<b>18</b>	<b>20</b>
<b>0.100</b>	1.587	1.579	1.574	1.565	1.561	1.559	1.558	1.545	1.534	1.499	1.310
<b>0.125</b>	1.659	1.631	1.623	1.619	1.605	1.604	1.601	1.589	1.583	1.583	1.583
<b>0.150</b>	1.703	1.699	1.697	1.682	1.674	1.669	1.663	1.663	1.648	1.646	1.645
<b>0.175</b>	1.738	1.737	1.736	1.722	1.713	1.707	1.703	1.695	1.675	1.675	1.665
<b>0.200</b>	1.782	1.777	1.775	1.763	1.751	1.741	1.738	1.736	1.734	1.728	1.727
<b>0.225</b>	1.806	1.805	1.796	1.793	1.792	1.790	1.790	1.781	1.778	1.771	1.770
<b>0.250</b>	1.834	1.833	1.831	1.830	1.829	1.826	1.826	1.816	1.816	1.816	1.816
<b>0.275</b>	1.850	1.849	1.849	1.845	1.845	1.844	1.843	1.841	1.839	1.837	1.836
<b>0.300</b>	1.942	1.912	1.894	1.859	1.857	1.854	1.853	1.852	1.851	1.850	1.848
<b>0.325</b>	2.028	1.976	1.955	1.875	1.869	1.864	1.861	1.859	1.858	1.858	1.857
<b>0.350</b>	2.096	2.051	2.036	2.001	1.873	1.869	1.867	1.865	1.864	1.864	1.862
<b>0.375</b>	2.215	2.200	2.178	2.086	1.925	1.877	1.873	1.872	1.870	1.869	1.868
<b>0.400</b>	2.280	2.276	2.192	2.166	2.017	1.880	1.878	1.878	1.876	1.875	1.874
<b>0.425</b>	2.369	2.324	2.252	2.218	2.099	1.953	1.886	1.884	1.882	1.880	1.878
<b>0.450</b>	2.393	2.357	2.329	2.278	2.166	2.023	1.890	1.886	1.885	1.884	1.883
<b>0.475</b>	2.455	2.418	2.387	2.319	2.216	2.096	1.974	1.892	1.889	1.887	1.886
<b>0.500</b>	2.511	2.481	2.437	2.348	2.271	2.161	2.028	1.928	1.896	1.890	1.890
<b>0.525</b>	2.542	2.497	2.473	2.377	2.310	2.208	2.099	2.000	1.924	1.901	1.894
<b>0.550</b>	2.569	2.539	2.507	2.417	2.342	2.257	2.157	2.059	1.996	1.903	1.899
<b>0.575</b>	2.579	2.563	2.524	2.446	2.362	2.298	2.202	2.117	2.053	1.908	1.903
<b>0.600</b>	2.621	2.581	2.565	2.476	2.390	2.325	2.237	2.166	2.098	1.910	1.906
<b>0.625</b>	2.635	2.596	2.587	2.494	2.413	2.351	2.287	2.205	2.148	1.912	1.907
<b>0.650</b>	2.654	2.613	2.606	2.512	2.447	2.365	2.317	2.244	2.191	1.912	1.909
<b>0.675</b>	2.674	2.629	2.621	2.548	2.470	2.393	2.341	2.284	2.226	1.913	1.910
<b>0.700</b>	2.700	2.660	2.640	2.578	2.483	2.418	2.356	2.315	2.268	1.915	1.910
<b>0.725</b>	2.727	2.688	2.665	2.603	2.498	2.446	2.369	2.339	2.299	1.915	1.911
<b>0.750</b>	2.738	2.696	2.688	2.617	2.520	2.470	2.395	2.351	2.324	1.916	1.914
<b>0.775</b>	2.754	2.721	2.708	2.630	2.537	2.480	2.420	2.374	2.344	1.917	1.914
<b>0.800</b>	2.766	2.753	2.739	2.681	2.560	2.495	2.450	2.388	2.366	1.918	1.915
<b>0.825</b>	2.796	2.790	2.756	2.693	2.600	2.516	2.466	2.408	2.377	1.918	1.915
<b>0.850</b>	2.809	2.807	2.766	2.700	2.611	2.529	2.478	2.434	2.396	1.919	1.916
<b>0.875</b>	2.819	2.817	2.779	2.711	2.646	2.542	2.488	2.449	2.414	1.920	1.916
<b>0.900</b>	2.834	2.827	2.786	2.723	2.674	2.558	2.512	2.470	2.436	1.922	1.919

**Appendix A. Network Simulator Output**

---

**Table A.4:** Point-to-Point Rate Performance for TIFR-4QAM

$\alpha$	Rician K-Factor [dB]										
	<b>0</b>	<b>2</b>	<b>4</b>	<b>6</b>	<b>8</b>	<b>10</b>	<b>12</b>	<b>14</b>	<b>16</b>	<b>18</b>	<b>20</b>
<b>0.100</b>	1.248	1.251	1.258	1.263	1.273	1.284	1.292	1.301	1.306	1.310	1.499
<b>0.125</b>	1.335	1.336	1.341	1.383	1.501	1.504	1.549	1.581	1.582	1.583	1.583
<b>0.150</b>	1.358	1.366	1.369	1.604	1.605	1.614	1.615	1.624	1.626	1.645	1.646
<b>0.175</b>	1.429	1.570	1.625	1.633	1.646	1.655	1.657	1.660	1.661	1.665	1.675
<b>0.200</b>	1.655	1.670	1.680	1.690	1.691	1.703	1.710	1.710	1.721	1.727	1.728
<b>0.225</b>	1.707	1.720	1.741	1.756	1.757	1.760	1.762	1.762	1.767	1.770	1.771
<b>0.250</b>	1.766	1.770	1.775	1.783	1.790	1.800	1.800	1.803	1.809	1.816	1.816
<b>0.275</b>	1.790	1.796	1.809	1.810	1.816	1.825	1.829	1.833	1.836	1.836	1.837
<b>0.300</b>	1.805	1.817	1.818	1.824	1.834	1.839	1.840	1.843	1.844	1.848	1.850
<b>0.325</b>	1.825	1.827	1.836	1.840	1.846	1.848	1.851	1.853	1.855	1.857	1.858
<b>0.350</b>	1.832	1.836	1.841	1.844	1.851	1.854	1.857	1.859	1.860	1.862	1.864
<b>0.375</b>	1.841	1.845	1.852	1.856	1.860	1.862	1.865	1.867	1.867	1.868	1.869
<b>0.400</b>	1.845	1.849	1.855	1.862	1.865	1.867	1.869	1.871	1.874	1.874	1.875
<b>0.425</b>	1.856	1.860	1.865	1.869	1.870	1.873	1.876	1.876	1.878	1.878	1.880
<b>0.450</b>	1.866	1.870	1.872	1.872	1.875	1.877	1.880	1.881	1.882	1.883	1.884
<b>0.475</b>	1.868	1.873	1.875	1.878	1.881	1.882	1.884	1.885	1.886	1.886	1.887
<b>0.500</b>	1.876	1.877	1.882	1.884	1.884	1.887	1.888	1.888	1.888	1.890	1.890
<b>0.525</b>	1.881	1.884	1.886	1.887	1.890	1.891	1.891	1.891	1.894	1.894	1.901
<b>0.550</b>	1.884	1.886	1.890	1.890	1.892	1.893	1.893	1.893	1.896	1.899	1.903
<b>0.575</b>	1.887	1.890	1.893	1.893	1.894	1.895	1.895	1.898	1.900	1.903	1.908
<b>0.600</b>	1.888	1.892	1.896	1.897	1.897	1.898	1.900	1.900	1.902	1.906	1.910
<b>0.625</b>	1.891	1.894	1.898	1.898	1.899	1.901	1.901	1.901	1.904	1.907	1.912
<b>0.650</b>	1.894	1.896	1.899	1.900	1.901	1.902	1.902	1.903	1.907	1.909	1.912
<b>0.675</b>	1.897	1.897	1.900	1.902	1.902	1.903	1.904	1.905	1.909	1.910	1.913
<b>0.700</b>	1.898	1.899	1.901	1.903	1.904	1.905	1.905	1.908	1.909	1.910	1.915
<b>0.725</b>	1.902	1.902	1.902	1.905	1.906	1.906	1.907	1.909	1.911	1.911	1.915
<b>0.750</b>	1.903	1.903	1.903	1.907	1.908	1.908	1.908	1.909	1.911	1.914	1.916
<b>0.775</b>	1.904	1.905	1.906	1.908	1.910	1.910	1.910	1.911	1.912	1.914	1.917
<b>0.800</b>	1.905	1.907	1.907	1.909	1.911	1.911	1.912	1.912	1.913	1.915	1.918
<b>0.825</b>	1.907	1.909	1.909	1.911	1.912	1.913	1.913	1.914	1.915	1.915	1.918
<b>0.850</b>	1.908	1.910	1.912	1.912	1.913	1.914	1.914	1.915	1.915	1.916	1.919
<b>0.875</b>	1.908	1.911	1.913	1.913	1.915	1.915	1.916	1.916	1.916	1.916	1.920
<b>0.900</b>	1.913	1.914	1.915	1.915	1.916	1.917	1.917	1.918	1.918	1.919	1.922

**Appendix A. Network Simulator Output**

---

**Table A.5:** Point-to-Point Rate Performance for CIFR-4QAM

$\alpha$	Rician K-Factor [dB]										
	0	2	4	6	8	10	12	14	16	18	20
<b>0.100</b>	1.142	1.149	1.150	1.151	1.152	1.153	1.153	1.159	1.167	1.172	1.243
<b>0.125</b>	1.145	1.155	1.165	1.258	1.261	1.268	1.274	1.283	1.293	1.301	1.319
<b>0.150</b>	1.148	1.159	1.174	1.272	1.276	1.282	1.291	1.299	1.307	1.331	1.339
<b>0.175</b>	1.151	1.162	1.284	1.289	1.298	1.303	1.315	1.333	1.351	1.364	1.379
<b>0.200</b>	1.154	1.298	1.301	1.305	1.319	1.336	1.358	1.369	1.386	1.397	1.538
<b>0.225</b>	1.158	1.305	1.310	1.323	1.333	1.358	1.377	1.395	1.578	1.655	1.697
<b>0.250</b>	1.319	1.325	1.334	1.350	1.351	1.370	1.399	1.566	1.711	1.755	1.766
<b>0.275</b>	1.331	1.338	1.351	1.368	1.391	1.511	1.619	1.742	1.778	1.779	1.780
<b>0.300</b>	1.344	1.353	1.363	1.389	1.449	1.683	1.717	1.759	1.788	1.791	1.798
<b>0.325</b>	1.357	1.366	1.386	1.410	1.630	1.714	1.773	1.798	1.804	1.804	1.815
<b>0.350</b>	1.371	1.385	1.399	1.535	1.733	1.785	1.800	1.803	1.811	1.814	1.823
<b>0.375</b>	1.388	1.399	1.482	1.716	1.747	1.793	1.811	1.817	1.820	1.831	1.837
<b>0.400</b>	1.400	1.451	1.625	1.759	1.798	1.819	1.822	1.825	1.838	1.839	1.842
<b>0.425</b>	1.470	1.588	1.769	1.772	1.803	1.823	1.828	1.833	1.843	1.847	1.856
<b>0.450</b>	1.593	1.726	1.776	1.807	1.831	1.833	1.837	1.849	1.851	1.859	1.861
<b>0.475</b>	1.727	1.782	1.813	1.835	1.835	1.838	1.841	1.852	1.857	1.862	1.864
<b>0.500</b>	1.785	1.817	1.832	1.841	1.843	1.846	1.855	1.862	1.867	1.869	1.871
<b>0.525</b>	1.790	1.821	1.844	1.848	1.851	1.859	1.864	1.871	1.872	1.874	1.879
<b>0.550</b>	1.794	1.825	1.846	1.851	1.855	1.861	1.866	1.874	1.876	1.882	1.883
<b>0.575</b>	1.799	1.828	1.848	1.854	1.859	1.863	1.871	1.876	1.880	1.885	1.886
<b>0.600</b>	1.802	1.831	1.854	1.856	1.862	1.867	1.875	1.879	1.882	1.887	1.888
<b>0.625</b>	1.805	1.835	1.856	1.859	1.866	1.869	1.878	1.881	1.884	1.890	1.891
<b>0.650</b>	1.809	1.837	1.860	1.862	1.868	1.872	1.880	1.884	1.887	1.893	1.893
<b>0.675</b>	1.814	1.841	1.861	1.864	1.871	1.873	1.882	1.886	1.888	1.894	1.895
<b>0.700</b>	1.817	1.843	1.863	1.867	1.872	1.875	1.884	1.889	1.890	1.896	1.897
<b>0.725</b>	1.820	1.846	1.865	1.869	1.877	1.877	1.886	1.891	1.892	1.897	1.900
<b>0.750</b>	1.823	1.849	1.871	1.872	1.879	1.879	1.887	1.893	1.893	1.898	1.901
<b>0.775</b>	1.826	1.851	1.875	1.875	1.881	1.883	1.889	1.894	1.896	1.900	1.902
<b>0.800</b>	1.831	1.853	1.876	1.877	1.882	1.884	1.891	1.897	1.898	1.902	1.902
<b>0.825</b>	1.834	1.856	1.878	1.880	1.883	1.886	1.892	1.899	1.902	1.902	1.905
<b>0.850</b>	1.836	1.859	1.879	1.882	1.884	1.888	1.893	1.900	1.903	1.904	1.907
<b>0.875</b>	1.839	1.862	1.880	1.883	1.886	1.889	1.894	1.901	1.905	1.905	1.907
<b>0.900</b>	1.841	1.863	1.883	1.885	1.889	1.891	1.896	1.903	1.906	1.906	1.909

## Appendix B

# Achievable Rate and Optimal Power Allocation Source Code

### Source Code for Two Link Relay Network:

```
load rate_matrix_2links
%%%%%%%%%%%%%%%%%%%%%%%%%%%%%%%%%%%%%%%%%%%%%%%%%%%%%%%%%%%%%%%%%%%%%%%%
%rate_matrix_2links is a 33x11x5 matrix of rate values%
%We look at 5 different transmission protocols:          %
%CIFR-4QAM (page 1 of rate_matrix_2links)                %
%TIFR-{4,16,32}QAM (pages 2-4 of rate_matrix_2links) %
%ADR (page 5 of rate_matrix_2links)                      %
%                                                         %
%%%%%%%%%%%%%%%%%%%%%%%%%%%%%%%%%%%%%%%%%%%%%%%%%%%%%%%%%%%%%%%%%%%%%%%%
alpha_2links = linspace(0.1,0.9,33);
Kf_dB = [0:2:20];
for p=5:5 %page index
    %looking at ADR rate values
```

## Appendix B. Source Code

---

```
rates = rate_matrix_2links(:,:,p);
for t=1:length(Kf_dB)
    alphaud = flipud(alpha_2links');
    chan_rate1 = rates(:,11); %K_1 = 20dB
    chan_rate2 = flipud(rates(:,t)); %K_2 = [0-20]dB
    i=1;
    for k=1:length(alpha_2links)
        for j =1:1
            pow_test(i,:) = [alpha_2links(k) alphaud(j)];
            y(i,:)=[chan_rate1(k) chan_rate2(j)];
            rate(k,j)=min(y(i,:));
            i=i+1;
        end
        alphaud(1)=[];
        chan_rate2(1)=[];
    end
    [rows cols] = find(rate==(max(max(rate))));
    optimal_power_levels(t,:) = [alpha_2links(rows(1)) ...
                                1-alpha_2links(rows(1))];
    optimal_rate(t) = (max(max(rate)));
end
ropt(p,:)=optimal_rate;
popt(:,:,p) = optimal_power_levels;
end
```

## Appendix B. Source Code

---

### Source Code for Three Link Relay Network:

```
load rate_matrix_3links
%%%%%%%%%%%%%%%%%%%%%%%%%%%%%%%%%%%%%%%%%%%%%%%%%%%%%%%%%%%%%%%%%%%%%%%%
%rate_matrix_3links is a 29x11x5 matrix of rate values%
%We look at 5 different transmission protocols:      %
%CIFR-4QAM (page 1 of rate_matrix_3links)          %
%TIFR-{4,16,32}QAM (pages 2-4 of rate_matrix_3links) %
%ADR (page 5 of rate_matrix_3links)                %
%                                                    %
%%%%%%%%%%%%%%%%%%%%%%%%%%%%%%%%%%%%%%%%%%%%%%%%%%%%%%%%%%%%%%%%%%%%%%%%
alpha = linspace(0.1,0.8,29);
Kf_dB = [0:2:20];
for p=3:3 %page index
    %looking at TIFR-16QAM rate values
    rates = rate_matrix_3links(:,:,p);
    for t=1:length(Kf_dB)
        alphaud = flipud(alpha);
        alphaud1 = flipud(alpha);
        chan_rate1 = rates(:,1); %K_1 = 0dB
        chan_rate2 = rates(:,1); %K_2 = 0dB
        chan_rate3 = flipud(rates(:,11)); %K_3 = 20dB
        i=1;
        for k=1:length(alpha)
            for j =1:length(alphaud)
                pow_test(i,:) = [alpha(k) alpha(j) alphaud(j)];
                y(i,:)=[chan_rate1(k) chan_rate2(j) chan_rate3(j)];
            end
        end
    end
end
```

## Appendix B. Source Code

---

```
        rate3(k,j)=min(y(i,:));
        i=i+1;
    end
    alphaud(1)=[];
    chan_rate3(1)=[];
end
[rows cols] = find(rate3==(max(max(rate3))));
optimal_rate(t) = (max(max(rate3)));
for u =1:length(y)
    if(min(y(u,:))==optimal_rate(t))
        pow_dist(t,:,p)=y(u,:);
    end
end
optimal_power_levels = [alpha(rows(1)) alpha(cols(1)) ...
    1-(alpha(rows(1))+alpha(cols(1)) )];
popt(t,:,p) = optimal_power_levels;
end
ropt(:,p)=optimal_rate;
end
```